Doctor of Philosophy

Experimental investigation on non-evaporative spray and combustion characteristics of gasoline-biodiesel blends under GCI conditions

The Graduate School

of the University of Ulsan

Department of Mechanical Engineering

Sakda Thongchai

Experimental investigation on non-evaporative spray and combustion characteristics of gasoline-biodiesel blends under GCI conditions

Supervisor: Prof. Lim, Ock Taeck

A Dissertation

Submitted to

the Graduate School of the University of Ulsan

In partial Fulfillment of the Requirements

for the Degree of

Doctor of Philosophy

by

Sakda Thongchai

Department of Mechanical Engineering

University of Ulsan, Republic of Korea

May 2019

Experimental investigation on non-evaporative spray and combustion characteristics of gasoline-biodiesel blends under GCI conditions

This certifies that the dissertation
of Sakda Thongchai is approved.

Committee Chair	**Prof. Park, Kyu Yeol**
Committee Member	**Prof. Lee, Sang Wook**
Committee Member	**Asst. Prof. Chang, Kyoung Sik**
Committee Member	**Dr. Lee, Young Jae**
Committee Member	**Dr. Chollacoop, Nuwong**
Committee Member	**Prof. Lim, Ock Taeck**

Department of Mechanical Engineering

University of Ulsan

June 2019

ABSTRACT

Experimental investigation on non-evaporative spray and combustion characteristics of gasoline-biodiesel blends under GCI conditions

Department of Mechanical Engineering
Sakda Thongchai

This research focused on the phenomena of the spray development process and combustion characteristics of gasoline-biodiesel blended fuels when used in the gasoline compression ignition (GCI) engine conditions. The experiments include the phase stability and physical/chemical property of gasoline-biodiesel blends. In addition, the effect of biodiesel concentration in the blends on the spray behaviors and combustion characteristics are clarified. The test fuels, commercial gasoline and diesel (sold in Korea) and pure biodiesel (soybean methyl ester) from the industrial plant, were used in the experiment. The gasoline-biodiesel blends were mixed by increasing the percentage of biodiesel. The experiments could be divided into three sections.

Firstly, a ternary phase diagram was utilized to indicate the effect of ambient temperature on the solubility. In this part, the major test fuels were commercial gasoline and biodiesel; however, diesel was also studied for clear understanding. The test fuels were separated into two groups which are gasoline-diesel-biodiesel and gasoline-ethanol-biodiesel, which were varied each fuel concentration from 0 to 100% by volume. Then, the selected GBs with the biodiesel concentration of 5, 10, 15 and 20% were analyzed their physical and chemical properties, especially for the lubricity. Neat gasoline, biodiesel and diesel were also tested as the reference.

Secondly, macroscopic spray visualization was observed to study the phenomena and characteristic of free spray in a constant volume combustion chamber (CVCC). The Schlieren, shadowgraph photography and particle image velocimetry / tracer-based planar laser-induced fluorescence (PLIF-PIV) technique were performed to obtain the image. Image processing via MatLab software was utilized to analyze the phenomena and characteristics such as spray

penetration, cone angle, the speed of spray, etc. The important parameters which strongly affect the fuel spray consisted of injection pressures and ambient pressures were varied.

Finally, the effects of the blended fuels on combustion characteristics and emissions based on GCI combustion were investigated with varying injection pressures and injection durations. A modified single-cylinder diesel engine (498cc displacement) with a compression ratio of 19.5, was implemented with the GCI concept. Heat release rate, in-cylinder temperature, mass fraction burned, etc. were analyzed by mean of in-cylinder. The exhaust emissions were also measured such as CO, NOx and THC.

The ternary phase diagram showed that all blends had the good solubility at ambient temperature $\geq 5\ ^{\circ}C$. The lubricity of GB mixed 5% of biodiesel was improved and better than the diesel standard (<400 μm). The spray visualization results showed that high biodiesel concentrations are not significantly affected to spray behavior and characteristics. Their behaviors are similar to diesel sprays. The combustion characteristic showed that the gasoline-biodiesel blends resulted in slightly lower performance than pure diesel due to its ignition delay time. However, the exhaust emissions tend to decrease due to low-temperature heat release. Relative to commercial diesel, exhausts emissions (exclude NO_X) were significantly decreased in some conditions when using GBs blends.

Gasoline blended with 5% biodiesel can be used in the GCI engine without phase separation and the failure of the high pressure injection system due to the excellent fuel lubricity. In addition, when using it with the common rail injection system could improve better air-fuel mixing process thus enhancing the combustion phenomena. However, the injection pressure should be optimized to prevent the occurrence of cavitation and worse combustion.

Keywords: Gasoline-biodiesel blended, Gasoline compression ignition (GCI), Gasoline spray, Single and multiple injections, Gasoline combustion strategies

ACKNOWLEDGEMENT

First of all, I would like to express my high gratitude to my supervisor, Professor Ocktaeck Lim, who always gives me great chances and excellent ideas. He also provides me good advice with effective directions to conduct my research. Moreover, he is a very kind person as well.

Second, I would like to sincerely thank Dr.Nuwong chollacoop and Dr.Manida Tongroon who give me the big opportunities and support me during studying abroad.

Third, I would also like to thank all lab members of the laboratory for next generation of fuel & smart powertrain who help me to conduct my experiments. I also have a lot of good life experiences with them during staying in Korea.

Fourth, I would like to express my thanks to the Graduate School of Mechanical and Automotive Engineering, University of Ulsan for supporting a full scholarship.

Finally, I would like to express my extraordinary gratitude to my parents (Mr.Sak Thongchai and Mrs.Somjit Sangsuwang) who always give me their endless love and support my aspiration. Without them, my dreams could not become true.

TABLE OF CONTENTS

LIST OF FIGURES

LIST OF TABLES

ABBREVIATION AND NOMENCLATURES

ATDC : after top dead center

B100 : neat biodiesel

BP : back pressure

BTDC : before top dead center

C_v : velocity coefficient

CAD : crank angle degree

CI : compression ignition

CVCC : constant volume combustion chamber

CO : carbon monoxide

CO2 : carbon dioxide

COV : coefficient of variation

dP/dt : pressure rise rate, MPa/ms

CR : compression ratio, dimensionless

DOC : diesel oxidation catalyst

GB00 : neat gasoline

GB05 : gasoline 95% + biodiesel 5%

GB10 : gasoline 90% + biodiesel 10%

GB15 : gasoline 85% + biodiesel 15%

GB20 : gasoline 80% + biodiesel 20%

GCI : gasoline compression ignition

GDCI : gasoline direct compression ignition

GHG : greenhouse gas

HC : hydrocarbon

HCCI : homogeneous charge compression ignition

HR : heat release

HRR : heat release rate

IMEP : indicated mean effective pressure

IP : injection pressure

K : constant depending on the spray internal distribution,

L : spray penetration length

LTC : Low-temperature combustion

M_f : fuel mass

M_a : air mass

M_0 : momentum flux

N_e : engine speed, rpm

NOx : nitrogen oxides

P : pressure, Mpa

P_i : injection pressure

P_b : back pressure

P_{vap} : the vapor pressure of the fuel

PPCI : partially premixed compression ignition

PON : pump octane number

Qin : input heat calorie, J/cycle

DPF : diesel particulate filter

PFV : photron fastcam viewer

PM : particulate matter

R : ideal gas constant, kJ/mol·K

RCCI : Reactivity controlled combustion ignition

Re : Reynolds number, dimensionless

PRR : pressure rise rate

RPM : revolution per minute

S : spray penetration length

SI : spark ignition

t : time,

T : time

T1 : pilot injection

T2 : pre injection

T3 : main injection

TDC : top dead center

THC : total hydrocarbon

t_r : transition time between initial and developed spray

U_{inj} : velocity of start of injection

$U_{spray.average}$: average of spray velocity.

V_d : displacement volume, cm^3

V_{in} : volume, cm^3

Δp : different pressure

θ : spray cone angle

λ :Air–fuel equivalence ratio

ϕ : Fuel–air equivalence ratio

γ_m : Surface tension of mixture

γ_i : Surface tension of component

ρ_a : gas density,

ρ_f : density of fuel

1. INTRODUCTION

1.1 Background and problems

The high demand of petroleum based fuel in conjunction with the decreasing of its availability (Figure 1-1) as well as the stringent emission regulations (Figure 1-2) are the main considerate issues in the world in particular for the transportation sector. Many researchers have discovered new sources of energy such as alternative fuels. Biodiesel has been successfully used in many countries. At the same time, researchers have developed the novel engine technologies for compression ignition (CI) concepts, for examples, homogeneous charge compression ignition (HCCI), low-temperature combustion (LTC), reactivity-controlled compression ignition (RCCI) and premixed charge compression ignition (PCCI) to improve the engine performance and reduce NO_X and PM emissions as shown in Figure 1-3. Especially, gasoline compression ignition (GCI) or gasoline direct compression ignition (GDCI), which based on PPCI combustion, has been developed to control combustion phasing and the fuel-air mixture. Gasoline compression ignition via a diesel common rail injection system has been investigated recently. These new combustion concepts allow the lengthening time for the fuel-air mixing process and result in the lower peak combustion temperature which leads to the high thermal efficiency with lowering NO_X and PM emissions.

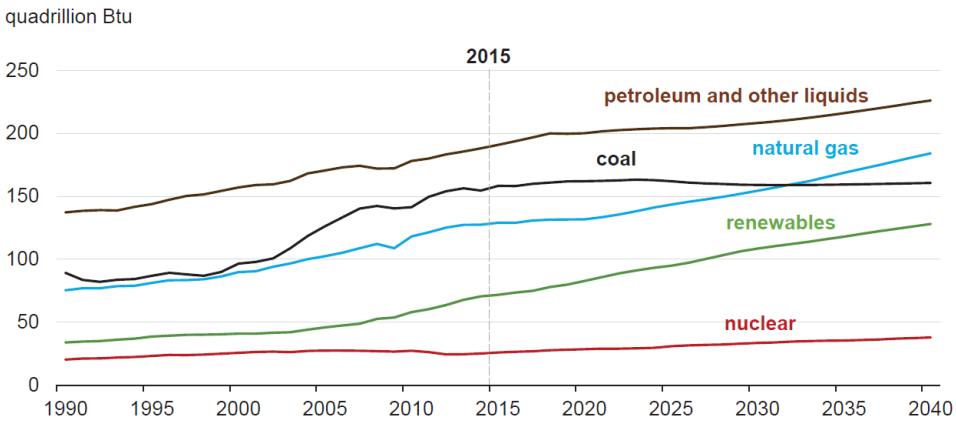

Figure 1-1 World energy consumption by energy source [1].

Due to its high cetane number, biodiesel fuel has been limited to use only in the compression ignition engines. Therefore, it is very interesting to apply biodiesel in the new types of engine, especially for gasoline compression ignition (GCI) engines. Because

gasoline has different properties with the diesel fuel, using biodiesel as the blends in GCI engines should compensate for some disadvantage of the gasoline fuel when applied in the diesel based engine. There is very few research about gasoline-biodiesel blended fuels applied in the GCI combustion concepts, both of the spray behavior and combustion characteristics.

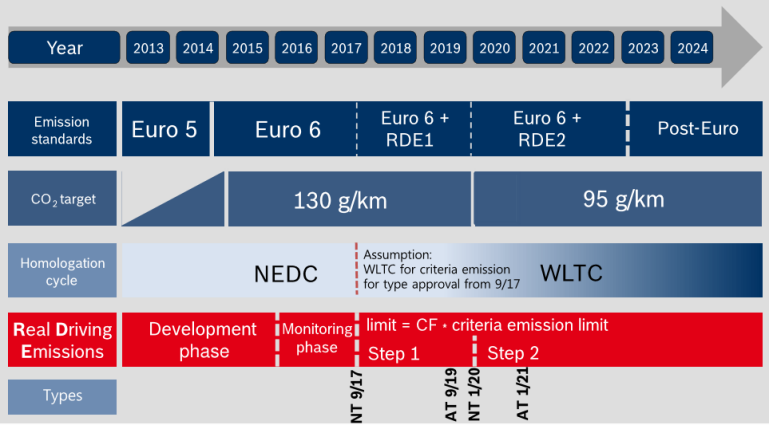

Figure 1-2 The EU legislation roadmap passenger cars (Bosch, FISITA2016).

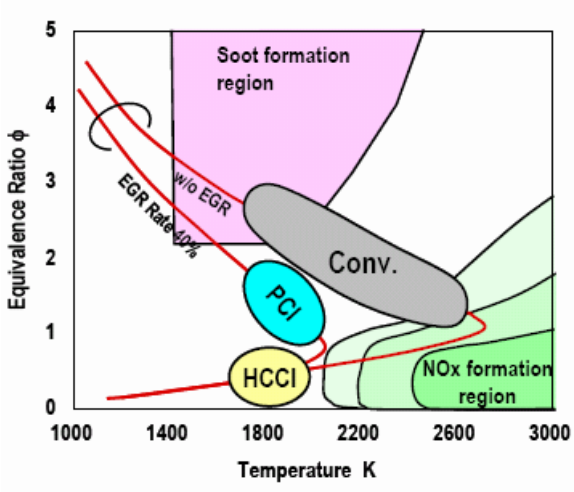

Figure 1-3 NO_X-soot map with the locations of conventional Diesel, PPC (PCI) and HCCI combustion [2].

Because gasoline has very low lubricity, there is a high possibility in which the high-pressure common rail injection system is damaged. The additive to enhance lubricity is required. It has been proved that biodiesel showed excellent lubricity and can improve the lubricity of blended fuel. Also, it is sustainable renewable fuels and decreases the exhaust emissions, especially soot and particulate matter. Therefore, to increase the fuel lubricity, it is

attractive to add biodiesel with the small amount into the gasoline injected by the high-pressure system.

Moreover, with the direct injection strategy, the combustion and exhaust emissions are significantly influenced by the spray characteristics. When injected with the different fuels, therefore, the spray behaviors which based on the fuel properties should be carefully investigated.

Because there is limited information available of GCI, It is very interesting to investigate the gasoline-biodiesel spray phenomena and consider the GCI combustion characteristics by using biodiesel as the high reactivity fuel blended in gasoline as the low reactivity fuel in some percentage by volume. One of the objectives by blending a small amount of biodiesel into gasoline is to increase lubricity, cetane number and oxygen content to reduce emission. And, the reason by using common rail is to obtain the stable high pressure of fuel and the homogeneity of the injection process will be achieved.

Before the spray phenomena and combustion characteristic test are conducted, fuel properties and the phase separation test were observed in order to confirm their properties and solubility of the blends. Then, the macroscopic spray visualization via Shadowgraph technique, Schlieren photography, were performed in a constant volume combustion chamber (CVCC) to understand the spray characteristics of gasoline-biodiesel blends. A single-hole injector was employed to investigate the effects of injection pressures and back pressures. The spray characteristics such as the spray penetration length, spray cone angle, average speed, spray area were analyzed by image processing via MatLab software. Subsequently, the microscopic spray structure including the velocity and vorticity are analyzed by means of the planar laser-induced fluorescence - particle image velocimetry tracer-based (PLIF-PIV) technique to characterize the flow field of the spray. Finally, the effects of the gasoline-biodiesel blended fuels on the GCI combustion characteristics were clarified by the in-cylinder pressure, the heat release rate and mass fraction burned. Moreover, the exhaust emission was also measured.

1.2 Objectives of the study

The objectives of this study are as follows:

(i) The main objective of this research is to study the spray behaviors of gasoline-biodiesel blends injected by the high pressure common rail injection system with varying the injection and back pressures.

(ii) To study the physical/chemical properties and phase stability of gasoline-biodiesel blends with various concentration of biodiesel.

(iii) To study the combustion characteristics of gasoline-biodiesel blends in the GDI engine with the various concentration of biodiesel.

1.3 Scope of the study

The scope of this thesis aims to study the spray phenomena and combustion characteristics when using gasoline-biodiesel blends. It does not only conduct the experiment but also design and modify equipment. The scopes of the study are included;

- Conducting the phase separation test of the "Gasoline-Diesel-Biodiesel" mixtures with the concentration from 0 to 100 percent and variation of ambient temperature.
- Measuring the fuel properties of GB00 - GB20, pure gasoline, diesel and biodiesel.
- Modifying a CVCC with injection ports to conduct the spray visualization under a variation of three injection pressures and two back pressures.
- Comparing the spay characteristic of GB00-GB20 with a single injection and two ambient pressures.
- Analysis of the spay characteristic of GB00-GB20 with multiple injection strategies and two different simulated engine speeds.
- Characterizing the flow fuel of the GB05 spray with velocity and vorticity.
- Modifying and repairing a single cylinder diesel engine to run on GCI mode
- Analysis of the combustion characteristics of GB00-GB20 at λ=1, through the cylinder pressure, mass fraction burned, and exhaust emissions.
- Clarifying the effect of two different injection pressures on the combustion characteristics of GB05 compared with diesel through the cylinder pressure, mass fraction burned, and exhaust emissions.

1.4 Organization of the thesis

- Chapter 1 addresses the background of this research including the objective and the scope of the study
- Chapter 2 reviews the relative works and relevant literature of the gasoline-biodiesel blends on the fuel spray and combustion. The new combustion concept is introduced,

and CGI is focused. The previous study of spray characteristics of biodiesel and gasoline are explained.

- Chapter 3 presents the theoretical of the spray visualization technique, the image processing via MatLab and the fundamental internal combustion engine in which the formula was used in this study shown. Moreover, the mechanisms of fuel spray development and the compress ignition combustion are explained.
- Chapter 4 details the experimental setups including the phase separation, the spray visualization and the GCI engine as well as the peripheral devices. The methodology and test procedure of each experiment are also explained.
- Chapter 5 presents the analytical results of each experiment, beginning with the phase stability and fuel properties. The macroscopic structure of gasoline-biodiesel blended fuels is firstly explained. Later, the microscopic behavior of the spray is detailed. Finally, the effect of gasoline-biodiesel blended fuels on the combustion characteristics is discussed.
- Chapter 6 provides the overall conclusions of this research. Suggestion for future research of GCI engine using gasoline-biodiesel blended fuels is also given.

2. LITERATURE REVIEW

2.1 Introduction

This chapter reviews the previous researches relative to the spray visualization and low temperature combustion concepts such as HCCI, PCCI and GCI. Many unconventional fuels, as well as the blends, have been explored their advantages when using in the compression ignition-based diesel engine. Especially, compression ignition engines using gasoline fuel have been extendedly experimented to compare with the ordinary diesel engine in the last decade. However, due to the limitations of gasoline properties and GCI operating range, there are some drawbacks of this technology. The researches have been continued by using several methods and strategies to overcome these disadvantages. Moreover, alternative fuels such as biodiesel are more interesting and important now; because, they are derived from renewable energy sources and contains oxygen molecule.

2.2 Biodiesel

In addition to the development of new engine technologies, sustainable renewable fuels, especially oxygenated fuels, have been used in the engine to reduce the automotive pollutions. Not only do they decrease the exhaust emissions, but they also reduce energy depletion problem. Biodiesel and its blends have been widely researched in the compression ignition engine because it can reduce the soot and particulate matter [3]. Moreover, due to its superior lubricity adding biodiesel in diesel fuel can improve the fuel lubricity [4], which can protect the wear and damage from the high-pressure operation of the common rail injection system. Because lubricity of gasoline is relatively poor, one challenge to use gasoline at the high-pressure injection operation is the failure and the damage of the high-pressure common rail system including high-pressure pump and nozzle. Therefore, biodiesel could be added in gasoline fuel as the lubricity enhancer additives [5]. In addition, viscosity and surface tension which affect the spray characteristics of gasoline differ from diesel while biodiesel has those properties in the opposite way. Adding biodiesel in gasoline could compensate for all these properties. Accordingly, it is interesting to combine the benefits of using gasoline in GCI engine and biodiesel fuels.

2.3 GCI concept

Generally, it is well known that when the air-fuel mixture in the CI engine is in the rich region, the engine will produce more soot. On the other hand, when the excess air is available in the charge mixture, the soot formation will be suppressed because of more complete combustion; however, the combustion temperature is high which results in the high concentration of NOx. Even though the combustion temperature is reduced in order to decrease the amount of NOx, It will also increase the amount of soot at the same time as shown in Figure 2-1. Therefore, the new combustion concepts have to develop to reduce the soot and NOx at the same time.

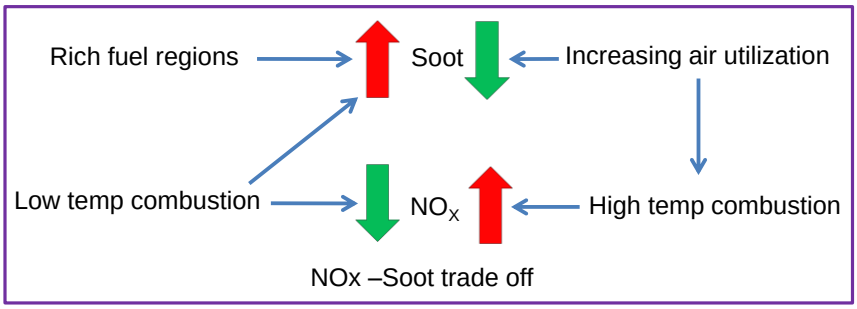

Figure 2-1 NOx –Soot trade off on commercial CI engines

Low-temperature combustion (LTC) [6,7] concept has been extendedly investigated to reduce the NO_X / PM trade-off emission in conventional compression ignition (CI) engines. Many approaches have been studied to achieve LTC concept for all operating regimes. For instance, homogeneous charge compression ignition (HCCI) [8–10] combustion, partially premixed compression ignition (PPCI), Reactivity controlled combustion ignition (RCCI) [2,11–13] and the Gasoline compression ignition (GCI) [14–18] combustion have been demonstrated their benefit to decrease the level of NO_X and soot like a spark ignition (SI) engine with the high thermal efficiency as the CI combustion. Nowadays, however, the limitation of narrower operating ranges of LTC when compared with the conventional SI and CI has still challenged researchers to overcome. For instance, in the high load range, an unacceptable rapid heat release rate of the HCCI engine is presented because of simultaneous spontaneous combustion [19–22] while a lower power output of LTC occurs due to high dilution.

The RCCI is designed to combine many engine technologies because the engine has to achieve the auto-ignition when using the blends of diesel-like and gasoline-like fuels. The

ratio of blended fuel and injection timing can be adjusted such that the definable reactivity fuel gradients initiate and control ignition. Therefore, the operating conditions can be tailored by enabling the direct control of the pressure rise rate and allowing combustion close to thermodynamically ideal conditions over wide speeds and load ranges, [23].

PPCI combustion, fueled with gasoline-like fuels, has been introduced and proved advantageous for lowering NO_X and PM by Kalghatgi [24,25]. Consequently, many researchers have continued the work on this combustion concept. The blends of gasoline and diesel, as well as pure gasoline with a 91 pump octane number (PON), were employed to control combustion phasing in a heavy duty diesel engine [26,27]. Like gasoline fuel, naphtha and ethanol have also been investigated and both demonstrated the capability to lower engine out exhaust emissions [28–31].

The partially premixed combustion of gasoline fuel, based on PPCI combustion, is known as gasoline direct compression ignition (GDCI), or more simply, gasoline compression ignition (GCI). It has been developed to control combustion phasing and improve the homogeneity of the fuel-air mixture as shown in Figure 2-2 [32,33]. Gasoline, a fuel with a high octane number, but a low cetane number, is directly injected into the in-cylinder at late timings, similar to a diesel injection at the compression stroke. Due to the difficulty of achieving self-ignition of low cetane number fuel, the ignition of the stratified charge is extended and delayed, resulting in lower combustion temperature. Subsequently, the heat transfer through the cylinder walls is reduced, which leads to higher thermal efficiency with lower NO_X, while the locally lean mixture suppresses the PM emission. However, the limited operating range of the GCI engine is the major challenge to overcome, especially at the low and high load conditions.

Based on diesel engine configuration, GCI engine applies the common rail injection system to directly inject gasoline at the high pressure through the nozzle into the cylinder. Unlike HCCI, the start of GCI combustion/combustion phasing could be controlled by the injection timing, hint the end of injection. Due to the low cetane number of gasoline, longer ignition delay allows the lengthen time for fuel to mix with the air as the premixed charge. This leads to the controllability of low NO_X and soot emissions [26,28,34,35]. Nowadays, Delphi has developed and optimized a four-cylinder GCI engine that enables operation from part load to full load operation [33,35]. With the new piston design, combined with a fuel injection system and multiple late injections, the fuel consumption of the GDCI engine was

greater than spark ignition engines and comparable or better than advanced diesel engine technology.

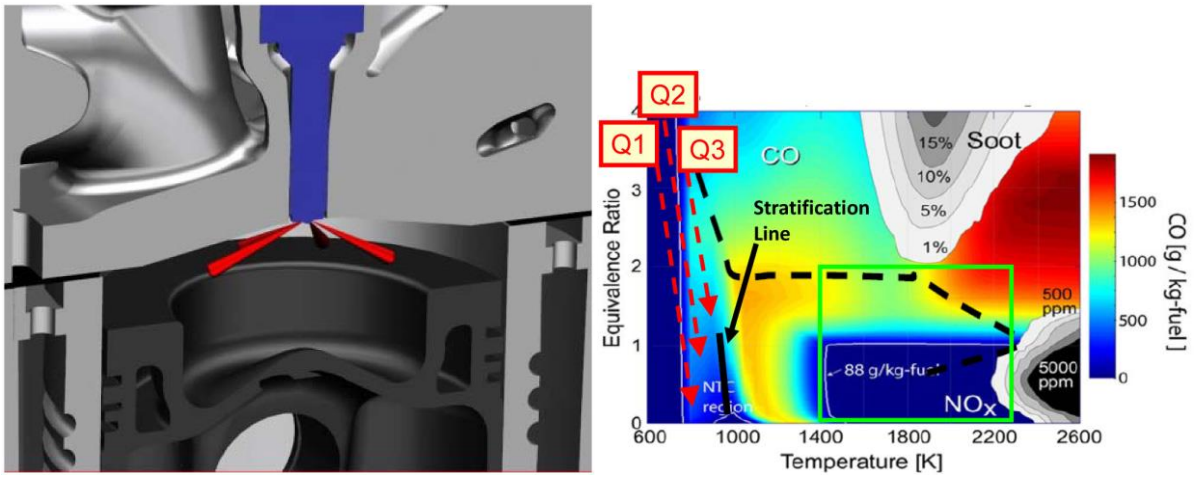

(a) (b)

Figure 2-2 (a) GDCI combustion chamber concept and (b) GDCI Injection Strategy depicted on Phi-T Diagram with NO_x, Soot, and CO Contours [32,33].

For more explanations, the principle of GCI operating concept is shown in Figure 2-3. The figure shows the combustion concepts of SI, CI and GCI engine in order to compare their combustion processes. The figure on the right-hand side shows the SI concept using the port fuel injection (PFI) to supply the homogenous fuel-air mixture into the cylinder. Then, the spark plug ignites the fuel-air mixture around the center of the combustion chamber. The flame prorogates from the center of the chamber to the cylinder wall. The middle figure exhibits the CI concept that only air is compressed during the compression stroke to obtain sufficiently high temperature before the fuel is injected for auto-ignition. The combustion starts at the periphery of the fuel spray and then the flame engulfs throughout the combustion chamber. For the last figure, the GCI operating concept is presented. The operation is analogous to the diesel but requires earlier injection timing when temperatures and pressures are lower than during typical diesel fuel injection. Due to the low CN fuel, the ignition timing is delayed, thus leading more available time for fuel-air mixing process. As the results, the combustion temperature is lower, hint low NOx and there is less rich zone to form the soot when the combustion happens.

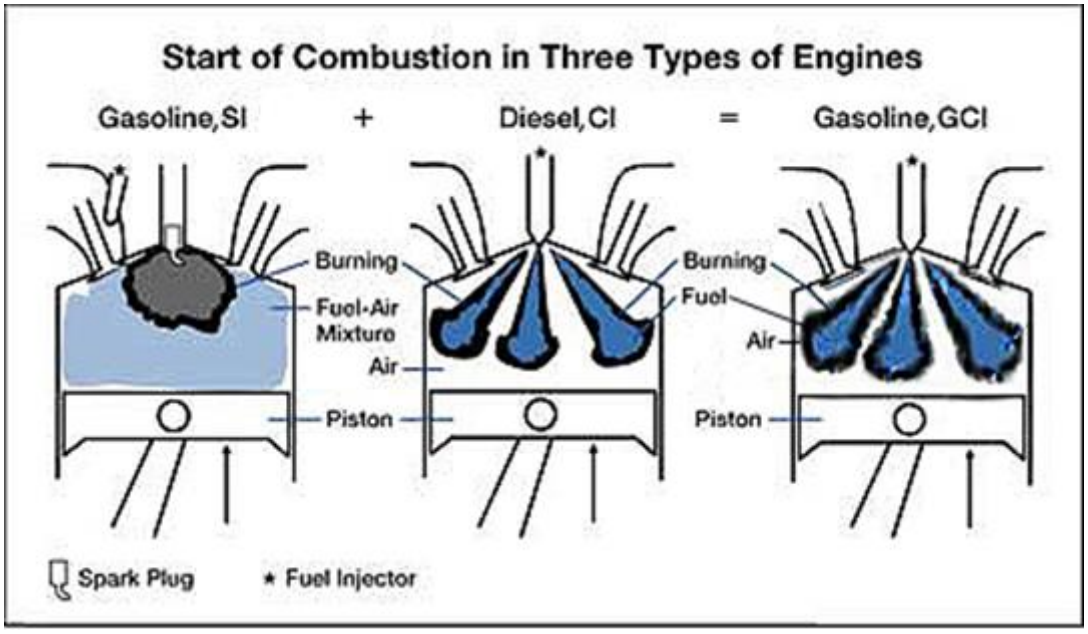

Figure 2-3 The operating concepts of SI, CI and GCI engine. (Applied from: http://thefraserdomain.typepad.com/energy/engines_turbines)

Therefore, it might be concluded the advantages and disadvantage of using the GCI concept as following;

- The advantages of GCI concept.
  - High thermal efficiency like diesel engines.
  - Possibility to use the low cetane number fuels.
  - Low emissions (NOx and PM).
  - Low combustion temperature.
- The disadvantages of GCI concept.
  - Need high injection pressure by using a common rail system.
  - Need a high compression ratio.
  - Need high air intake temperature for achieving autoignition.
  - Gasoline is very low lubricity.

2.4 Macro/micro spray structure

Gasoline

Since GCI complies the direct injection strategy to introduce the fuel into the chamber, the combustion and emissions are strongly depended on the spray characteristics. Not only does the nozzle geometry affect the spray behaviors, but the fuel properties also alter the

spray shape. When injected with different fuels, therefore, the spray behaviors which based on the fuel properties should be carefully investigated.

Previous researches have shown that there is no difference between the vapor penetration tip of gasoline and diesel. But for the liquid phase, the spray tip of gasoline is shorter and the cone angle is wider than that of diesel [36]. With the low resistant of gasoline because of its lower viscosity [14], the injector needle is opened earlier and closed faster when compared with diesel injection. In addition, the injection rate of gasoline is lower than that of diesel when the injector is fully opened [37].

Biodiesel

Szybist and Boehman found that biodiesel can advance the injection timing and shorten the injection duration when compared with diesel [38]. Densantes et al [39] showed that biodiesel had the longer penetration length and the narrower spray angle than those of diesel. However, none of the significant difference of spray patterns between diesel and biodiesel was found by Allocca et al [40]. The nozzle geometry strongly affected spray behaviors. The more compact spray of biodiesel (higher length and smaller angle) was observed with the cylindrical type nozzle while the diesel spray had the longer tip with similar angles when using the conical injector [41].

As reported above, most researches have investigated the spray characteristics of neat gasoline and biodiesel injected by the high-pressure common rail system, but less available data for the spray of gasoline blended with biodiesel. In particular, the study of the internal spray structure and the flow field of gasoline spray injected as the CI engine condition has not found in the literature. The spray structure and its flow field strongly relate to the fuel-air mixing process which significantly influents the combustion process.

Spray density and air entrainment

The light extinction method is one of the methods used to define the spray density [42]. Manaka et al. evaluated the air access ratio in the diesel spray [43] by this approach. The diesel spray was injected into an in-cylinder of the ultra-high boost engine. When the ambient density is high, the spray density rapidly spreads out from the middle to the end of spray formation. On the other hand, at the low ambient density, the free spray expands straightforward. Zama et al. employed the shadow and tomographic image method to analyze the diesel spray behavior in the ultra-high ambient pressure [44]. The results showed that the

density of surrounding gas affects the inner structure of the diesel spray. The spray structure is altered, which depended on its surrounding pressures.

The general concept of the air entrainment process , which based on the conservation of mass, is exhibited in Figure 2-4 [45]. In the beginning, the momentum of liquid fuel and surrounding air exhibit in the initial velocity stage. After injection commences, the air entrainment process prepared. Permeable air mass is accumulated with the spray mass, thus increasing the spray mass. Then, the velocity of the spray is gradually resisted by the ambient pressure. The average momentum velocity of fuel spray can be calculated by the conservation of momentum as the following equation.

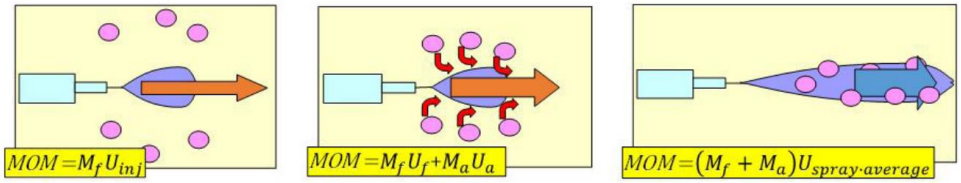

Figure 2-4 Air entrapment process and momentum conservation.

$$M_f U_{inj} = (M_f + M_a) U_{spray.average} \tag{2.1}$$

where M_f is fuel mass, U_{inj} is the velocity at the start of injection, M_a is air mass and $U_{spray.average}$ is average of spray velocity.

Internal flow characteristic

Macian et al studied the influence of the cylindrical and conical diesel nozzle geometry on the inception of cavitation [46]. They found that the upper and lower rounding radius at the inlet of the orifice, area reduction of the nozzle and diameter at the outlet of the orifice play the major role in the onset of cavitation. Moreover, the injection pressure and black pressure have the strong effect on the occurrence of the cavitation [47]. When the injection pressure increases, Reynold number is increased. This leads to the high turbulence level of the flow. Thus, the higher injection pressure is, the smaller critical cavitation number becomes (higher cavitation). The cavitation number was introduced by Nurick (Nurick's theory of cavitation flow) [48] as shown in Figure 2-5 and can be calculated by equation 2.2.

$$\mathrm{KN} = \frac{P_i - P_b}{P_i - P_{vap}} \tag{2.2}$$

where P_i is injection pressure, P_b is back pressure, P_{vap} is the vapor pressure of the fuel.

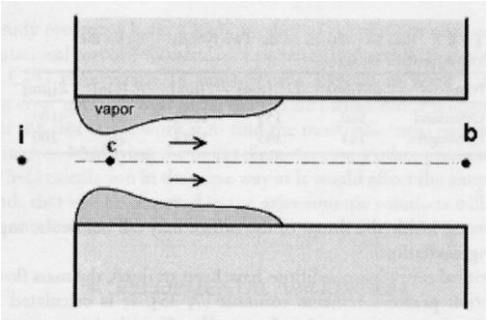

Figure 2-5 Simplified diagram of cavitation flow.

The high cavitation can induce the choked flow and affects the spray behaviors. The effect of injection pressure and back pressure on spray break up could be characterized by using the cavitation number. However, the influence of cavitation on spray phenomena is still not clear.

Flow field characteristic

To investigate the spray phenomena such as velocity and vorticity distribution, the time-resolved particle image velocimetry (PIV) is utilized [49]. PIV introduced by Adrian [50] is an advanced measuring method and generally used to analyze the two or three dimensional flow fields. With this method, the tiny particles mixed in the fluid and at least, two correlation images with very short time interval are required. The interrogation area between the two correlation images is correlated to specify the displacement vectors. Then, the displacement vectors corresponding to the spatial time in the area of interest are converted into a map of velocity vectors. For the planar measurement of spray induced gas motion, LIF-PIV (laser induced fluorescence-particle image velocimetry) technique has been validated to be one of the most potential measuring methods [51–53]. However, for measuring the internal flow of the spray, it has still challenged for the researcher to investigate spray droplets' velocity and internal gas flow velocity with the high resolution of the liquid dense core of non-evaporating fuel spray.

Sepret et al. applied the particle image velocimetry and fluorescent tracer technique to measure the flow field of the surrounding gas around the spray with the air mixing rate [54]. The surrounding of the spray could be classified into three zones and two identifications which are gas aspiration zone and gas pushed out zone as shown in Figure 2-6.

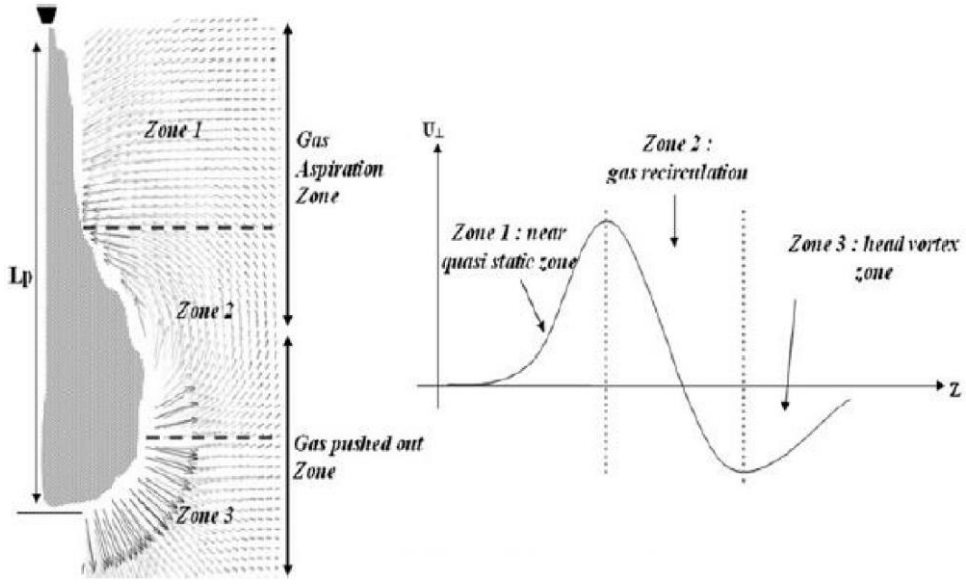

Figure 2-6 Average gas velocity field and evaluation of normal component.

Rhim et al. investigated the boundary of the surrounding gas of the spray structure [55]. The surrounding gas could be divided into three parts which are gas entrainment through side periphery, air pushed-out by head-vortex and gas entrainment by spray-capturing at the spray tip region as shown in Figure 2-7. The results showed the significant differences between the total spray volume and the accumulated gas volume entrained under the non-evaporating transient spray conditions. They demonstrated that the important segments of the gas entrainment into the spray structure is developed near the liquid spray tip.

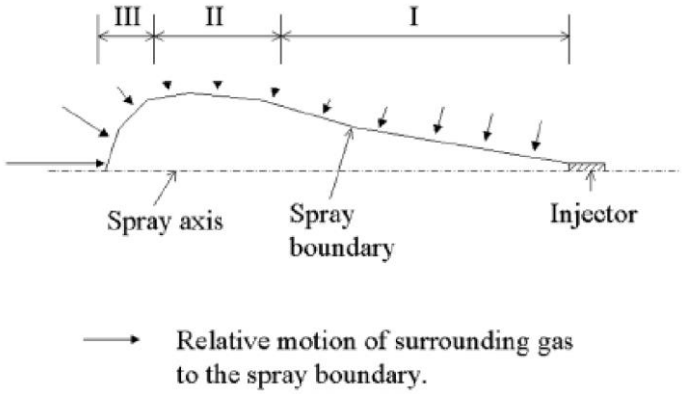

Figure 2-7 Gas entrainments corresponding to the spray boundary for non-evaporating transient spray.

3. PRINCIPLE OF OPTICAL METHOD, IMAGE PROCESSING AND ENGINE PERFORMANCE

This chapter shows the principle of image processing and the internal combustion engine as background knowledge. Firstly, the basis of optical measurement techniques is illustrated how to capture the images of spray phenomena at which fluid medium is transparent to pass the light. Then, the post image processing via MatLab is shown how to calculate the spray characteristics such as the spray length and cone angle. Finally, the principle of the internal combustion engine is explained to analysis the engine performance and combustion characteristics.

3.1 Optical methods

3.1.1 Shadowgraph and Schlieren technique

Settles [56] introduced the details of Mie scattering, Schlieren and Shadowgraph technique in 2001. These optical techniques have been widely used to capture the fuel spray for investigating and analyzing the macroscopic and microscopic spray structure in transparent media. The techniques provide both the qualitative information such as the liquid/vapor phase development and distribution as well as the quantitative data, for instance, the spray length and cone angle. The basic layout of Shadowgraph and Schlieren technique are shown in Figure 3-1 and 3-2 [57], respectively.

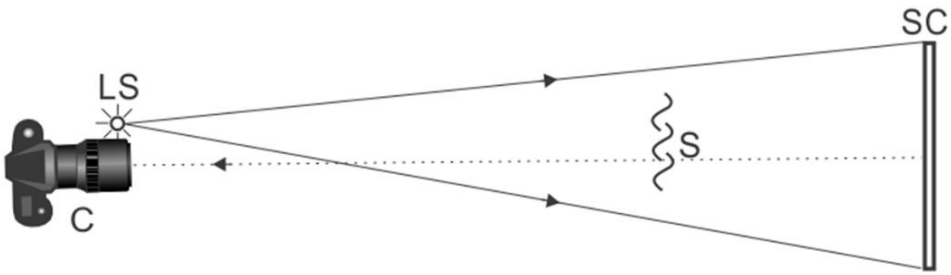

Figure 3-1 Direct shadowgraph technique [57].

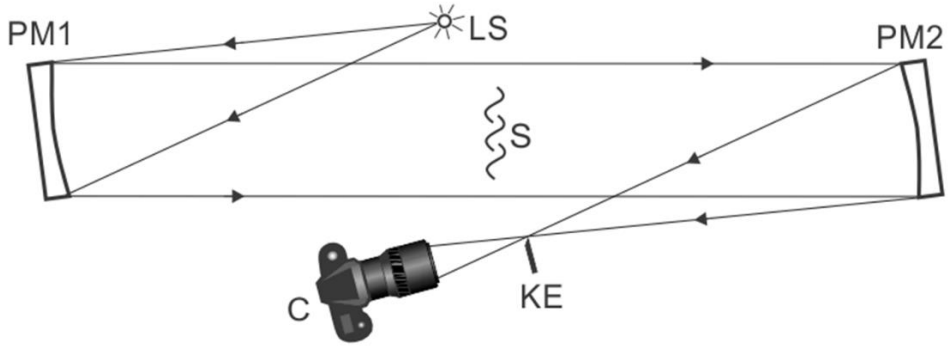

Figure 3-2 Z-type Schlieren technique with two parabolic mirrors [57].

The simple arrangement of the direct shadowgraph setup has only a light source (LS) with small diameter (≤ 1mm.), a camera and a projection screen (SC). A transparent schlieren object (S) such as the spray is placed midway between the small bright light source and the reflective screen, to cast its telling shadow named a shadowgraph on the screen. On the other hand, Z-type Schlieren technique requires two parabolic mirrors (PM) to reflect the light and the knife-edge (KE) for blocking the part of the light. The light ray is refracted by the parabolic mirrors like a Z-shape through the knife-edge and then captured by the camera.

According to the Gladstone–Dale law, the relation of the refractive index (n) and the density (ρ) of the fluid between can be calculated as the following equation:

$$n - 1 = \rho k \tag{3.1}$$

where k is a constant for a given fluid.

3.1.2 PLIF-PIV technique

Particle Image Velocimetry (PIV) is another non-intrusive method for flow visualization. This technique is used to trace the element flow in a short time interval. To determine the displacement vector, Cross-correlation of the two PIV images shot controlling by the exposure method is applied. The former PIV image records the particles at the initial position and the latter PIV image capture the particles at the point of the element trace.

Planar Laser Induced Fluorescence - Particle Image Velocimetry (PLIF-PIV) is also widely used as a non-intrusive optical diagnostic tool [58]. Laser Induced Fluorescence (LIF) is frequently used to solve the high-speed flow and spatial resolution problems. The principle

of this technique is simple. The laser light, fluorescence, emits the specific wavelength to identified atom or molecule in the interesting area for absorption.

To analyze the flow field in two dimensions, the laser beam is adjusted as a thin sheet by using the set of cylindrical lenses. As following the above methodology, this technique is named the planar laser-induced fluorescence (PLIF) which suitably used to investigate the gaseous fuel concentration and combustion temperature.

3.2 Post image processing

3.2.1 Spray penetration and spray cone angle

Based on the commercial MatLab software, the image processing technique [59,60].and PIVlab tool (a time-resolved particle image velocimetry) [61] were utilized to analyze the spray characteristics, and the vector and vorticity distribution. In order to define the spray penetrating length and cone angle as shown in Figure 3-3, the spray penetration length (L) is the distance from the injector tip to the end of the fuel spray which can be calculated by using equation 3.2 The spray angle (θ) is the angle which created by the two lines covering the spray from the injector tip to the middle length of the fuel spray (L/2) as calculated in equation 3.3 [62].

$$L = (A_{injector\ tip} - A_{spray\ end}) \times P_{size} \tag{3.2}$$

where L is denoted the spray penetration length, $A_{injector\ tip}$ is the address of the pixel at the end of injector tip, $A_{spray\ end}$ is the address of the pixel at the end of the spray, and P_{size} is the resolution of the pixel (mm/pixel).

$$\theta = 180 - cos^{-1}\left(\frac{V_1 \cdot V_2}{L_1 L_2}\right) \times \frac{180}{\pi} \tag{3.3}$$

where θ is denoted the spray cone angle, V_1 and V_2 is the vector along the boundary of the spray image, and L_1 and L_2 is the vector length of V_1 and V_2.

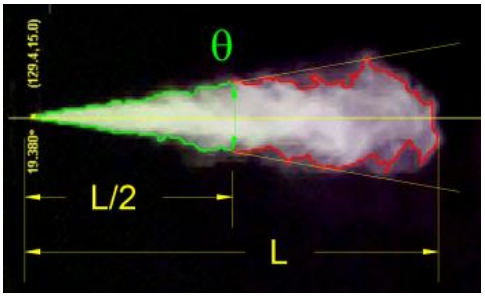

Figure 3-3 Defining of the spray penetration length at L, and the spray cone angle (θ) at L/2.

3.2.2 Particle velocity of the two images

To measure the flow velocity, the discrete cross-correlation function determining the particle displacement is illustrated in equation 3.4 [63]. Two PLIF-PIV images exploded in the very short time interval were analyzed with the FFT window deformation algorithm (direct Fourier transform correlation with multiple passes and deforming windows) as shown in Figure 3-4. The initial pass which was the relatively large interrogation area (size 32x32 pixels) was used to calculate the particle displacement of the data-target range. The second, third and fourth interrogations area were reduced by 50%, respectively. Then, the velocity of a vector could be calculated as shown in equation 3.5 [64].

$$C(m,n) = \sum_i \sum_j A_1(i,j) A_2(i-m, j-n) \tag{3.4}$$

where A_1 and A_2 are representative interrogation areas between the pair images.

$$v = \frac{\sqrt{dx^2 - dy^2}}{dt} \tag{3.5}$$

where *dx* and *dy* is the displacement calculating from the coordinate of the location of the cross-correlation parameter.

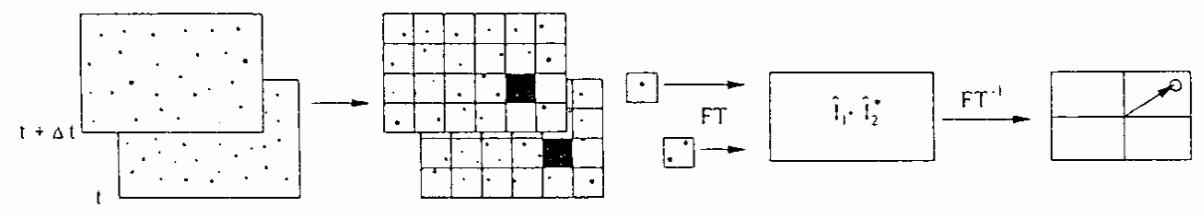

Figure 3-4 Cross-correlation method with multiple passes.

3.3 Engine performance

3.3.1 CI engine

The combustion process in the CI engine totally differs from the SI engine. CI engine is an engine in which only air is drawn into the combustion chamber during the intake stroke and compressed during the compression stroke before the fuel is injected directly into the chamber . Then, the fuel-air mixture is ignited at the elevated temperature and pressure. Because the fuel is introduced into the chamber shortly before the top dead center, there is less available time for evaporation and mixing. The fuel is dispersed and mixed with the air non-uniformly throughout the chamber; so called a heterogenous air-fuel mixture. The mixing process in which the oxygen in the air diffuses into the fuel spray occurred during the combustion process and induced the subsequent combustion. This means that the CI engine is operated in a diffusion flame mode. Moreover, the torque of the CI engine is controlled by manipulating the fuel quantity and the air/fuel ratio. Therefore, the CI engine relies on altering the amount of injected fuel and excess air.

3.3.2 Compression ratio

The compression ratio is the ratio between the maximum volume and the minimum volume of the cylinder as shown in Figure 3-5 and calculated as in equation 3.6.

Compression ratio (r_c):

$$r_c = \frac{maximum\ cylinder\ volum}{minimum\ cylinder\ volume} = \frac{V_d + V_c}{V_c} \tag{3.6}$$

where V_d is the displacement or swept volume and V_c is the clearance volume.

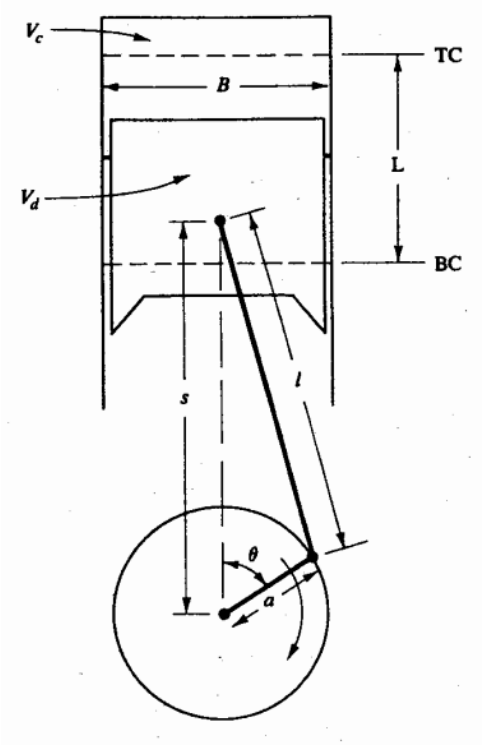

Figure 3-5 The Geometry of cylinder, piston connecting rod and crankshaft. [65]

3.3.3 Break torque and power

The engine is attached by a shaft to rotate a dynamometer usually measuring the engine torque. The principle of the dynamometer operation is shown in Figure 3-6. Beak Torque and power can be calculated as following.

Torque (T):

$$\mathrm{T} = \mathrm{Fb} \tag{3.7}$$

Power (P):

$$\mathrm{P(kW)} = 2\pi \mathrm{N(rev/min)T}(N \cdot m) \times 10^3 \tag{3.8}$$

where N is the engine speed

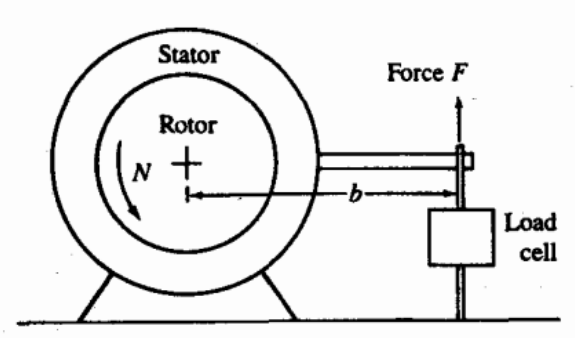

Figure 3-6 The principle of operation of a dynamometer. [65]

3.3.4 Indicated work per cycle

The in-cylinder pressure during engine operation can be used to calculate the work produced by the engine. Pressure versus cylinder volume can be plotted on a P-V diagram. The area under this plot is called the indicated work and calculated by the following equation:

Indicated work (Wi):

$$W_i = \oint PdV \tag{3.9}$$

Indicated work can be defined as;

- Gross indicated work per cycle (Wc,ig): Work calculated during the compression and expansion strokes.
- Net indicated work per cycle (Wc,in): Work calculated for the entire four-stroke cycle.

3.3.5 Mean effective pressure (MEP)

Mean effective pressure (MEP) is calculated by the work per cycles divided by the displacement volume as shown in the following equation;

$$MEP(kPa) = \frac{p(kW)n_r \times 10^3}{V_d(dm^3)n(rev/s)} \tag{3.10}$$

where P is work per cycle and Vd is the engine displacement volume.

Moreover, the mean effective pressure can be defined by using different work terms. Therefore, indicated work is used to calculate the indicated mean effective pressure (IMEP). On the other hand, brake mean effective pressure (BMEP) use brake work measured by the engine dynamometer to calculate.

3.3.6 Heat release rate

To analyze the heat release in the CI engine by the pressure inside the cylinder at a specific crank angle, the first law of thermodynamics and the ideal gas law at the steady state condition with the chemical energy are applied. The rate of heat release can be calculated by using the following equation;

$$\frac{dQ_n}{d\theta} = \frac{\gamma}{\gamma-1} p \frac{dV}{d\theta} + \frac{1}{\gamma-1} V \frac{dp}{d\theta} \tag{3.11}$$

where γ is the ratio of specific heat (C_p/C_v), p is the pressure inside the cylinder, and V is the instantaneous volume of the combustion chamber. The appropriate value of γ for a CI engine is approximately 1.3 to 1.35.

3.3.7 Mass fraction burned

In the combustion process, the air-fuel mixture is the most effect on the heat rerelease rate. The combustion starts burning process from a small amount of the charge mixture and then rapidly increases until the middle of the burning process. After that, the combustion gradually decreases to near zero at the end of combustion. Therefore, the heat release rate can be used to define the ignition delay and combustion duration by accumulating the heat releases. The mass fraction burned can be explained the combustion process as following;

The combustion process starts when the small amount of fuel is burned with the mass fraction of 10 percent or CA10 generally. The end of combustion is usually defined by the mass fraction of 90 percent or CA90 and CA50 means the mass fraction of 50 percent burned. Therefore, ignition delay can be considered from SOI to CA10 and combustion duration can be recognized by the time from CA10 to CA90.

3.3.8 Cylinder temperature

Combustion temperature can be calculated by using ideal gas law in which the temperature is derived from the in-cylinder pressure measured by the piezoelectric sensor as in the following equation.

$$T = \frac{p.V}{n.R} \tag{3.12}$$

where p is the in-cylinder pressure measured by the sensor, V is the cylinder volume, n is the moles of substance and R is the gas constant.

3.3.9 Coefficient of variation of IMEP (COV_{imep})

To analyze the cycle to cycle variation of combustion from one hundred cycles for each test, the coefficient of variation of indicated mean effective pressure is utilized as the following equation.

$$\boldsymbol{COV_{imep}} = \frac{\mathbf{1}}{\boldsymbol{IMEP_{mean}}} \sqrt{\frac{\sum_{i=1}^{N}(\boldsymbol{IMEP_i - IMEP_{mean}})^2}{\boldsymbol{N-1}}} \times 100 \tag{3.13}$$

With this equation, the cyclic variability in indicated work per cycle is represented. Therefore, if the COV_{imep} is over than 10 percent, it indicates that there are some vehicle driveability problems

4. EXPERIMENTAL SETUP AND PROCEDURES

The test fuels, including commercial gasoline and diesel (sold in Korea) and neat biodiesel from an industry source, were utilized throughout this study to investigate the physical/chemical properties, phase stability, spray characteristics, and combustion characteristics. Gasoline-biodiesel blends were mixed by increasing the percentage of biodiesel. Therefore, the test fuels were called D100 for pure diesel and B100 for pure biodiesel; meanwhile, gasoline-biodiesel blends were named GBs where G stands for gasoline, B stands for biodiesel, and the numeric number is specified to the mixing percent by volume of biodiesel mixed with gasoline. For example, GB05 means the gasoline blended with 5% biodiesel by volume.

4.1 Phase stability and fuel property

4.1.1 Phase stability

To investigate two major drawbacks of gasoline-biodiesel blends, which having low miscibility and high instability at low temperature [66], the ternary blends consisted of gasoline, diesel and biodiesel (G-D-B) were experimented. The blended ratios were varied from 0 to 100% by increasing 10% volume of each fuel. For this study, the ternary blends were measured and prepared by using a 2 and 3 ml measuring pipette with accuracy of 0.01 ml. Each ternary blend was mixed and contained in a 16 ml glass test tube which sealed with a screw cap. The test condition is shown in Table 4-1.

Table 4-1 Test conditions of phase stability.

Test fuel	Gasoline, diesel and biodiesel (0-100%)
Ambient temperature 25°C	30 days
Ambient temperature 20°C	1 hour
Ambient temperature 15°C	1 hour
Ambient temperature 10°C	1 hour
Ambient temperature 5°C	1 hour
Ambient temperature 0°C	1 hour

The total samples of 132 were separated into 2 groups equally (66 blended ratios). The first group of 66 samples was examined at 25 °C of ambient temperature within 30 days. In the first day after the mixing process, the 66 samples were observed at every hour for 10 hours and then at every day for 30 days. The latter one was refrigerated by using incubator

with the accuracy of 0.1 °C. The temperatures were controlled at 20, 15, 10, 5 and 0 °C respectively. The samples were monitored for 1 hour at each controlled temperature.

4.1.2 Fuel property test

The physical/chemical properties of the gasoline, diesel, biodiesel and GBs according to the Korean fuel standard were measured by K-Petro. For this test, the gasoline-biodiesel blends were varied between 0 to 20% with 5 % increment of biodiesel (GB00-GB20). The important properties of test fuels consisting of distillation, cetane number, viscosity, lubricity, cloud point, pour point, density and heat of combustion were evaluated to clarify the effect of biodiesel on spray phenomena and combustion characteristics in Chapter 5.

Because neat gasoline has relatively low lubricity, it is not suitable to use it in a high-pressure injection system. Therefore, some additive should be considered to add in the gasoline for avoiding the wear problems in the common rail diesel system. For this point of view, biodiesel could be used as lubricity enhancer because it comprises of the neat fatty compound. A few percentages of biodiesel (1-5%) can extraordinarily improve the lubricity property of mixing fuel without a commercial lubricity additive [4,67,68]. Using the small amount of biodiesel less than 1% can increase the lubricity up to 30% [69]. The physical/chemical properties of the test fuels assessed in this research and the test standard method following the Korean standard requirement are shown in Table 4-2.

Table 4-2 Physical/chemical properties of the test fuels.

Test Item	Unit	Test Method
Distillation		ASTM D86:2012
Initial Boiling Point	°C	
10% Evaporated	°C	
50% Evaporated	°C	
90% Evaporated	°C	
End Point	°C	
Cetene Index	-	KS M ISO 4261:2003
Kinematic Viscosity (40°C)	mm^2/s	KS M ISO 3104:2008
Lubricity	μm	KS R ISO 12156-1:2012
Cloud Point	°C	KS M ISO 3015:2008
Pour Point	°C	ASTM D6749:2002
Density (15°C)	kg/m^3	KS M ISO 12185:2003
Heat of combustion of liquid hydrocarbon fuels	MJ/kg	ASTM D240:2009

4.2 Spray visualization

Three different photography techniques were employed to investigate the gasoline spray characteristics. The spray images were captured by using Shadowgraph and Schlieren photography as well as PLIF-PIV technique. Gasoline-biodiesel blend sprays were formed in the constant volume combustion chamber (CVCC) with varieties of injection pressures and ambient pressures. The injection pressure (IP) was controlled through a common rail diesel system. The spray images were recorded by a high-speed camera. Then, the image processing technique via Matlab was employed to analyze the spray features such as length, cone angle, etc.

4.2.1 Shadowgraph, Schlieren, and PLIF-PIV setup

The CVCC, approximately 1,295 ml, was used to simulate the combustion chamber condition for the gasoline-biodiesel spray test. It consists of six changeable ports such as quartz windows, injector holder, and gas inlet/outlet. The injector was mounted on the top port while N_2 gas flowed into the chamber through the bottom port. The flow rate of N_2 was metered in order to control the chamber pressure (ambient density). A Sensys pressure transducer was used to monitor the in-chamber pressure. The spray features were accessed through two 110 mm quartz windows, fitted on the side ports. The other side ports were used for the light or laser source and one of the side port was used for the high-speed camera. The common rail injection system comprises a common rail, oil filter, fuel tank, and a low and high-pressure pump. This common rail system can provide the maximum pressure at 1350 bar. The injection pressures were handled by the common rail PCV Driver (ZB-1100) and the multi-stage engine controller was employed to control injection duration and timings. A single-hole injector utilized to develop the spray shape was Bosch & Hyundai common rail diesel injector model 33800_27400 with orifice diameter 0.30 mm and 0.25 mm. (shown in Figure 4-1). A common rail solenoid injector peak & hold driver (ZB-5100) and multi-stage injection engine controller (ZB-8035) were employed to drive the single-hole injector and control injection timings. Moreover, the engine controller was utilized to generate a trigger signal sent to a high-speed camera for recording images and the peak & hold driver for injecting the fuels simultaneously.

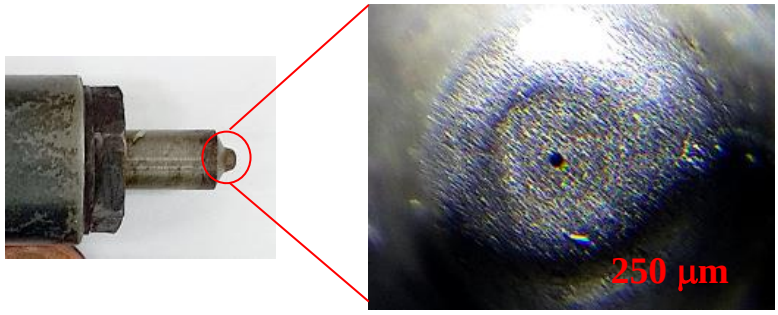

Figure 4-1 The orifice of the single-hole injector with a diameter of 250 µm.

The schematic diagram of the shadowgraph photography technique is exhibited in Figure 4-2. The spray characteristics were analyzed by using imaging behind a diffuse screen [62]. The knife-edge technique was used to enhance the shadow of spray image, formed from the light source through a corrector lens. A high-speed camera, Photron model FASTCAM SA3, CMOS image sensor with 17 µm pixel size, equipped with Nikkor lens 50 mm. f1.8 was used to record the spray image with the spatial resolution of 256x256 pixels. After recording at a speed of 10,000 frames/second, a thousand spray images were transferred and saved on a personal computer via Photron FASTCAM Viewer (PFV) software.

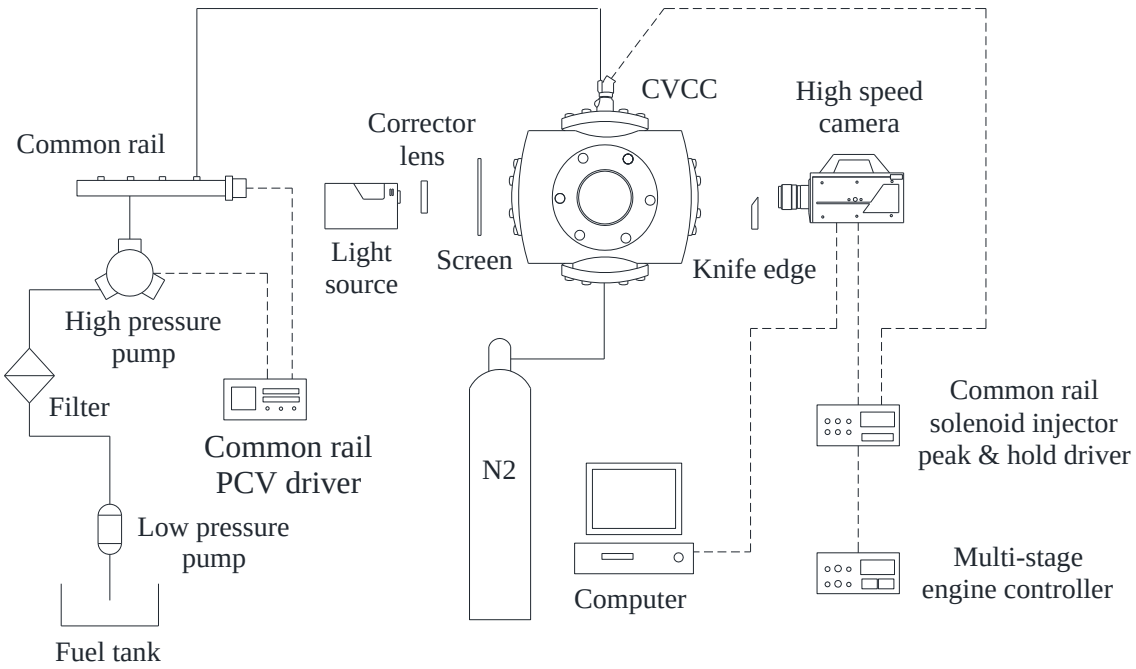

Figure 4-2 The schematic diagram of the spray image recording system using the shadowgraph technique.

The setup of Schlieren photography technique is presented in Figure 4-3. Two concave mirrors Model SM300 were used for deflecting LED light form LED light source to the high-speed camera. The high-speed camera Photron model FASTCAM SA3 was used to record the spray pattern formed from the LED light source. The Schlieren images having resolution 256x512 pixels were recorded at a speed of 10,000 frames/second and speed shutter 1/200,000 second. Thus, the time interval for recording the two images was 100 μs. Consequently, a thousand spray images were transferred and also saved in the personal computer via PFV software.

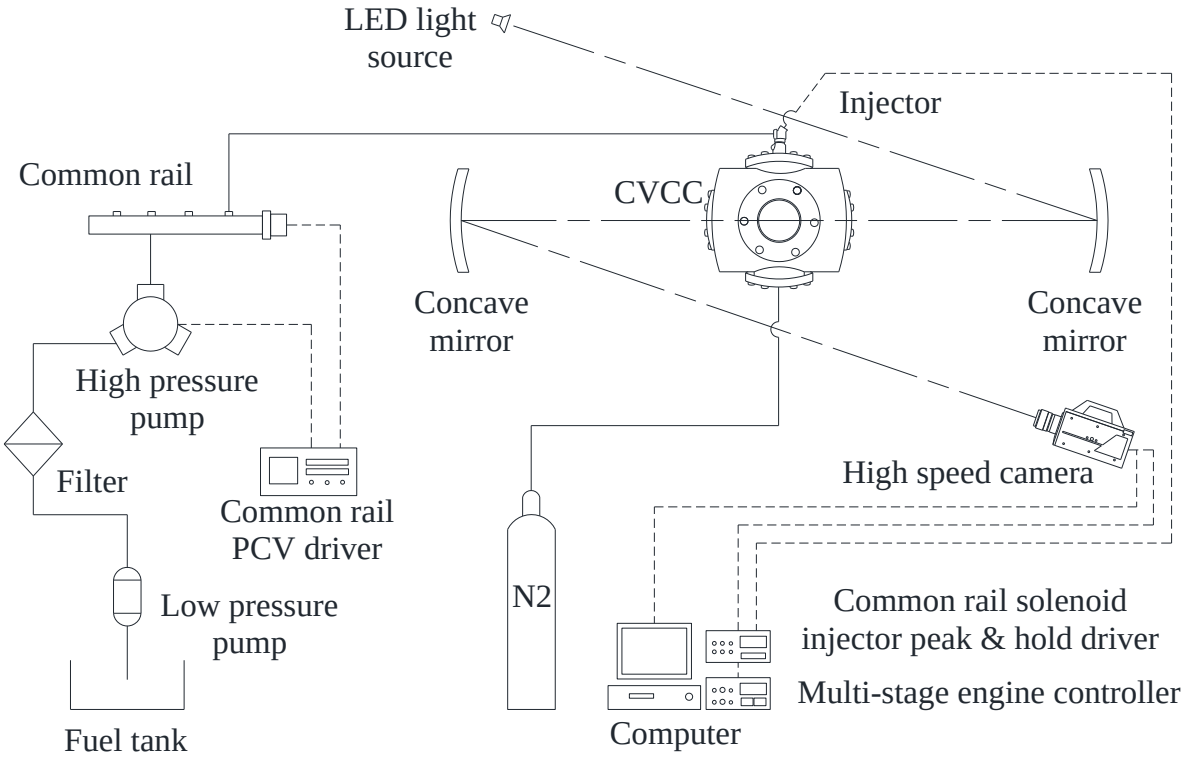

Figure 4-3 The schematic diagram for the spray image recording system using Schlieren photography techniques.

Figure 4-4 illustrates the tracer-based PLIF-PIV technique setup. A diode-pumped solid-state (DPSS) laser which continuously emits light illumination and a cylindrical lens (fl=-25) were used to create a laser sheet. The wavelength of DPSS laser is 532±1 nm and the laser sheet thickness is approximately 2 mm. The high-speed/resolution camera Photron model FASTCAM SA1.1 was employed. The PLIF-PIV images were shot at 8,000 frames/second and speed shutter 1/104,000 second with the resolution of 750x1024 pixels. The time interval

between the two images was 125 μs. All PLIF-PIV images were also managed by PFV software. The examples of images recorded by Schlieren photography and PLIF-PIV techniques are shown in Figure 4-5.

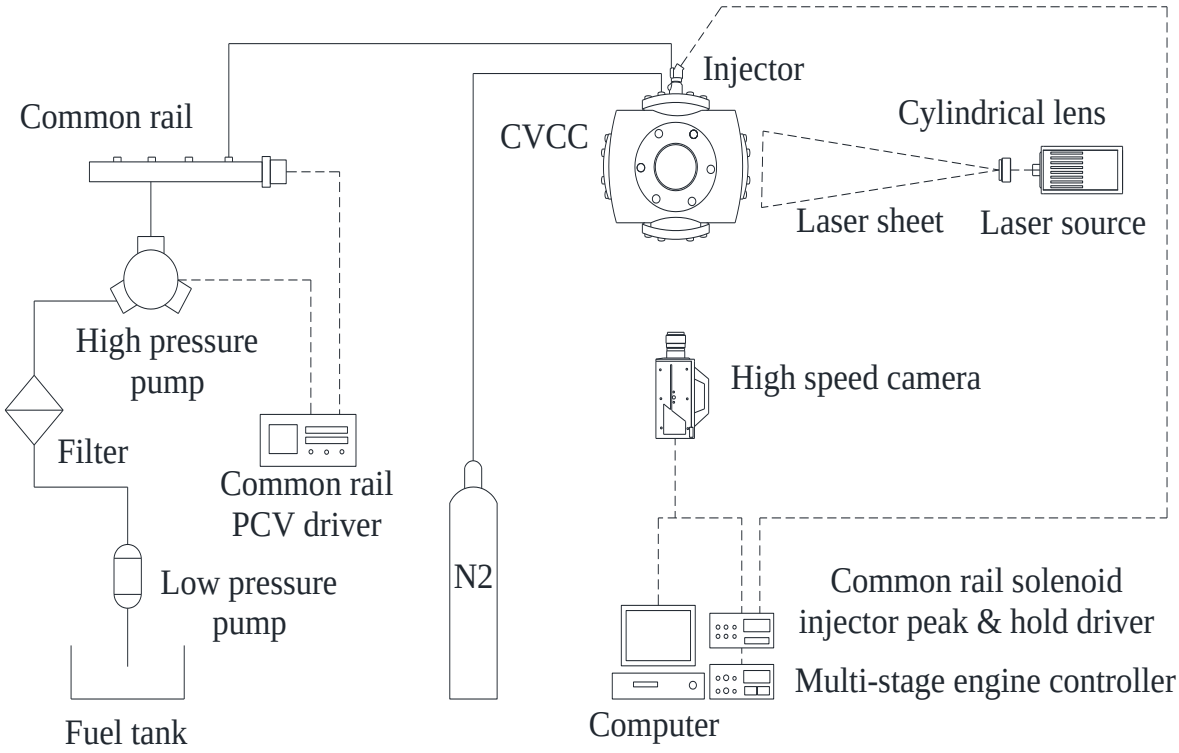

Figure 4-4 The schematic diagram for the spray image recording system using PLIF-PIV technique.

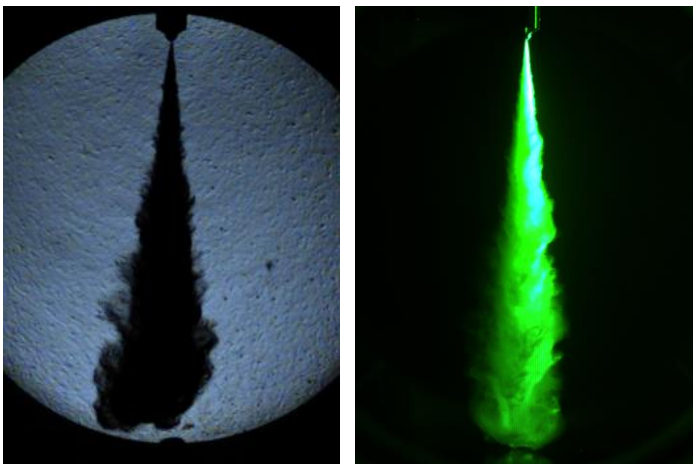

(a) (b)

Figure 4-5 (a) An image of Schlieren photography techniques and (b) an image of PLIF-PIV techniques.

4.2.2 Experimental procedure and conditions

The influence of biodiesel blended gasoline-based fuels on macroscopic spray structure when injected from a diesel injection conditions

The spray characteristics of five GBs were evaluated. The factors and test conditions, investigated in this study, are listed in Table 4-3. Besides the type of fuels, the injection and chamber pressure, also known as the back pressure, were varied to verify their effect on the fuel spray. Firstly, the high-speed camera was triggered at the same time as the injector started. Then, the injector was activated continuously at the engine-simulated speed of 2,000 rpm while the camera continuously recorded the fuel spray at 10,000 frames/second. Depending on the onboard memory of the high-speed camera, only the first ten cycles of the injection event were recorded. Finally, a post-processing method was performed for each cycle. The results are the average value from ten cycles. The mean value of standard deviations was less than 1 mm for spray-penetration length and 1.6° for the cone angle.

Table 4-3 Test conditions.

Simulated Engine Speed	2,000 rpm
Injection Pressure	1,000 bar, 1,200 bar and 1,350 bar
Injection Duration	800 μs
Chamber Pressure	30 bar and 50 bar
Fuels	GB00, GB05, GB10, GB15, GB20 and B100

The effects of gasoline-biodiesel blended fuels on spray characteristics with multiple injections

The blended fuels, GB00-GB20 and B100, were injected into the CVCC with the simulated speed of 1,500 and 2,000 rpm. Each of simulated speed has three injection timings including a pilot injection (T1), pre-injection (T2) and main injection (T3) which detailed in Table 4-4. The injection pressures were controlled at 800, 1,000 and 1,350 bar. When the test fuel was injected into the CVCC, the common rail peak and hold driver triggered the high-speed camera to record the image. The back pressure was set constantly at 20 bar. Each test condition was repeated five times.

Table 4-4 Test conditions with the simulated speed.

1,500 rpm		2,500 rpm	
Timing	Duration (ms)	Timing	Duration (ms)
Pilot: 10CAD BTDC (T1)	300	Pilot: 31CAD BTDC (T1)	260
Pre : 3CAD BTDC (T2)	300	Pre : 3CAD BTDC (T2)	330
Main: 6CAD ATDC (T3)	700	Main: 7CAD ATDC (T3)	840

Macroscopic/microscopic structure of gasoline spray added biodiesel 5% injected with a single-hole common rail diesel injector by varying injection pressure

In the current study, the spray characteristics including spray penetration length, cone angle, spray area, average velocity and instantaneous velocity were investigated. To observe their behaviors by using Schlieren photography techniques, GB05 and D100 were injected into the CVCC with the simulated speed of 2,000 rpm. The injection duration for all test conditions was kept constantly at 1,000 μs. The injection pressures were controlled at 500, 750, and 1,000 bar. When the test fuel was injected into the CVCC, the high-speed camera was triggered by the signal from the engine controller to record the images at the same time. The back pressure (BP) was set at 10 and 50 bar. Each test condition was repeated three times. In order to evaluate the spray distribution and vorticity with PLIF-PIV technique, only GB05 was performed by adding 1% of silicone oil (KF-96) as a particle tracer seed. The test conditions for each fuel are shown in Table 4-5.

Table 4-5 The summary of fuel injection condition.

Description	Schlieren	PLIF-PIV
Test fuel	GB05 and D100	GB05
Particle tracer seed (KF-96)	-	1%
Injector type	Single hole injector, Dia. 300 μm	
Fuel injection system	Diesel common-rail system	
Simulate speed	2000 rpm	
Injection duration	1,000 μs	
Injection pressure	500, 750 and 100 bar	
Ambient pressure (N_2) in CVCC	10 and 50 bar	

4.3 Experimental setup of engine test

The combustion characteristics were performed by using the single-cylinder diesel-based engine applying the diesel common rail injection system with gasoline-biodiesel blended fuels. The in-cylinder pressures were recorded by a data acquisition system. The exhaust emissions were analyzed by a gas analyzer.

4.3.1 Engine specifications, fuel injection system and measurement system

Figure 4-6 shows a schematic diagram of the engine test bed system. A single cylinder four-stroke engine modified from the commercial four-cylinder Hyundai engine was used throughout the experiment. The 4 valve engine has 498 cm^3 of displacement and a single overhead cam (SOHC). The detailed engine specification is given in Table 4.6. To introduce the fuel into the cylinder, a common rail injection system used for fuel flow rate measurement was installed in the engine. To control the engine speed and torque, the engine was mounted with a 57 kW AC dynamometer, Elin AVL Puma type model MCA325MO2. The AC dynamometer was used to drive the engine during motored conditions and absorb load during fired operations. The in-cylinder pressure was measured by a Kistler type 6056 piezo-electric pressure transducer connected to a charge amplifier, Kistler type 5018. The encoder, Autonics type model E40S8-1800-3-T-24, was attached to the crankshaft to position the engine crank angle.

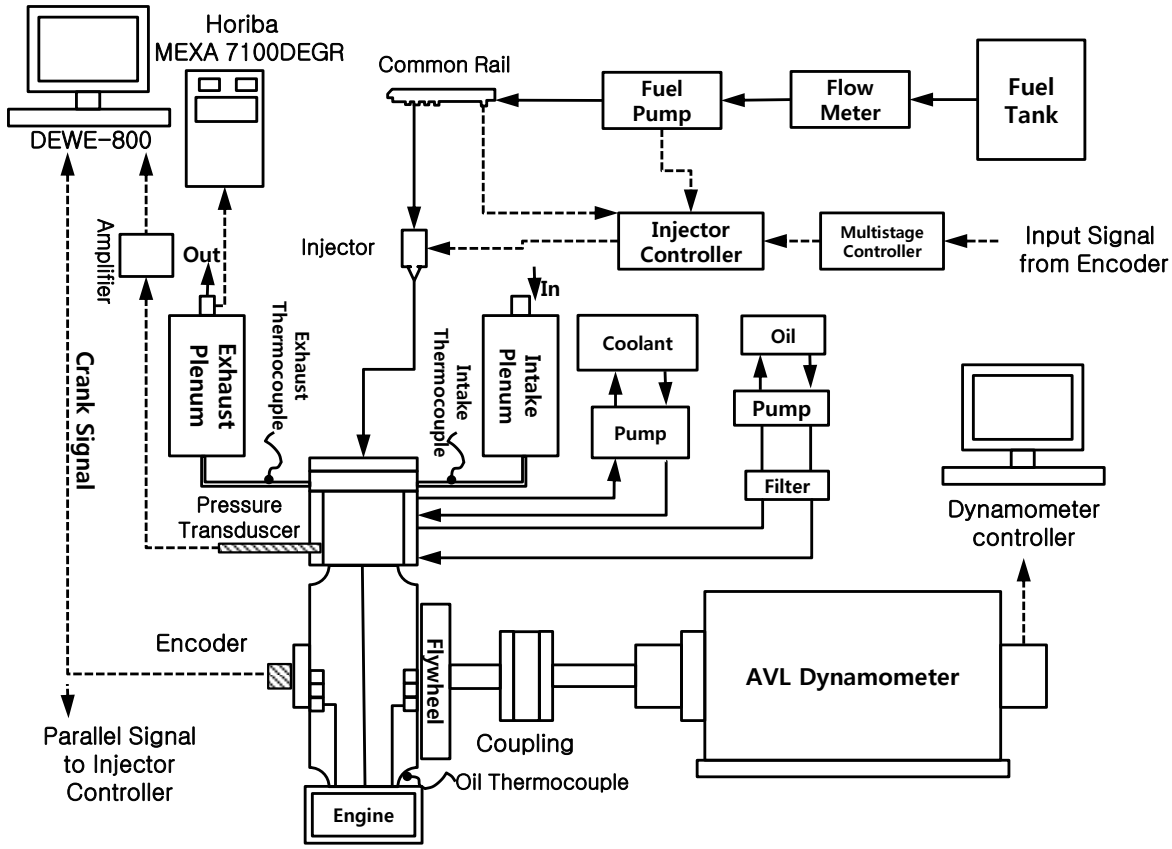

Figure 4-6 Schematic diagram of the test bed for the combustion characteristics and gas emission experiment.

An exhaust gas analyzer, Horiba model MEXA 7100 DEGR, was used to analyze the components of the exhaust emissions. The non-dispersive infrared method (NDIR) measures the carbon monoxide (CO) levels while the oxide of nitrogen (NO_X) concentration is quantified by chemiluminescence detection (CLD). A flame ionization detector (FID) is used to determine the total hydrocarbons (THC).

Table 4-6 Engine specifications.

Engine Parameters	Value
Displacement	498 cm^3
Bore x Stroke	83 x 92 mm
Compression ratio	19.5
Con. rod length	145.8 mm
Crank radius	43.74 mm
Valve System	SOHC 4 valve
Fuel System	Electronic common rail

4.3.2 Fuel injection flow rate measurement

The fuel injection flow rate system, operated under the non-evaporative condition, is shown in Figure 4-7. A diesel common rail system with a Bosch high-pressure pump was used to provide the stability of high-pressure conditions up to 1350 bar. The desired injection pressure was controlled using a common rail PCV driver ZB-1100. A Bosch solenoid-type seven-hole injector located at a measuring vessel was employed to determine the fuel injection rate. The injection timing and duration were controlled independently by a Zenobalti multistage injector engine controlled ZB-8035 combined with the ZB-5100.

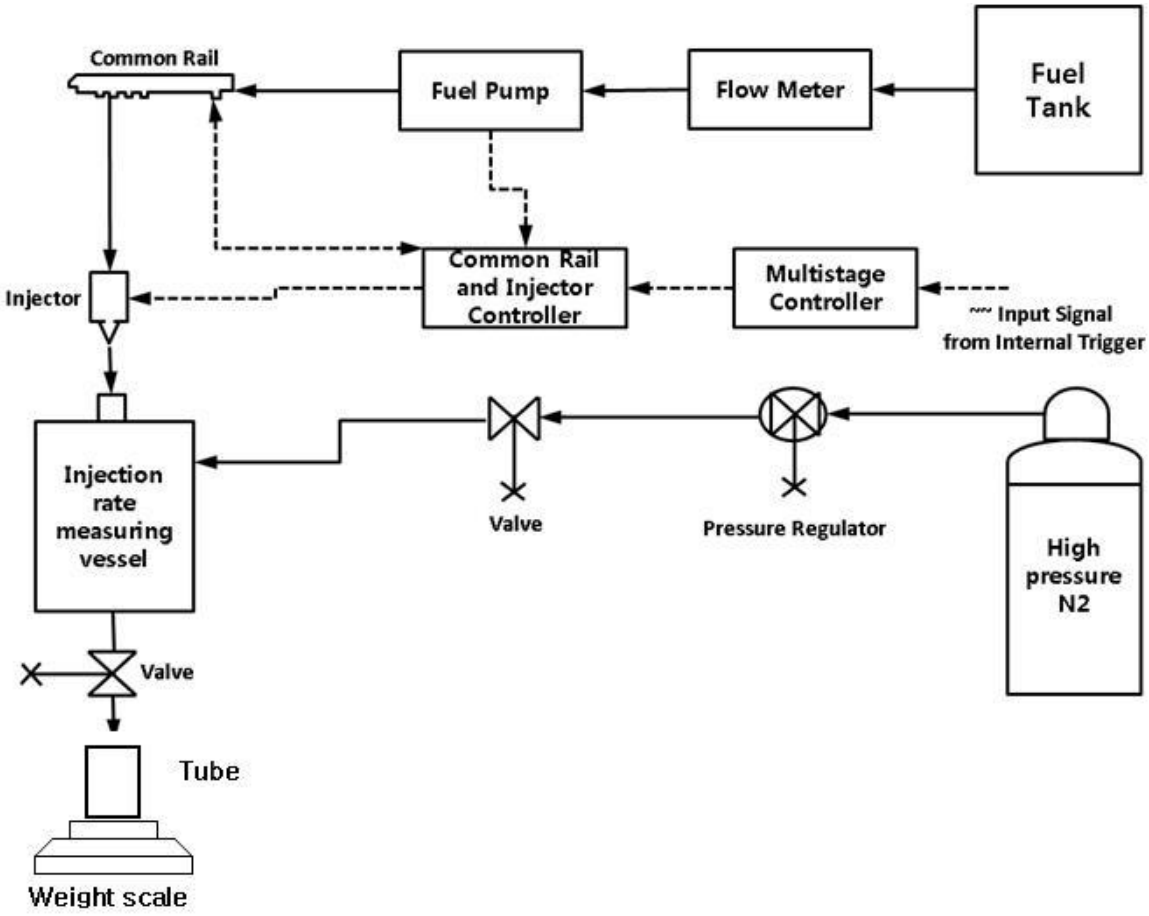

Figure 4-7 Schematic diagram of the fuel injection flow rate system.

4.3.3 Experimental procedure and conditions

Combustion characteristics and exhaust emissions of GCI engine fueled with Gasoline-biodiesel blends

The concentrations of biodiesel blended with gasoline were varied in the range of 5, 10 and 20 %. Furthermore, pure biodiesel and neat diesel were employed in this experiment for the reference. The engine speed and load were set at 1200 rpm and 7 bars of IMEP, respectively. The injection timing was varied, and the injection duration was altered to keep the stoichiometric equivalent ratio (λ=1). The combustion characteristics were represented by the heat release analysis and mass fraction burned. Moreover, the effect of injection timing on the diesel and GB20 combustion were observed by running the engine at 1200 rpm with the rail pressure of 800 bar, the single injection duration of 800 μs and the injection timing at 18 to 75 degree bTDC. The test condition is presented in Table 4-7.

Table 4-7 Engine operating condition.

Parameters	**Setting**
Engine speed	1200 rpm
Rail pressure	800 bar
SOI	varying
Duration	varying
IMEP	7 bar
Lambda (λ)	1

Fuel injection flow rate

The injection pressures were varied from 200−1350 bar increment form 200 bar. The injection duration was varied in the range of 800 to 1,050 μs. To simulate the ambient pressure of a combustion chamber at 40ºCA bTDC, nitrogen gas was filled into the vessel up to 8 bar. This ambient pressure was derived from the pressure traces [29] when a single-cylinder engine was operated during the motored mode at 1200 rpm. In order to increase the accuracy of the measurement, the fuel was injected into the vessel repeatedly 1,000 times. Then, a three-digit precision balance was used to measure the fuel quantities on a mass basis. The test conditions of the fuel injection flow rate experiment are summarized in Table 4-8.

Table 4-8 The test conditions of the fuel injection flow rate.

Item	Value
Fuel	GB05, 10, 20 and D100
Engine speed (simulate)	1200 rpm
Injection pressure	200-1350 bar
Injection duration	800-1,050 μs
SOI	40ºCA bTDC

Combustion characteristics of gasoline compression ignition engine fueled with gasoline-biodiesel blends at different injection pressure

The engine speed was set at 1200 rpm. To maintain smoothly normal engine operation, the engine oil and water coolant were controlled at 90 ± 5 ºC and 80 ± 5 ºC, respectively. The effect of the injection pressure was investigated at 600 and 1,000 bar. The injector was activated once to commence at 40 degree bTDC. The injection duration was altered to keep the stoichiometric equivalent ratio (λ=1). As a result, the injection duration of GB05 lasted for 1,020 and 750 μs while diesel durations were prolonged to 1,775 and 775 μs at respectively at the low and high injection pressures. The combustion characteristics were

analyzed by heat release analysis and the mass fraction burned. The test condition is presented in Table 4-9.

Table 4-9 Engine operating condition.

Item	Parameters
Engine speed	1200 rpm
Rail pressure	600 / 1,000 bar
SOI	40ºCA bTDC
Lambda (λ)	1

5. RESULTS AND DISCUSSION

5.1 Fuel characteristics and properties

5.1.1 The effect of gasoline-biodiesel-diesel blends on phase stability

Phase separations and liquid phases are defined by different color circles as shown in Figure 5-1 and 5-2. The phase separations were classified in three types; i) clear liquid single phase (green), ii) clear liquid two phases (light blue) and iii) clear liquid three phases (navy blue) as shown in Figure 5-1(a)-(c) respectively. When the ambient temperature decreased some of the samples showed the crystalline colloid. Therefore, the phase separations were classified more detail with the number of crystalline colloid as a few (purple), medium (orange) and full amount (red) of colloid as seen in Figure 5-2 (b),(c) and (d). In addition, the clear liquid single phase or homogeneous phase (green color) is still presented to compare.

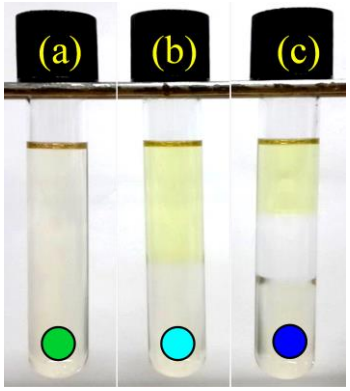

Figure 5-1 The phase separation of G-D-B blends with (a) clear liquid single phase (green), (b) clear liquid two phases (light blue) and (c) clear liquid three phases (navy blue).

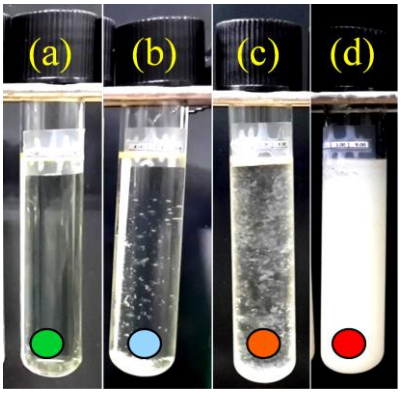

Figure 5-2 The crystalline colloids of G-D-B blends with (a) no (green), (b) a few (purple), (c) medium (orange), and (d) full (red) amount of crystalline colloids.

Phase separation of G-D-B

The phase separation test was conducted in two environmental conditions which were room temperature about 25 ºC and cold condition. At the beginning when gasoline, diesel and biodiesel were blended with various ratios, they could well dissolve in each other in the test tubes.

Figure 5-3(a) exhibits the ternary diagram of G-D-B blends with ambient temperature at 25^{o}C after 30 days. G-D-B blends at all ratios show only green color. This means that no phase separation and crystal colloid occurred in this condition. Due to the exact same results Figure 5-3(b) shows the ternary diagram of G-D-B blends conducted in cold temperature at 20, 15 and 10^{o}C after one hour. The results are similar to ambient temperature condition, in which no phase separation and crystalline colloids appear. The blends could maintain the single liquid phase (homogeneous) throughout the test period. Because gasoline and diesel are non-polar solutes, they can readily dissolve in each other following “like dissolve like” rule. Biodiesel has the polar in one end and the non-polar at the others [66]. Therefore, they can use the non-polar end to dissolve into gasoline or diesel.

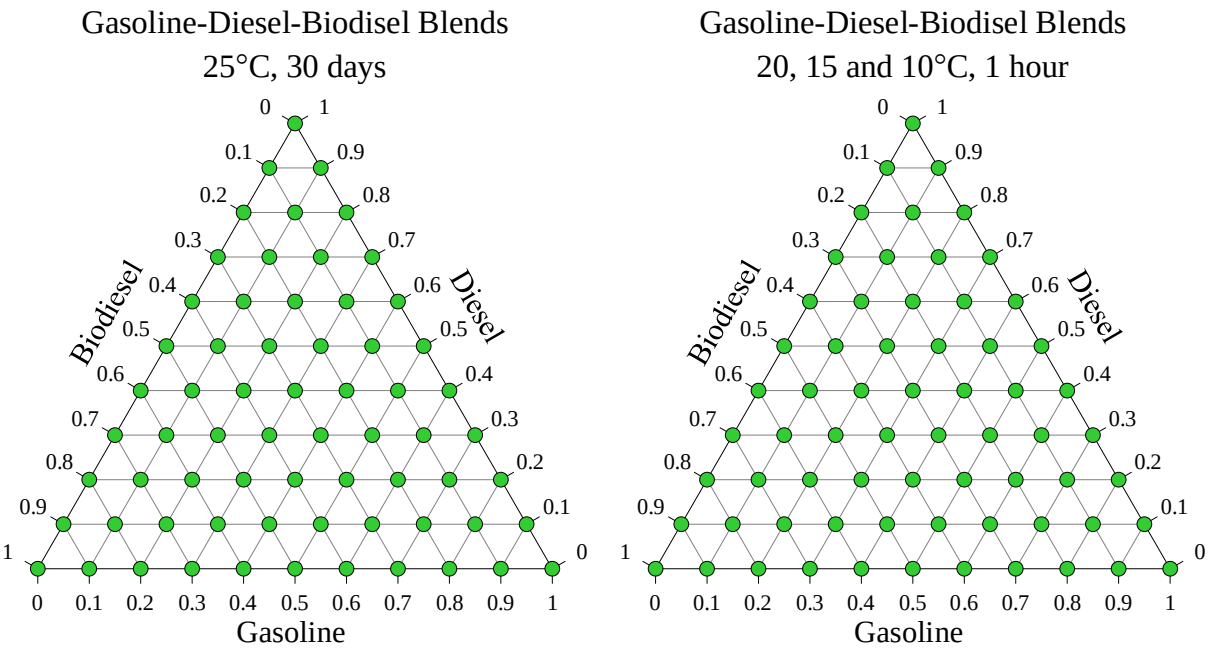

(a) (b)

Figure 5-3 The ternary phase diagram of G-D-B at (a) room temperature 25^{o}C and cold temperature (b) 20, 15 and 10^{o}C.

When the cold temperature was decreased to 5^{o}C, the crystalline colloids occurred in the region of high biodiesel concentration. The purple color (a few colloids) appeared when the biodiesel concentration was blended more than 30%. Increasing the percentage of biodiesel higher than 50%, the orange color (medium colloids) circles were indicated as shown in Figure 5-4(a). After continuingly decreasing the temperature to 0^{o}C for one hour in Figure 5-4(b), the full amount of crystal colloids (red color) occurred when the 70 % of biodiesel concentration was blended in the test fuels. In addition, the region of all crystalline colloids levels covered the biodiesel concentration ranging from 20% to 100% at this 0°C condition. The higher cloud point of higher biodiesel concentration as shown in Table 5-1 is the cause to form crystalline colloids.

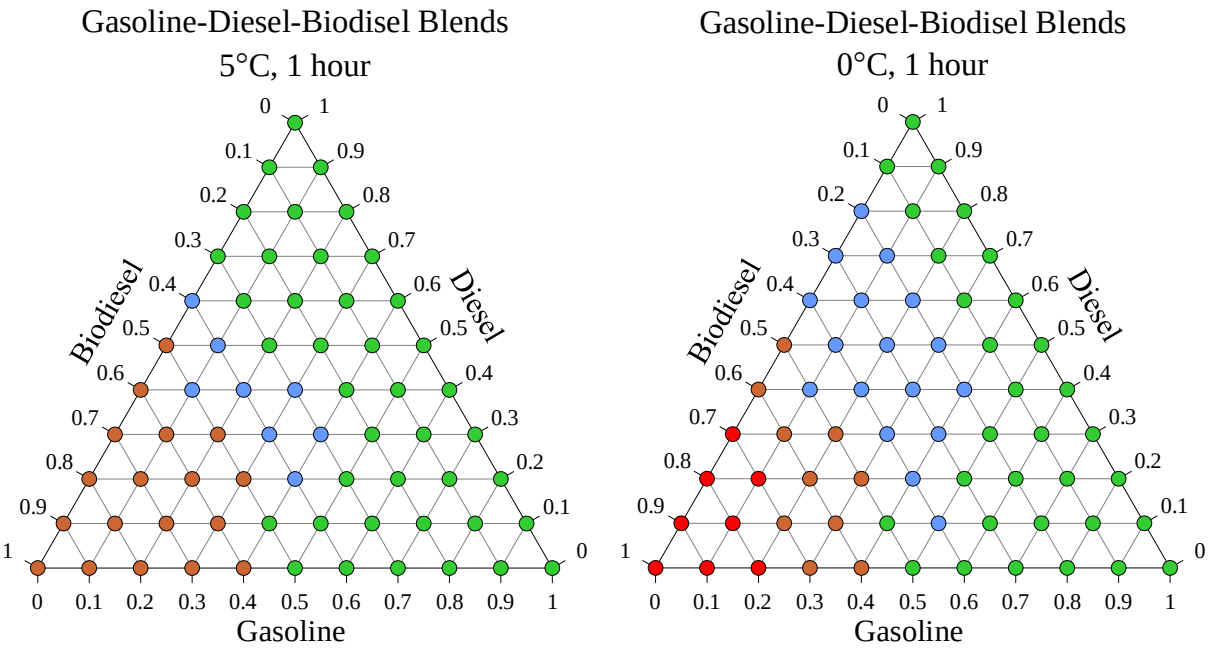

Figure 5-4 The ternary phase diagram of G-D-B at cold temperature (a) 5^{o}C and (b) 0^{o}C.

5.1.2 Fuel properties

The chemical and physical properties of the GB blends including viscosity, density, lubricity, cloud point and pour point were characterized to clarify the effect of biodiesel content. Except for surface tension, the physical properties of the GBs according to the Korean standard were measured by K-Petro. The property values are exhibited in Table 5-1 and their appearances are shown in Figure 5-5.

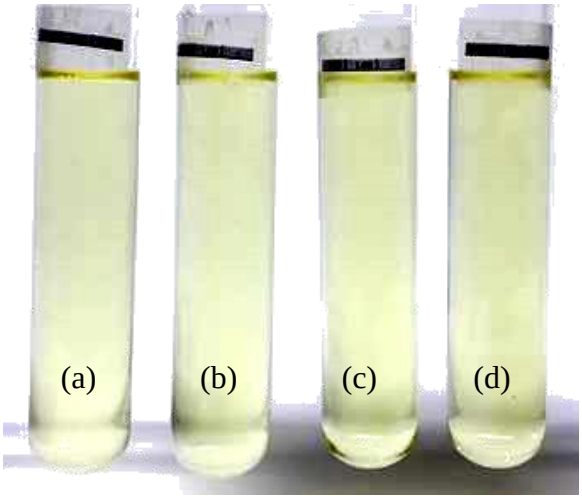

Figure 5-5 The appearance of gasoline-biodiesel blended fuels (GB) with biodiesel concentrations of (a) 20%, (b) 15%, (c) 10% and (d) 5%.

The density of neat biodiesel (B100) is the highest value, whereas that of gasoline (GB00) is the lowest as shown in Figure 5-6. Therefore, the density of the GB increases with the concentration of biodiesel. However, the values are still lower than that of diesel. Generally, the amount of injected fuel in the cylinder is based on a volume basis. With a lower density for the GB than for diesel, the characteristics of the spray, combustion, and emissions of the GCI engine should differ from the commercial diesel engine.

Table 5-1 Physical properties of the test fuels.

Test Item	Unit	Test Method	GB00	GB05	GB10	GB15	GB20	B100[1]	Diesel
Distillation		ASTM D86:2012							
Initial Boiling Point	°C		25.3	28.5	26.9	-	-	-	164.5
10% Evaporated	°C		40.5	43.3	45.1	-	-	-	198.3
50% Evaporated	°C		74.2	79.9	86.4	-	-	-	280.6
90% Evaporated	°C		156.4	174.6	316.2	-	-	-	335.3
End Point	°C		205.9	328.9	334.9	-	-	-	361.1
Cetene Index	-	KS M ISO 4261:2003	26	24.6	10.6	-	-	-	57.9
Kinematic Viscosity (40°C)	mm^2/s	KS M ISO 3104:2008	0.735[2]	-	-	-	-	4.229	2.798
Lubricity	μm	KS R ISO 12156-1:2012	548	290	282	252	236	189	238
Cloud Point	°C	KS M ISO 3015:2008	-57	-37	-32	-20	-16	3	-5
Pour Point	°C	ASTM D6749:2002	-57	-57	-57	-57	-57	1	-9
Density (15°C)	kg/m^3	KS M ISO 12185:2003	712.7	722.3	732.2	742.6	757.1	882.3	826.3
Surface Tension	mN/m		22.6[3]	22.9[5]	23.1[5]	23.4[5]	23.6[5]	27.1[4]	-
Heat of combustion of liquid hydrocarbon fuels	MJ/kg	ASTM D240:2009	45.86	45.323	44.924	44.569	43.58	39.794	45.933

[1] Soybean fatty acid methyl ester, [2] (Bao et al., 2014), [3] (Park et al., 2013), [4] (Ejim et al., 2007), and [5] Calculated based on (Ejim et al., 2007)

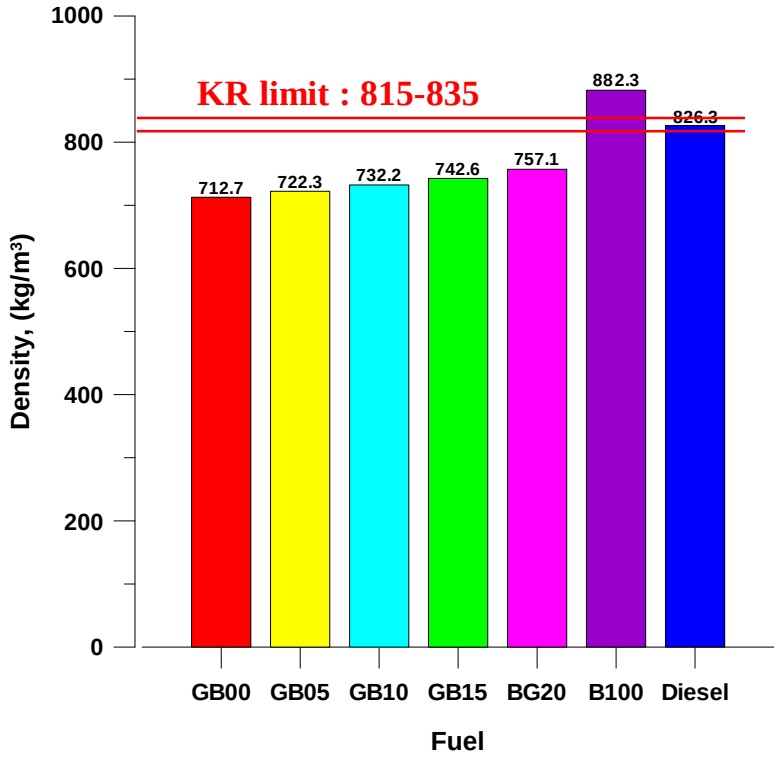

Figure 5-6 The density of test fuels at 15°C

Because of their relatively low value, the kinematic viscosities of the GB could not be measured with the same standard as diesel and biodiesel as shown in Figure 5-7. Therefore, the viscosity of GB00 shown in Table 5-1 refers to the reference [70], but those of the other GBs are not presented. The cloud point and pour point of B100 are higher than those of GB00 and diesel. As a result, the cloud point of the GB increases with increasing biodiesel concentration. However, the amount of biodiesel did not affect the pour point which remains constant at -57° C for all GB.

Shown with the lower value of a wear scar in micrometers, the lubricity of B100 is better than that of GB00 and diesel as shown in Figure 5-8. When biodiesel is added to gasoline, the lubricity of GB05-GB20 is drastically improved because of the fatty acid compound in biodiesel [4]. The excellent lubricity of biodiesel was proved by many researches and blending only 1% of biodiesel can improve lubricity by 30% [69]. Five percent of biodiesel can improve the lubricity of GB blend by 53 % in this study. When increasing the percentage of biodiesel in the blends, the lubricity is reduced. However, all results of the gasoline blended with biodiesel in this study qualify the standard limit of 400 µm wear scar, according to Korea regulation [71].

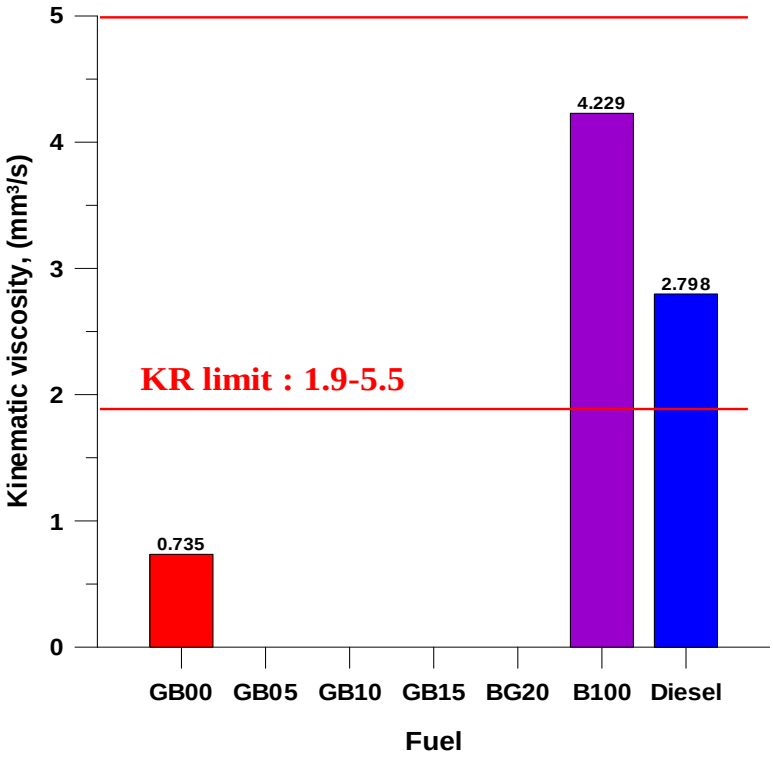

Figure 5-7 The kinematic viscosities of test fuels

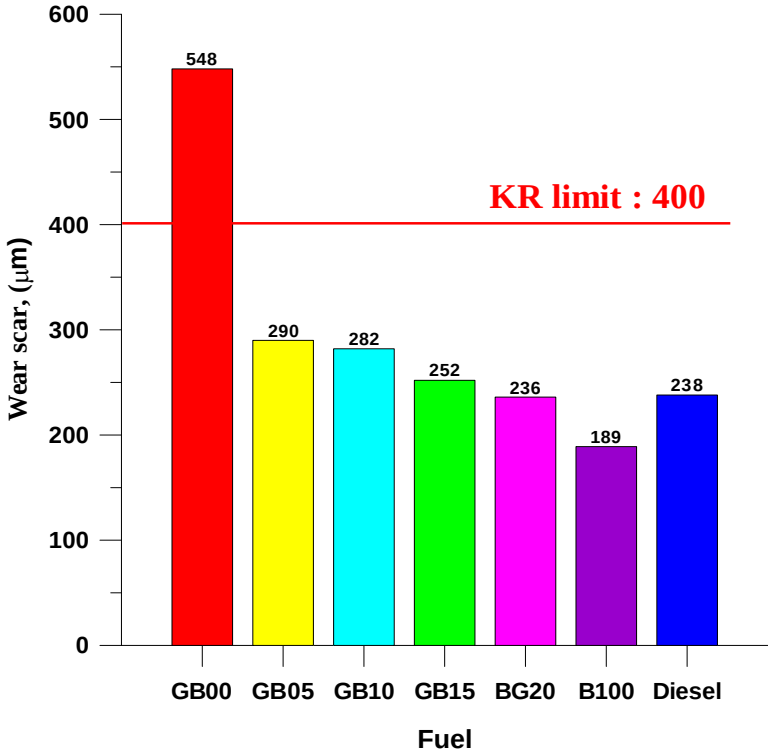

Figure 5-8 The lubricity of test fuels

Therefore, adding biodiesel in gasoline may protect the wear from the mechanical movements of high-pressure pumps and injectors. On the other hand, neat gasoline showed very poor lubricity, which is out of the range of the standard. Hence, when using gasoline in GCI engine with the common rail injection system, the failure of the injection system, caused by the low lubricity fuel, has to be considered.

Due to the limitation of testing equipment, surface tension has not been directly measured for the current study. Based on the Macleod-Sudgen correlation, however, the mixture surface tension can be calculated as in equation 1 [72].

$$\gamma_m = \left[\sum_{i=1}^{n} y_i (\gamma_i)^{1/4}\right]^4 \quad (5.1)$$

Where, γ_m is denoted Surface tension of the mixture

5.2 Spray phenomena

5.2.1 The influence of biodiesel blended gasoline-based fuels on macroscopic spray structure when injected from a diesel injection conditions

This current study investigates the spray characteristics of gasoline-biodiesel blended fuels (GB), which expected to be utilized in a gasoline compression ignition (GCI) engine. Commercial gasoline blended with 0 - 20 % by volume of biodiesel, called GB00 - GB20, were used to experiment. In addition, neat biodiesel and pure gasoline were also investigated as the references. The spray features of the fuels injected into a constant volume combustion chamber (CVCC) with the common rail injection system of a diesel engine were studied. Spray macroscopic visualization was performed by the shadowgraph technique. The test fuels at injection pressures of 1,000, 1,200, and 1,350 bar were injected into the CVCC with an engine-simulated speed of 2,000 rpm. The constant back pressures in the CVCC were set at 30 bar and 50 bar. A high-speed video camera was employed to record the spray pattern with a frame speed of 10,000 f/s. The spray penetrating length and cone angle were analyzed by an image processing technique. Biodiesel is characterized as the widest angle and longest spray length while gasoline has the narrowest cone angle and shortest penetration. There is no correlation between the spray angle/penetration length and the percentage of biodiesel in the blends among the GB. When the injection pressure was increased, the spray cone angle was slightly decreased, while the spray-penetrating length was increased for all test fuels.

5.2.1.1 Results and discussion

Appearance of the sprays

The example of temporal images of biodiesel (B100) and gasoline (GB00) spray in the non-evaporative condition at the back pressure of 50 bar and the injection pressure of 1,000 bar are illustrated in Figure 5-9. The spray boundary of each image is confined by the red line contour. Both gasoline and biodiesel show the similar pattern of spray development. To quantitatively compare the spray characteristics of the blends pure gasoline and biodiesel, the liquid spray penetration tip, the cone angle and the average speed are derived from those images and presented in the following section.

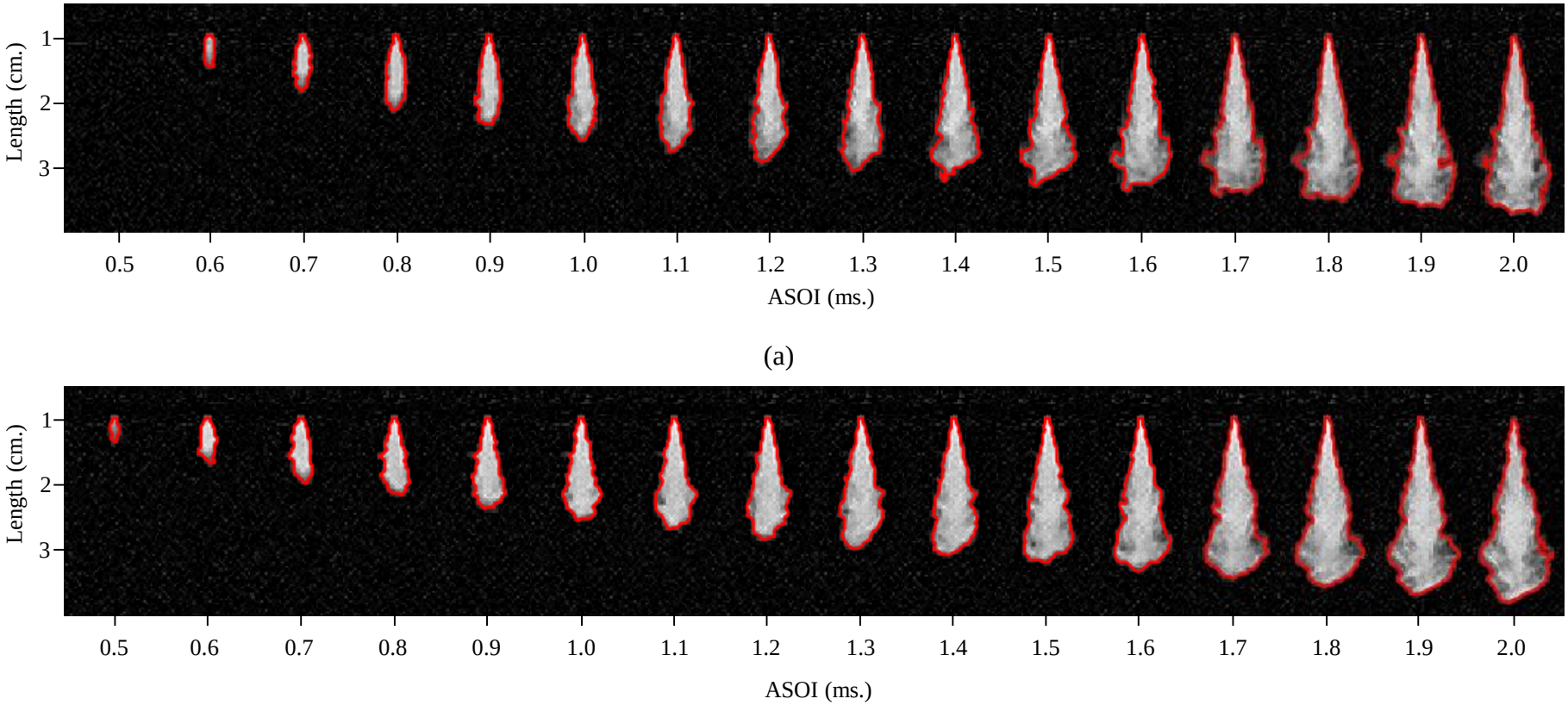

Figure 5-9 The spray pattern of (a) B100 and (b) GB00 at the injection pressure 1,000 bar and the back pressure of 50 bar.

Liquid spray penetration length

Effect of injection pressure

Figure 5-10 shows the effect of injection pressure on the liquid spray penetration length of each test fuel at the back pressure of 30 and 50 bar. When the injection pressure increases, the spray penetration length increases as expected. All test fuels present the same trend at both ambient pressures. The main reason for the increased penetration length is the increased spray jet momentum.

Although the increased spray length with the increased injection pressure because of the increased momentum flux is not depended directly on the test fuel (fuel properties), biodiesel added in the gasoline alters the pattern of increased spray length of GB blends, like neat biodiesel spray. The increased injection pressures increase the spray length of biodiesel from the initial spray tip until the end of length, but gasoline shows the effect of injection pressure after 0.8 ms. In general, the penetration length increases with the increased injection pressure both the beginning and the fully developed spray. The spray length at the initial or transient region can be calculated as in equation 5.2, proposed by Naber and Siebers [73].

$$S(t) = C_v\sqrt{\frac{2\Delta P}{\rho_f}} \qquad \text{at } t < t_r \tag{5.2}$$

where, C_v is velocity coefficient, Δp is the different pressure, and ρ_f is the density of the fuel.

According to this equation, the spray length at the beginning is depended on the pressure difference, hint injection pressure. Because the spray formation at the nozzle exit is strongly dominated by the internal nozzle flow [74], the different fuel properties between gasoline and biodiesel should induce different nozzle flow phenomena such as turbulent and cavitation. For this study, cavitation flow should be the main cause to reduce the effect of the increased injection pressure at the initial length of gasoline spray. With the relatively low viscosity of gasoline leading to high Reynold number, the cavitation is strongly induced in the nozzle hole rather than the high viscosity fuel [75]. When the injection pressure is increased, the formation of cavitation is readily occurred as indicated in the cavitation number [76] in equation 5.3 due to the large difference between chamber and injection pressure.

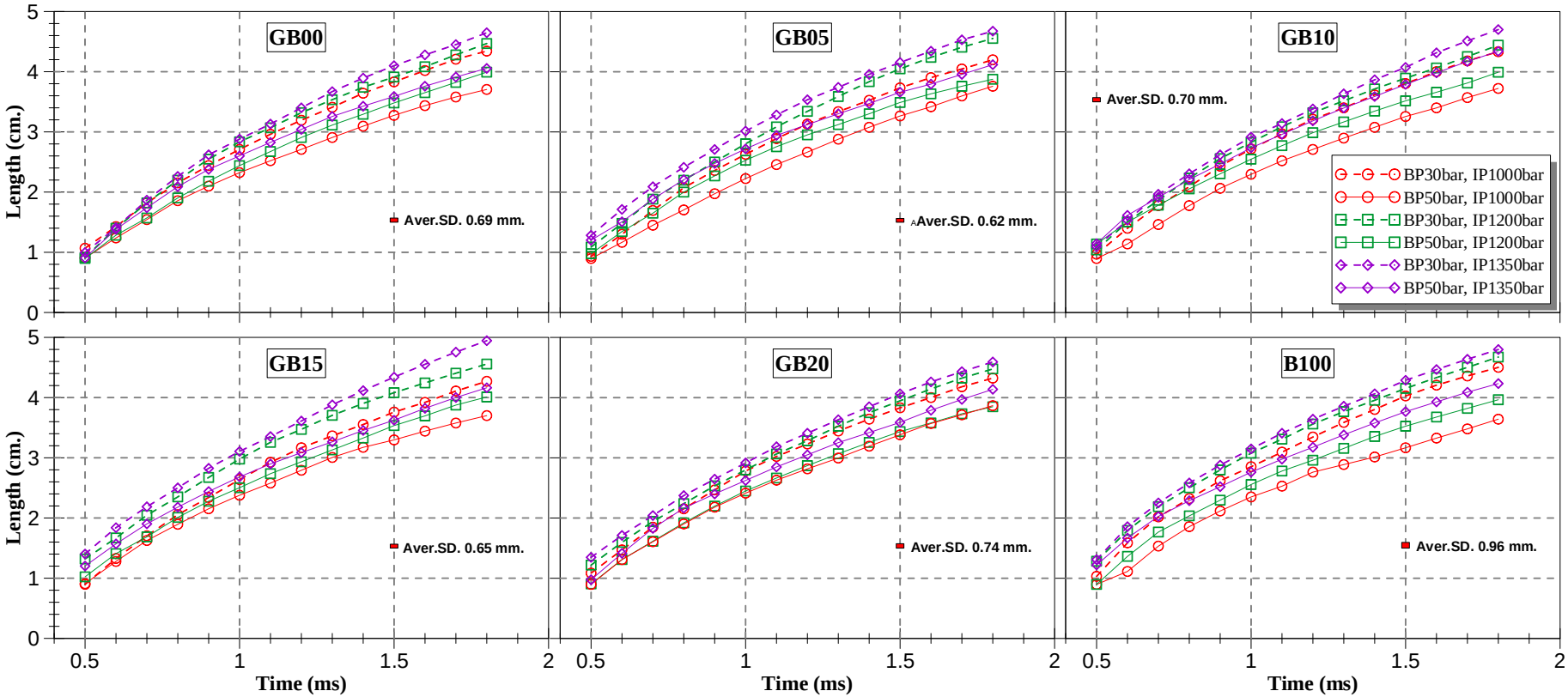

Figure 5-10 The spray penetration length of GB00, GB05, GB10, GB15, GB20, and B100 spray at various injection pressures and back pressures.

In addition, the magnitude and the occurrence of the cavitation are enhanced during the low needle lift period [46,77]. At fully needle opening, the cavitation is reduced and then the effect of injection pressure dominates.

$$K = \frac{P_i - P_v}{P_i - P_b} \tag{5.3}$$

where P_i is injection pressure, P_v is vapor pressure and P_b is back pressure.

Effect of back pressure

The back pressure has the significant effect on the penetration length, as shown in Figure 5-10. For all test fuels, the liquid spray lengths, which injected at the same injection pressure, are obviously decreased when the back pressure increases. Moreover, the effect of the back pressure dominates the influence of the injection pressure. As a result, the spray penetration lengths at 50 bar are shorter than those of 30 bar although the injection pressure is increased. More dense air in the chamber resists the moving of the spray jet. Accordingly, the increased drag force decreases the liquid length.

Effect of test fuel

Figure 5-11 presents the comparison of the liquid penetration length of all test fuels at the injection pressure of 1000, 1200 and 1350 bar as well as at the back pressure of 30 and 50 bar. The results show the effect of the test fuel on the liquid length at the low back pressure, but no significant difference of the penetration tip is observed at the high back pressure. At the back pressure of 30 bar, B100 results in the longest length where GB00 has the shortest travel distance. However, the penetration length does not relate to the amount of biodiesel blended into gasoline. The penetration lengths of the blends are nearly the same and close to that of GB00. This implies that blending biodiesel into gasoline up to 20 % does not affect the liquid spray length.

The higher viscosity (6 times), density (1.2 times) and surface tension (1.2 times) of biodiesel lead to the longer penetration length when compared with gasoline. The result corresponds well with the finding of Desantes et al [78] when compared biodiesel with diesel fuel. With the higher viscosity and surface tension of biodiesel, the fuel droplets are hardly broken, and liquid spray can travel further along with the chamber with the higher inertial mass.

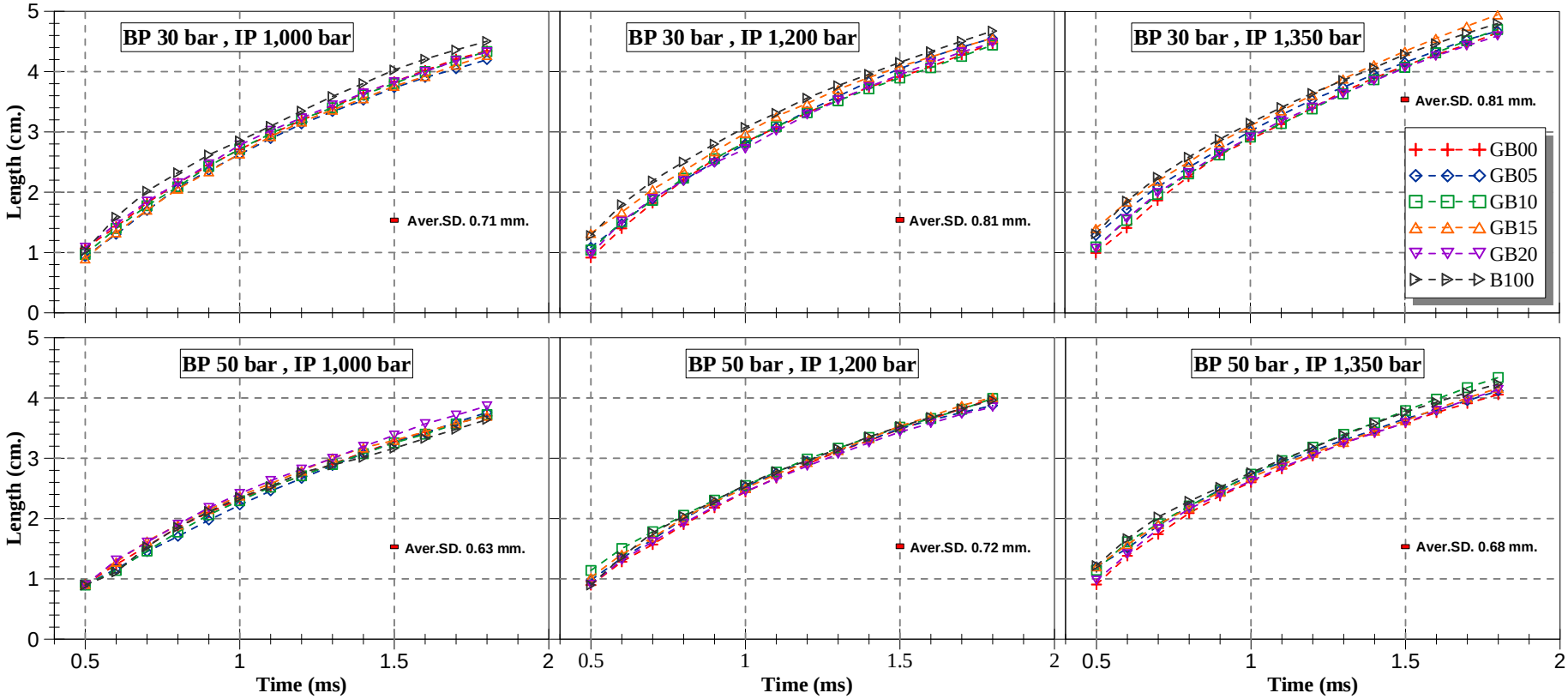

Figure 5-11 The spray penetration length at the back pressure of 30 and 50 bar with the injection pressure of 1,000, 1,200, and 1,350 bar.

In addition, due to the high density of biodiesel, the lower ambient entrainment could decelerate the fuel atomization and breakup process as found by Kook and Pickett [79]. Moreover, with the low volatility of biodiesel (i.e. high boiling point and T90), the liquid length is longer than the high-volatility multicomponent hydrocarbon fuels as suggested by the correlation of Siebers [80], Cannan et al [81] and the study of Higgnins [82].

As stated above, the effect of the fuel properties on the spray length could not observe at the high back pressure. Hint, the effect of back pressure overcomes the effect of fuel properties. Because biodiesel is hardly atomized and vaporized, its droplet sizes are bigger than those of gasoline. Therefore, when the back pressure increases, the increased drag force acts opposite to B100 spray higher than gasoline because the drag force is proportional to the moving object area. Consequently, the increased spray length of B100 is reduced and closed to GB00 and the blends.

Spray cone angle

At the beginning of injection, when the needle is lifting, the instability of the spray is formed and results in the difficulty of the analysis. Therefore, the spray cone angle will be acquired only after the needle is fully opened.

Effect of injection pressure

Unlike the liquid spray penetration length, the effect of injection pressure on the cone angle is not clearly observed. As seen in Figure 5-12, the cone angles of GB00 are relatively identical except for the angle at the injection pressure of 1350 bar which is lower than that of the injection pressure of 1000 and 1200 bar. For B100, the cone angles at the injection pressure of 1200 and 1350 bar are lower than that of 1000 bar at the ambient pressure of 50 bar while at the ambient pressure of 30 bar the cone angles at injection pressure at 1000 bar is close to that of 1200 bar which higher than that of 1350 bar. As reported previously [83], the cone angle is related to the spray penetration tip. The spray having the small cone angle could travel in the chamber longer than the wider spray. The spray penetration tip is not well related to the cone angle at all test conditions from this study. Nevertheless, the trend of cone angle seems to decrease with the injection pressure.

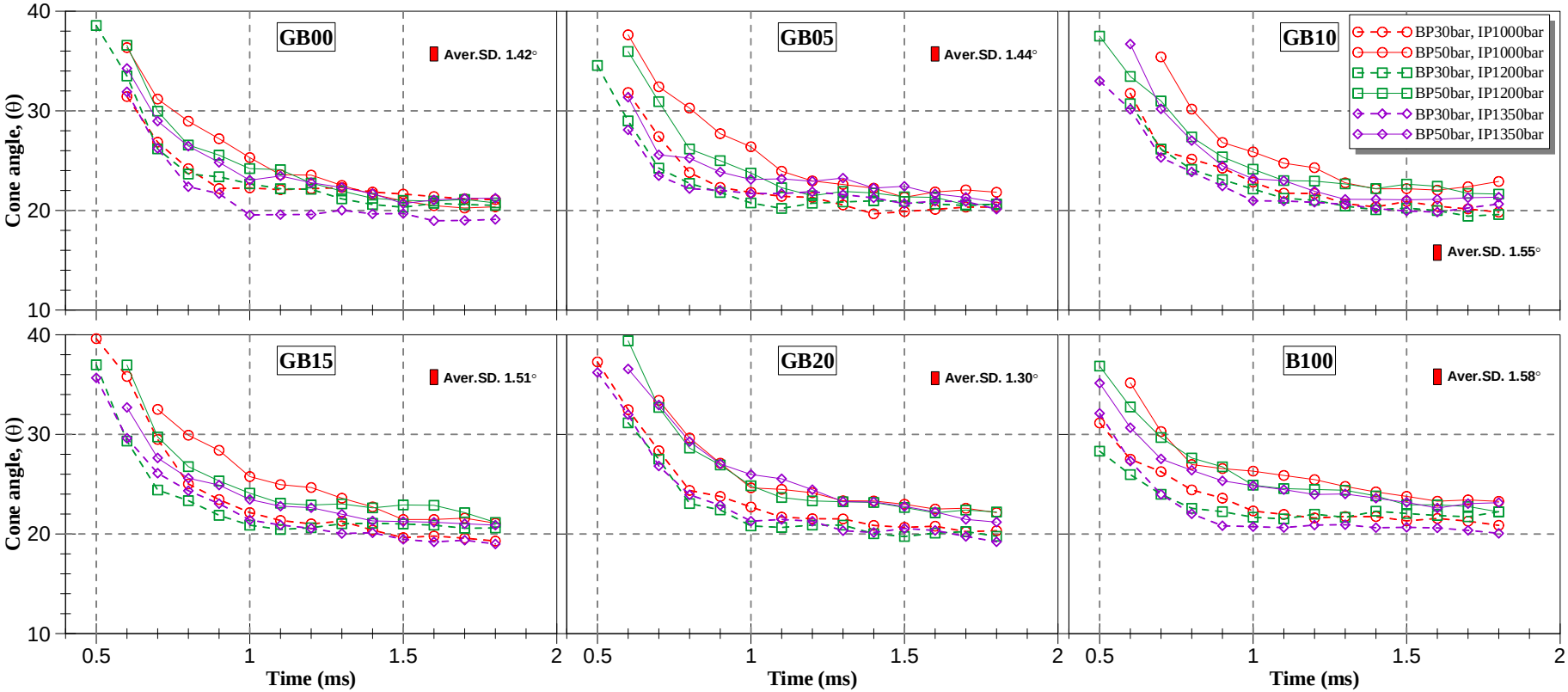

Figure 5-12 The spray cone angle of GB00, GB05, GB10, GB15, GB20, and B100 spray at various injection pressures and back pressures.

Effect of back pressure

The effect of back pressure on the cone angle for each test fuel is presented in Figure 5-12. The result indicates that when the back pressure is increased the cone angle is increased for all test fuels. At the back pressure of 30 bar, the spray cone angles range from 19° to 21° and at the back pressure of 50 bar the spray cone angles are around 20° to 23°. Following with the results of Payri et al [84], the spray cone angle strongly correlates with the gas density, meaning the ambient/back pressure. With the higher ambient density, the drag force increases thus enhancing the spray dispersion.

Considering for each fuel, the cone angles of B100 fuel at 30 and 50 bar show the most different. This indicates that the back pressure has the most effect on the spray cone angle of B100 fuel. When the back pressure increases, biodiesel spray is readily dispersed because of the increased drag force acting on the larger droplet size. On the other hand, the effect of increased drag force has the less extension on the gasoline fuel because of its smaller droplet size, resulted from the evaporation process.

Effect of test fuel

The cone angles of all test fuels at each injection and ambient pressure are presented in Figure 5-13. The results obviously show that most of the biodiesel spray is formed with the widest cone angle at each condition while almost gasoline characterizes the narrower spray. However, there is no correlation between the biodiesel content in the blends (0-20%) and the cone angle.

The result could not be compared directly with the previous studies because no comparison between gasoline and biodiesel was found. Nevertheless, this result is compared with the relevant literature relating to gasoline and biodiesel. This result agrees well with the finding of the previous studies -- Postrioti et al. [41], Agarwal and Chaudhury [85] and Battistoni and Grimaldi [86] -- in which biodiesel had the wider angle than that of diesel (lower density and viscosity like gasoline in this case) because of the higher fuel density. However, it is opposite to the result of Kim et al [87] in which gasoline spray produced the wider cone angle than that of diesel (higher density and viscosity like biodiesel in this case).

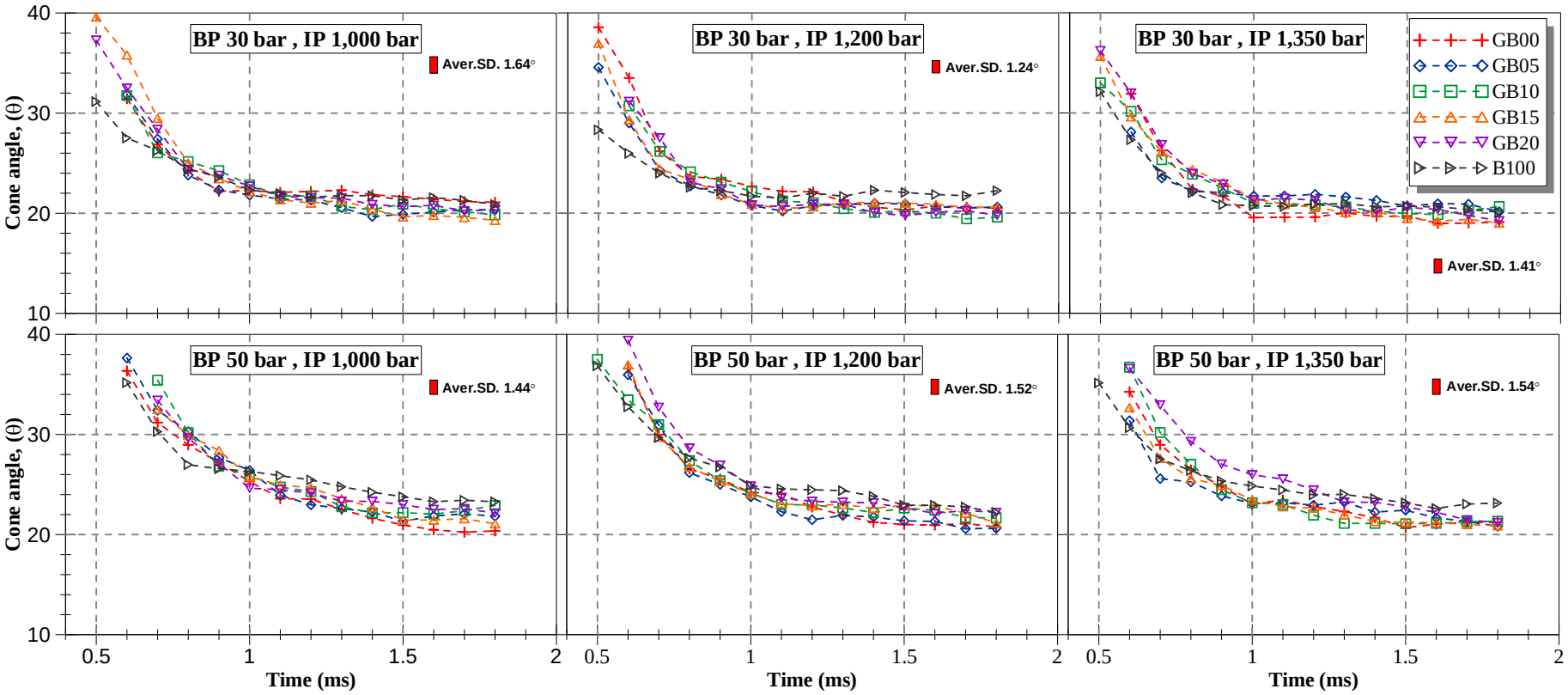

Figure 5-13 The spray cone angle at the back pressure of 30 and 50 bar with the injection pressure of 1,000, 1,200, and 1,350 bar.

It is possible that the type and the geometry of the nozzle is the main cause of this discrepancy. The cone angle of gasoline and diesel is sensitive to the nozzle geometry. The wider cone angle of gasoline from the result of Kim is due to the flow regime in the nozzle in which cavitation is possible to induce sometime. Biodiesel is less sensitive to the nozzle geometry and has a lower tendency of the cavitation [41]. To clarify and link the relationship between these three fuels and the cone angle, the experiment of diesel spray will be future conducted.

Average speed of the spray

Calculated from the spray penetration tip divided by the time, the average speed of the spray under the back pressures of 30 bar and 50 bar are shown in Figure 5-14. Following the spray penetration, B100 results in the fastest speed and GB00 has the slowest velocity. The average speeds of GB05-GB20 are in the range between GB00 and B100. The average speeds of the blended fuels trend to increase when the injection pressure is increased as seen in Figure5-15, due to the spray jet momentum. Furthermore, the average speed is decreased with the increased ambient pressure. As a result, the spray injected with the injection pressure of 1,350 bar (the maximum injection pressure) under the back pressure of 30 bar (the minimum back pressure) shows the highest average speed. In contrast, the lowest average speed is observed under the back pressure of 50 bar (the maximum back pressure) and the injection pressure of 1,000 bar (the minimum injection pressure).

Unlike the spray penetration tip, the average speeds increase after the injection is started. Then, they reach their maximum speed at around 0.7-0.8 ms after SOI, depending on the test conditions and fuels. Afterward, the speeds gradually decrease with the lengthen time. The effect of fuel properties on the average speed shows the most extent at the start of injection and decreases later when the spray further travels in the chamber. It is possible that fuel vaporization and atomization after the breakup time are the cause to decrease average speed and reduce the effect of fuel properties.

Considering the GB00 spray, the average speeds at the initial region do not depend on the pressure difference. Following Bernoulli equation, the outlet velocity of fluid flowing in the nozzle can be calculated in equation 5.4.

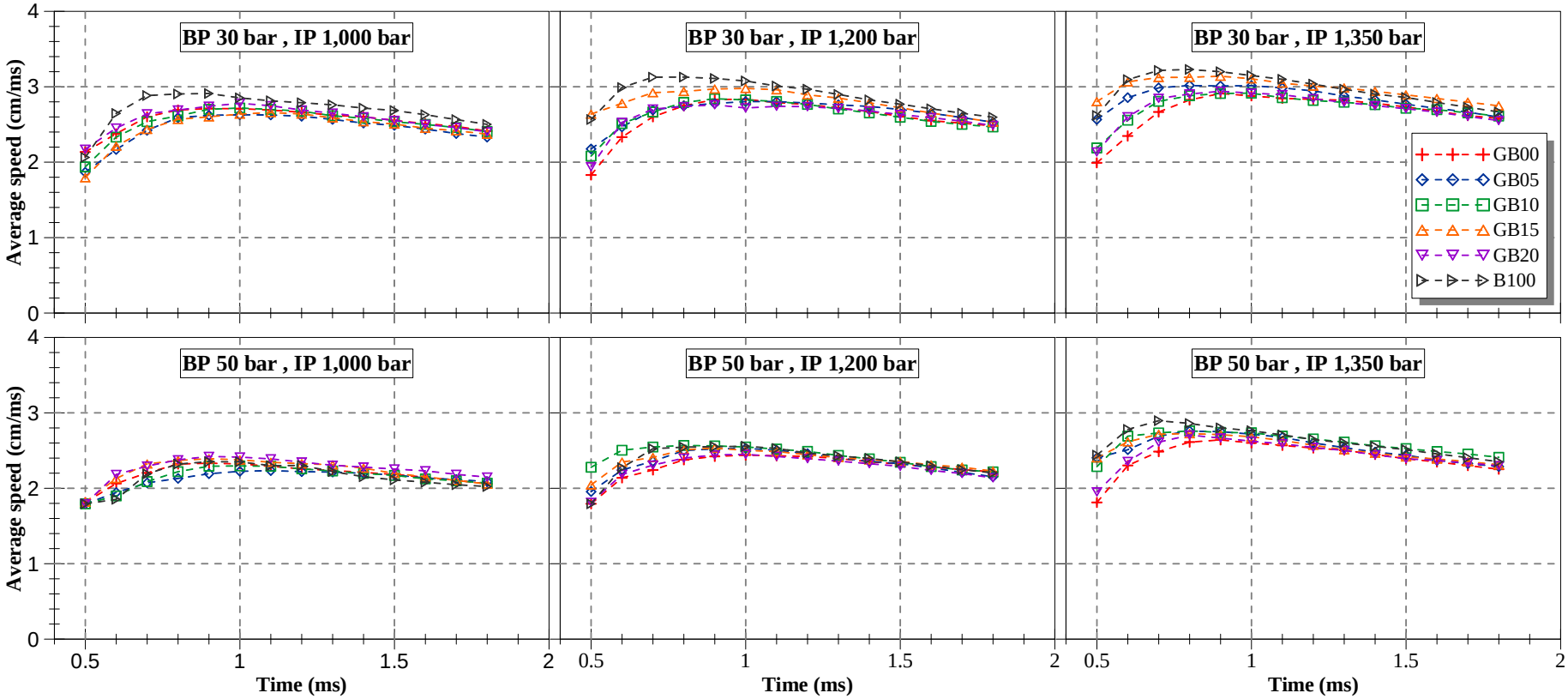

Figure 5-14 The average speed of the spray at the back pressure of 30 and 50 bar with the injection pressures of 1,000, 1,200, and 1,350 bar.

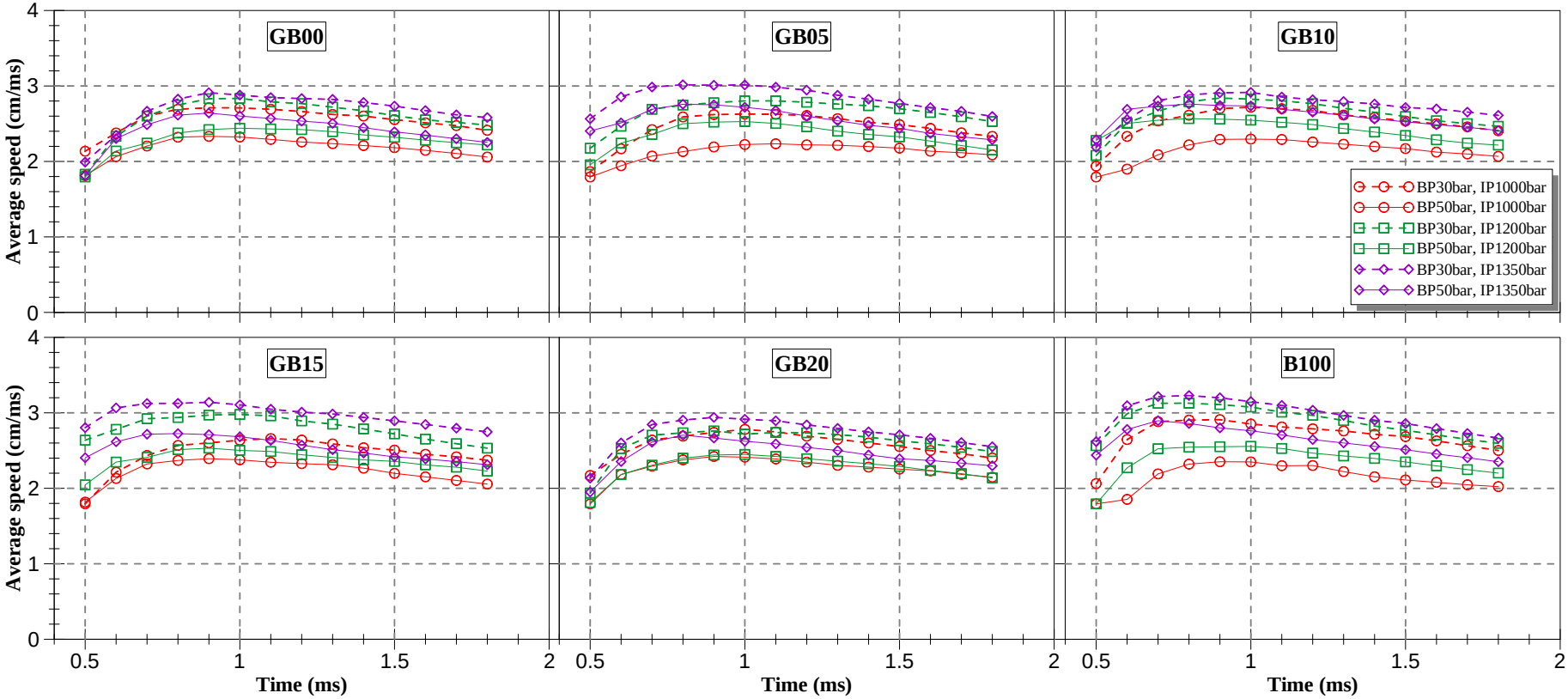

Figure 5-15 The average speed of GB00, GB05, GB10, GB15, GB20, and B100 spray at various injection pressures and back pressures.

$$\text{Velocity} = \sqrt{\frac{2\Delta P}{\rho_f}} \tag{5.4}$$

The equation indicates that when the pressure difference increases, the velocity should be increased. In the opposite way, the velocity of gasoline decreases with the increased injection pressure at the back pressure of 30 bar and is nearly the same value at the back pressure of 50 bar. This confirms the development of cavitation at the needle lift period. When cavitation occurs, the spray is dispersed in the radial direction thus reducing the axial velocity. When adding biodiesel in the gasoline, the cavitation seems to suppress. As the results, the average speeds at the initial spray of GB blends increase with the increased injection pressure.

Instantaneous speed of spray

Figure 5-16 show the instantaneous speed under back pressure 30 and 50 bar. The instantaneous speed of GB blends trends to increase when injection pressure increases. The highest instantaneous speed is observed at the lowest backpressure 30 bar and the maximum injection pressure at 1,350 bar. On the other hand, at the maximum back pressure 50 bar and the lowest injection pressure 1,000 bar the spray has the slowest instantaneous speed. At 0.5 ms of the start of injection, the instantaneous speeds for all blends are approximately 2 cm/sec. Then the instantaneous speed suddenly increases within 0.1 milliseconds and results in the maximum instantaneous speed at 0.6 ms. consequently, the instantaneous speeds drastically decrease until the end of injection timing.

The instantaneous speed of blended fuels under backpressure 30 bar and injection pressure 1000, 1200 and 1350 bar are shown in Figure 5-16, the upper row. B100 shows the highest instantaneous speed whereas GB00-20 do not show the clear difference. At the instantaneous speed of blended fuels under backpressure 50 bar and injection pressure 1000, 1200 and 1350 bar. There is no clear the relation between the instantaneous speed and the blended ratios in this test condition.

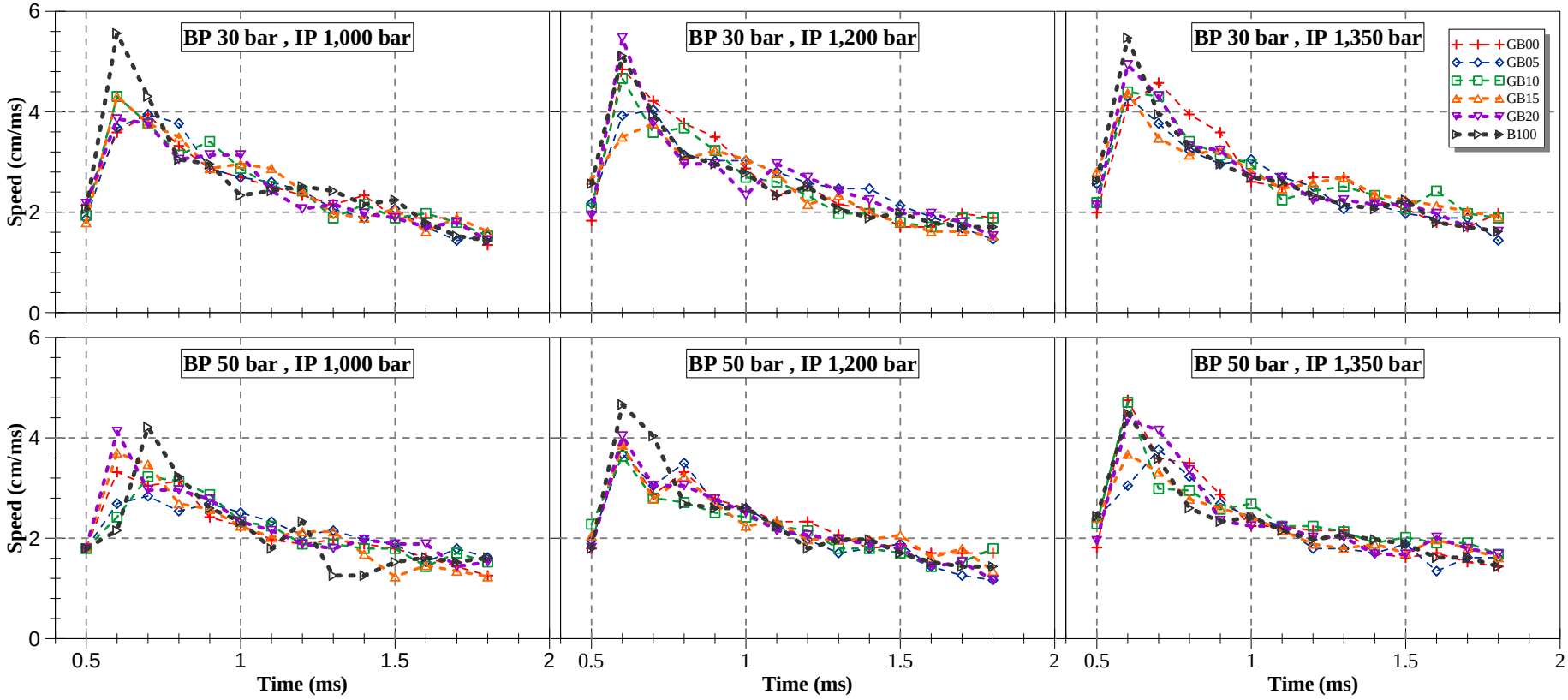

Figure 5-16 The instantaneous speed of the spray at the back pressure of 30 and 50 bar with the injection pressures of 1,000, 1,200, and 1,350 bar.

5.2.1.2 Conclusion

This current study investigates the spray characteristics of gasoline-biodiesel blended fuels in a common rail diesel system in order to be utilized in GDCI engines. The spray-penetrating length, spray cone angle and average speed of the spray at various back pressures and injection pressures are investigated in the CVCC. Subsequently, the spray characteristics were analyzed by image processing with Matlab software. The main conclusions drawn from the study are as follows:

- Adding biodiesel 5-20 % into gasoline has no effect on the spray characteristics including the liquid length, cone angle and average speed when compared with those of pure gasoline.

- Compared with gasoline, biodiesel is characterized as the wider spray with the longer liquid length and faster average speed.

- The higher the back pressure is increased, the more the spray penetration length is diminished, whereas the higher the injection pressure is increased, the longer the spray penetration length for all test fuel.

- The back pressure has the significant effect on the cone angle while the injection pressure shows the marginal influence. When the back pressure increases, the cone angle is increased.

- Adding biodiesel in gasoline can suppress the cavitating flow in the nozzle during the needle lift period.

- The instantaneous speeds of blend fuel suddenly increase at 0.5-0.6 ms of the start of injection and then abruptly decrease and their relations are not clear.

5.2.2 The effects of gasoline-biodiesel blended fuels on spray characteristics with multiple injections

The current study has investigated the effects of biodiesel blended with gasoline on the spray characteristics in a Constant Volume Combustion Chamber (CVCC). With the concentration of 5, 10, 15 and 20% by volume, biodiesel was blended with commercial gasoline and performed on the macroscopic visualization test. Pure gasoline and biodiesel were also tested as the reference. The shadowgraph technique was conducted in the constant volume chamber. The spray images were recorded by a high-speed video camera with frame speed 10,000 frames/second. Fuel injection was set at 800, 1000 and 1,350 bar with the simulated speed 1,500 and 2,000 rpm. The back pressure was controlled at 20 bar. The spray angle and penetration tip were measured and analyzed using image processing.

At the high injection pressure, the spray penetration length with the simulated speed 1,500 rpm showed that B100 was lower than GB00-20 whereas the spray penetration length with the simulated speed 2,000 rpm exhibited that GB blends and B100 were insignificantly different. Due to biodiesel concentration, its effects on spray angles were observed throughout injection periods (T1, T2 and T3). At the simulated speed 1,500 rpm, the spray angle of GB blends and B100 presented the same pattern following injection timing. In addition, when the simulated speed increased to 2,000 rpm the different spray angle of all blends disappeared at the main injection (T3).

5.2.2.1 Results and discussion

The spray patterns of tested fuels with the simulated speed 1,500 rpm are fully developed after start of injection (SOI) at 3.3 ms as shown in Figure 5-17(a). The results show that with the lower biodiesel concentration, the spray pattern is narrower and more uniform distribution.

The spray patterns of tested fuels with the simulated speed 2,000 rpm are fully developed at 5.4 ms as shown in Figure 5-17(b). They have the similar trend to the spray patterns at 1,500 rpm but the spray lengths are longer because of their longer injection period (840 ms).

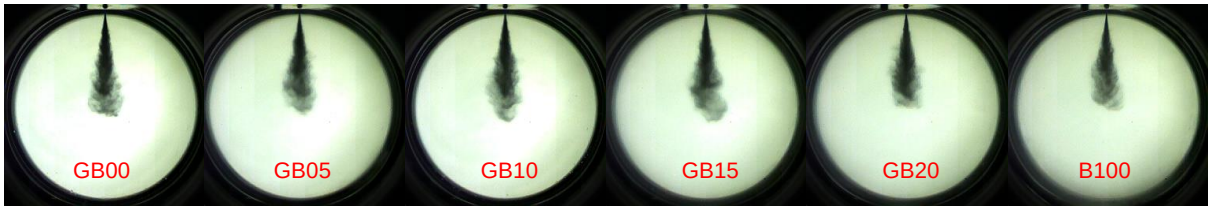

(a)

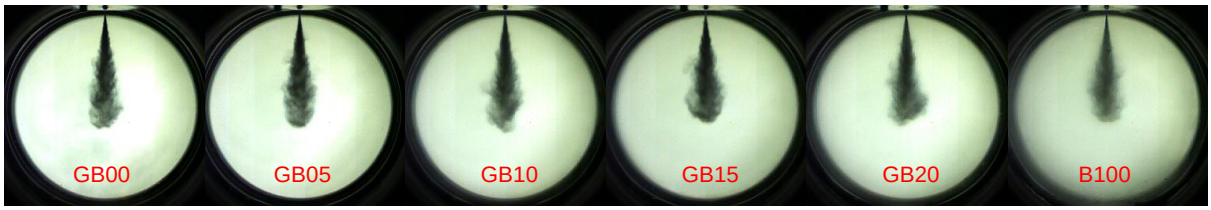

(b)

Figure 5-17 The fully developed spray length and cone angle at injection pressure 1,350 bar with the simulated speed (a) 1,500 rpm and (b) 2,000 rpm.

The injection timing and duration with the simulated speed 1,500 and 2,000 rpm and ambient temperature 25^{o}C are shown in Figure 5-18 and 5-19 respectively. The spray images show the injection time in which the fuel is injected from the nozzle. At simulated speed 1,500 rpm, the images show that the injector is energized for T1 from 0.5 to 0.8 ms, T2 from 1.2 to 1.5 ms and T3 from 2.1 to 3.3 ms as well as the simulated speed 2,000 rpm, the injector are driven for T1 from 0.5 to 0.7 ms, T2 from 3.2 to 3.5 ms and T3 from 3.6 to 5.4 ms.

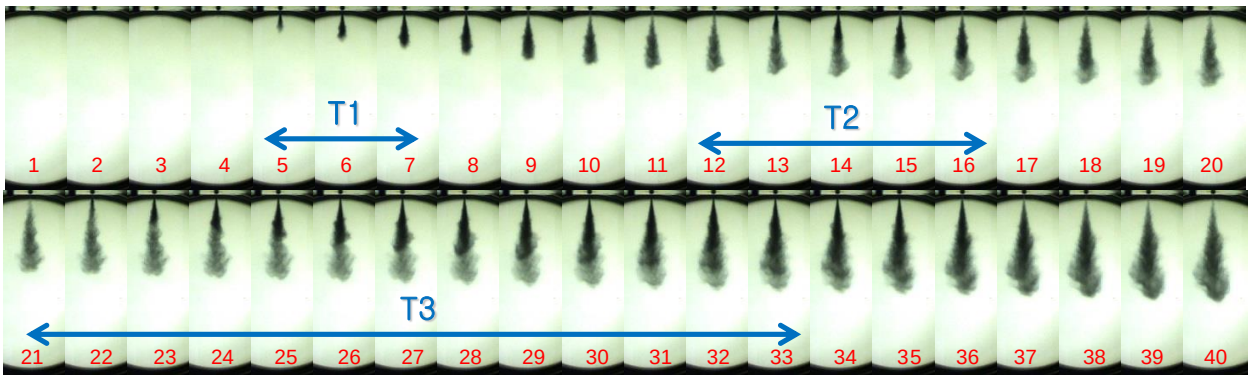

Figure 5-18 Fuel injection times (x 0.1 ms) of 1,500 rpm at 25^{o}C (GB05@1350 bar).

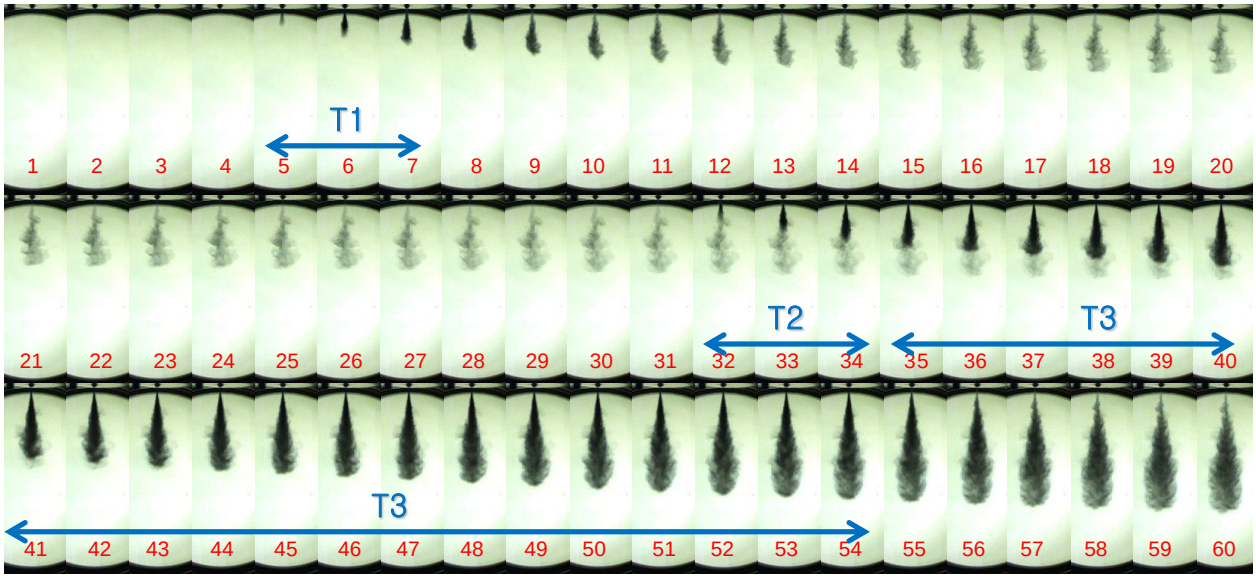

Figure 5-19 Fuel injection times (x 0.1 ms) of 2,000 rpm at 25^{o}C (GB05@1350 bar).

The spray penetration lengths and the spray cone angles are clearly specified by using the image processing. With the simulated speed 1,500 rpm and injection pressure 800-1,350 bar, GB00-20 and B100 show the similar patterns during T1, T2 and T3.

With the simulated speed 1,500 rpm, the spray penetration lengths of GB00-20 are in the vicinities due to the low concentration of biodiesel. When GB00-20 are compared with B100, their spray penetration lengths are slightly longer at the injection periods of T2 and T3 as shown in Figure 5-20-22(a). At the simulated speed 2,000 rpm, there is no significant difference of the spray penetration lengths between the blended fuels and B100 at all injection timing due to continuous injection period of T2 and T3 as shown in Figure 5-20-22(b)

The spray cone angles at injection pressure 800-1,350 bar with the simulated speed 1,500 and 2,000 rpm are shown in Figure 5-23-25 (a) and (b). The results exhibit that the similar trends are observed for all tested fuels. At the T1 injection period, the spray cone angles of all test fuels fluctuate and relatively broaden. According to Table 5-1, when the percentage of biodiesel is increased in the gasoline, the density of the blends increases due to the higher density of the biodiesel. The GB blends have lower density when compared with the Korean standard (815-835 kg/m^3) [88]. Thus, higher density results in larger fuel flow resistance which is the cause of higher viscosity.

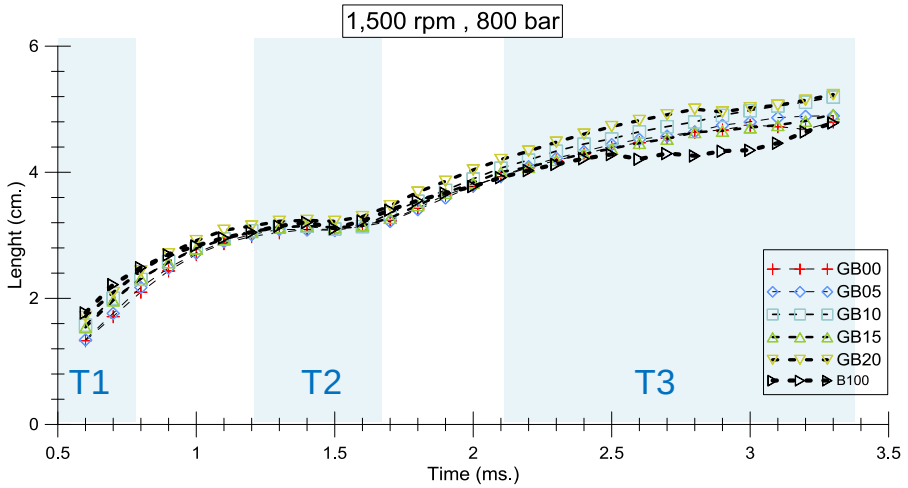

(a)

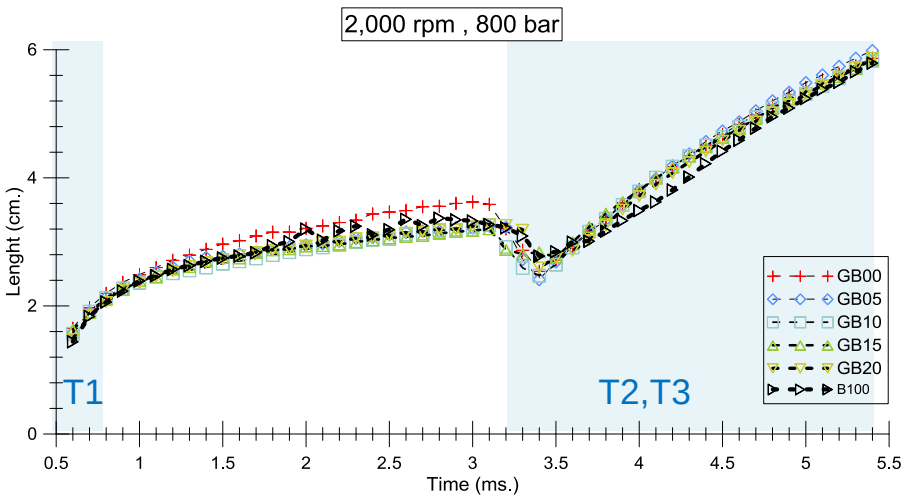

(b)

Figure 5-20 The spray length at injection pressure 800 bar with the simulated speed (a) 1,500 rpm and (b) 2,000 rpm.

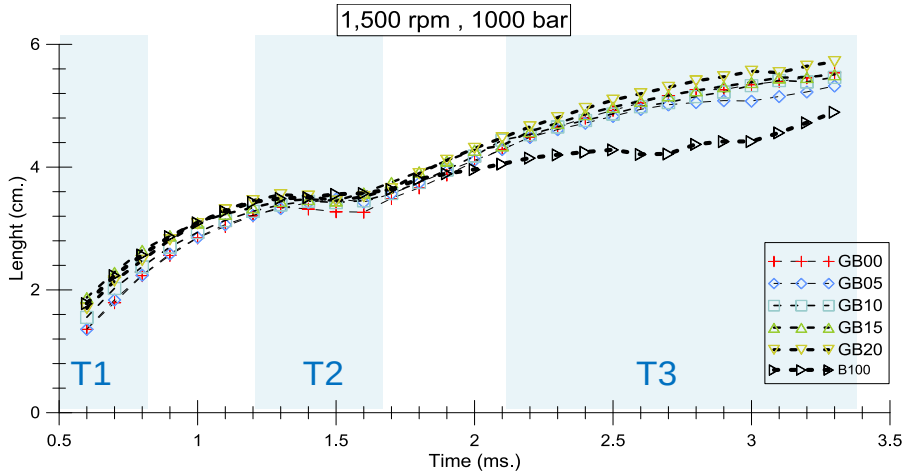

(a)

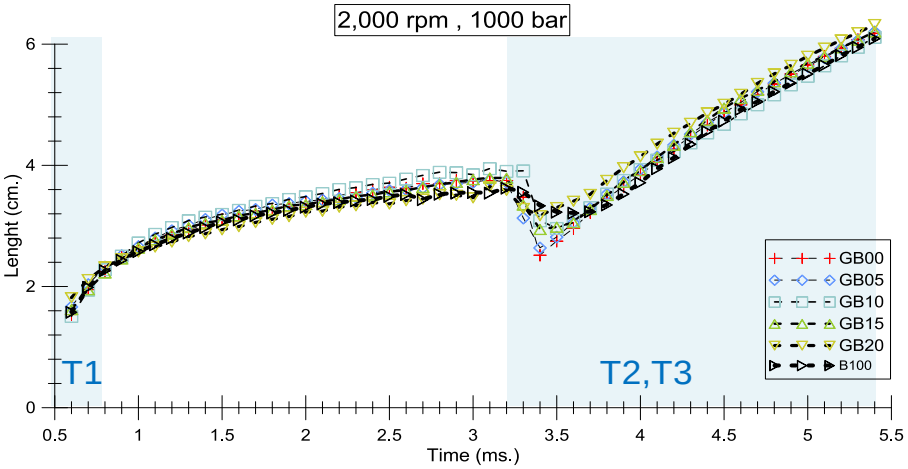

(b)

Figure 5-21 The spray length at injection pressure 1,000 bar with the simulated speed (a) 1,500 rpm and (b) 2,000 rpm.

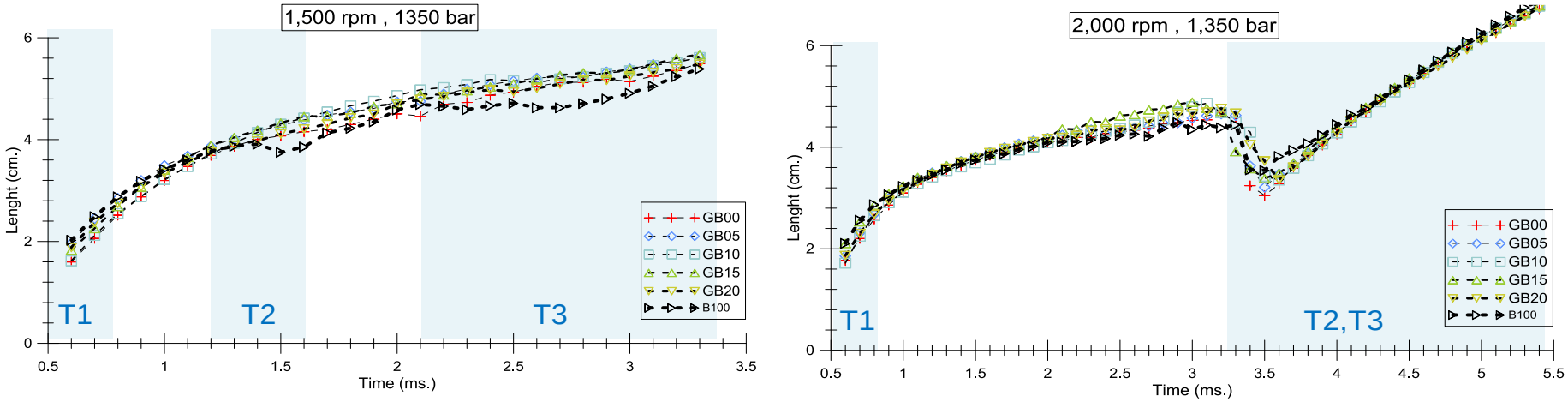

(a) (b)

Figure 5-22 The spray length at injection pressure 1,350 bar with the simulated speed (a) 1,500 rpm and (b) 2,000 rpm.

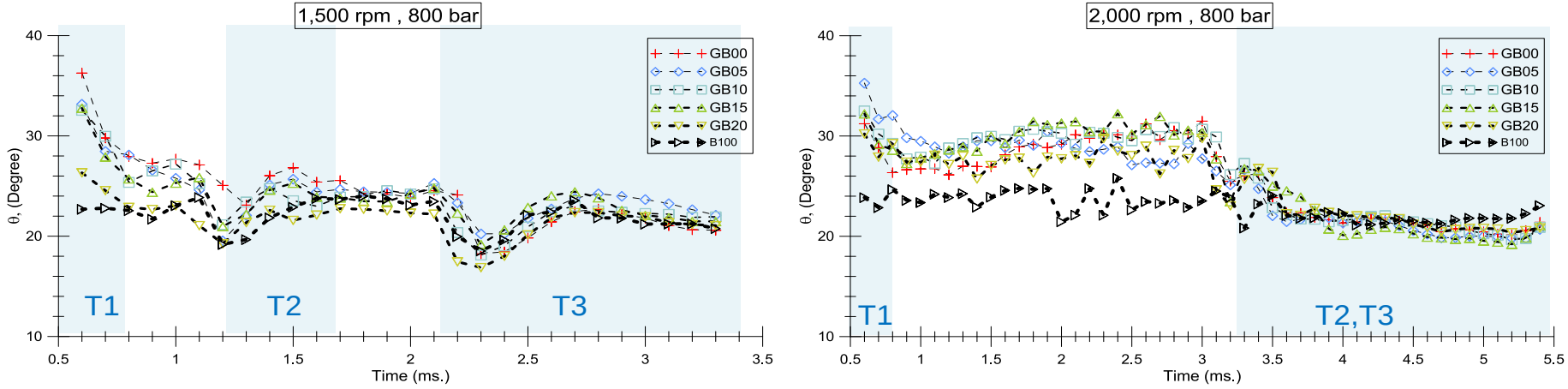

(a) (b)

Figure 5-23 The spray angle at injection pressure 800 bar with the simulated speed (a) 1,500 rpm and (b) 2,000 rpm.

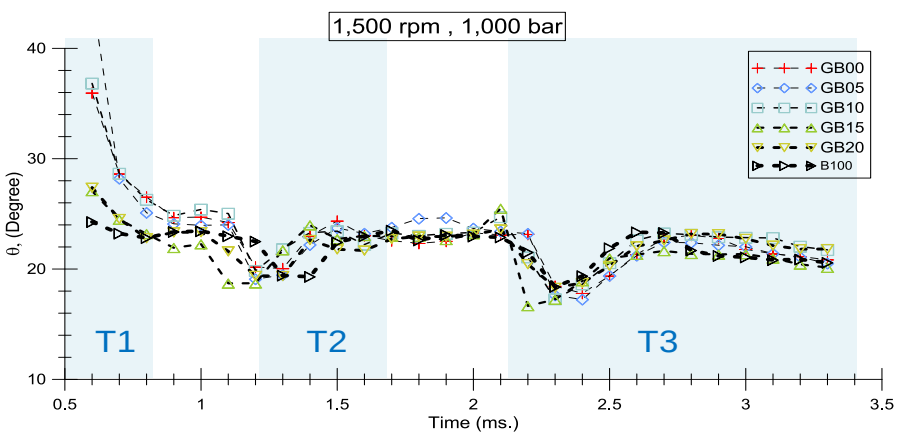

(a)

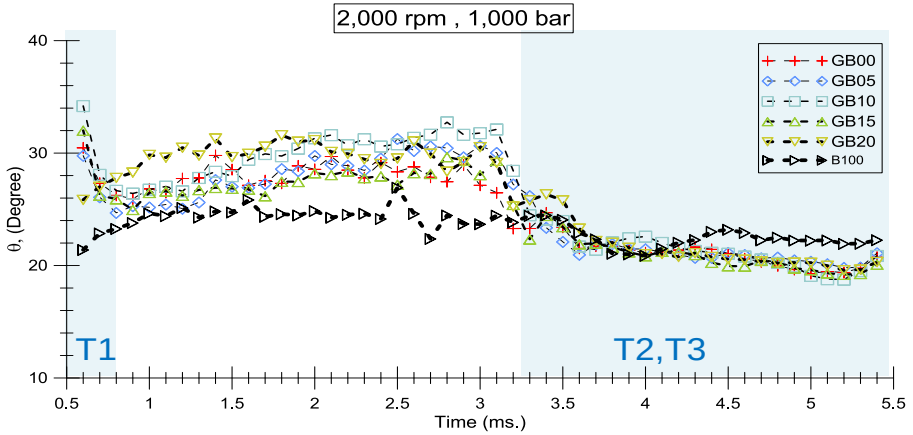

(b)

Figure 5-24 The spray angle at injection pressure 1000 bar with the simulated speed (a) 1,500 rpm and (b) 2,000 rpm.

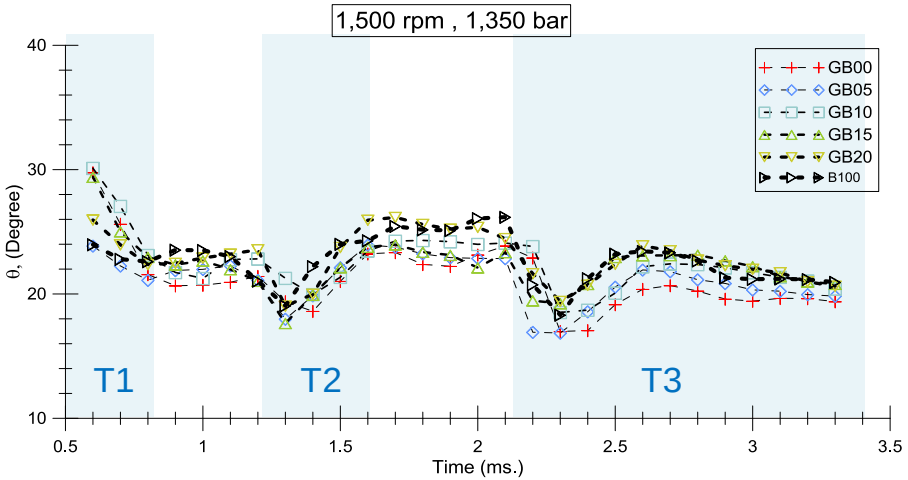

(a)

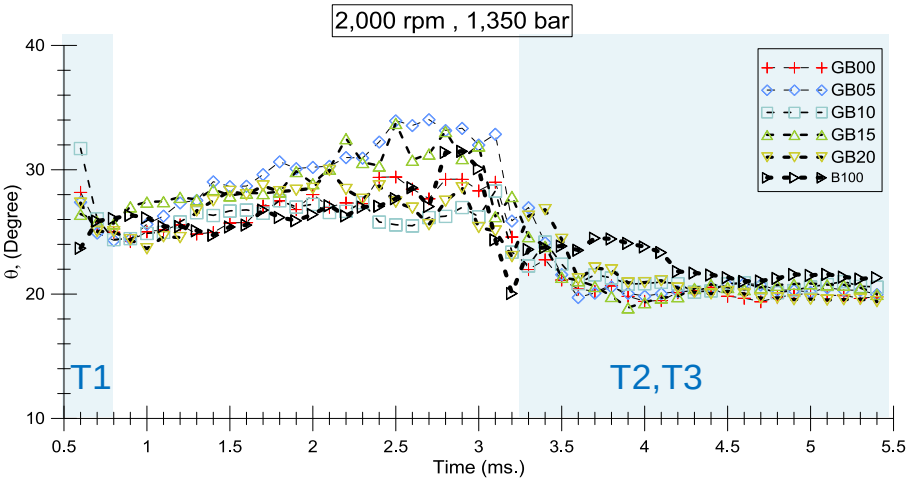

(b)

Figure 5-25 The spray angle at injection pressure 1,350 bar with the simulated speed (a) 1,500 rpm and (b) 2,000 rpm.

The kinematic velocity of neat biodiesel is higher than neat gasoline. Therefore, it may lead to inferior fuel injection [66]. Meanwhile, GB00 at the injection periods of T2 and T3 shows the smallest spray cone angle due to its low density and viscosity value. Whereas, the B100 has the biggest spray cone angle which is similar to GB20. In addition, the cone angles of GB05-15 locate between GB00 and B100 values.

At the simulated speed 2,000 rpm and injection pressure 1,350 bar, the spray cone angles at the T1 injection period also fluctuate like the spray cone angles with the simulated speed 1,500 rpm. The spray cone angle of the GB00-20 at the injection periods of T2 and T3 are lower than B100 due to density and viscosity. The spray cone angles of all tested fuel become narrow angle at the end of T3 injection period.

Moreover, the spray penetration lengths and the spray cone angle of injection pressure 800 and 1,000 bar with the simulation speed 1,500 and 2,000 rpm showed the similar trends with the injection pressure at 1,350 bar.

5.2.2.2 Conclusion

The results of spray penetration length and spray cone angle can be concluded as following:

- GB00-20 and B100 at high injection pressure show the same spray penetration length and the spray cone angle patterns when the blended fuels are injected by diesel common rail injection system.

- During the injection duration T3, the spray penetration length of B100 at 1,350 bar with simulation speed 1,500 rpm is lower than GB00-20. However, there is no significant difference in the spray penetration length between B100 and GB00-20 at 2,000 rpm and 1,350 bar.

- For the spray cone angle, B100 is bigger than that of blended fuels.

5.2.3 Macroscopic/microscopic structure of gasoline spray added biodiesel 5% injected with a single-hole common rail diesel injector by varying injection pressure

This research studies the macroscopic/microscopic structure of gasoline spray added biodiesel 5% injected with a single-hole common rail diesel injector by varying injection pressure in order to further utilize on compression ignition engines. To reduce the NO_X/PM trade-off emission, gasoline used in a compression ignition (CI) engine called gasoline compression ignition (GCI) combustion has stimulated many researchers to investigate. Because gasoline is injected directly into the combustion chamber, its spray has a significant effect on the combustion and emission of engines. Therefore, the spray characteristics of gasoline were studied in this research. Due to its low lubricity, gasoline was added with 5% of biodiesel (GB05), as the lubricity enhancer, to prevent the failure of the high-pressure common rail injection system, which used in the CI engine. The macroscopic spray structures were investigated through Schlieren photography and planar laser-induced fluorescence – particle image velocity (PLIF-PIV) techniques. The injection pressure was handled by a conventional common rail diesel system while ambient pressure (back pressure) was controlled by supplying nitrogen gas into the constant volume combustion chamber (CVCC). The effects of injection and ambient pressure on the gasoline spray were clarified by taking advantage of image processing. In addition, the magnitude of spray variation was compared with the variation of diesel spray. The results show that the spray penetration tip of gasoline increased with the increased injection pressure and decreased with the increased ambient pressure as the diesel spray. The cone angles for both fuels decreased with the increased injection pressure. However, the injection pressure had the effect on the diesel spray higher than gasoline at the low ambient pressure. The cavitation seemed to induce for gasoline injection. Moreover, PLIF-PIV images show the remarkable turbulent structure of gasoline spray under the higher injection pressure.

5.2.3.1 Results and discussion

Spray characteristics

Figure 5-26 presents the effect of different injection pressure (between rows) and the ambient pressure (between columns) on the spray developing patterns of GB05 from the raw images. Considering on the left-hand side of the Figure 5-26, the influence of injection

pressure at the ambient pressure of 10 bar is clearly observed, like those of the right-hand side presented for 50 bar ambient pressure condition.

In addition, the effect of ambient pressure when comparing between two columns is significantly noticed for all injection pressures. When injection pressure was increased from 500 to 750 and 1,000 bar at ambient pressure of 10 bar, the spray tip impacted on the chamber. Hence, there is a high chance of wall/piston impingement. However, when the ambient pressure (back pressure) was increased to 50 bar, the spray could not travel to strike the chamber. The following section has discussed in detail of the macrostructure of the spray, quantified from Figure 5-26. Furthermore, the characteristics of diesel spray have been included for reference. Unfortunately, the results of GB05 and diesel derived from the different technique. Therefore, it is impossible to compare the spray of GB05 and diesel. However, the effect of injection pressure and ambient pressure on the variation of GB05 and diesel spray can be drawn.

The spray penetration lengths when varying injection pressure and back pressure are presented in Figure 5-27; GB05 is exhibited on the left-hand side while diesel is illustrated on the right (throughout this paper). For the top row, the ambient pressure was kept constant at 10 bar whereas the bottom row indicates the data at 50 bar of back pressure (throughout this paper).

When the injection pressure is increased, the momentum flux is increased. As the results, the spray lengths increased for both fuels and both ambient pressures. At the lower back pressure of 10 bar, the spray length reached the maximum value at the injection pressure of 750 and 1,000 bar for both test fuels due to the chamber impingement as seen in Figure 5-26. However, at ambient pressure of 50 bar, the length continued to increase without striking on the chamber because the increased drag force by the air surrounding resisted the momentum flux of liquid spray, thus lowering the spray penetration. Therefore, the lengths of the spray at the higher back pressure were lower than those of lower conditions at the same injection pressure.

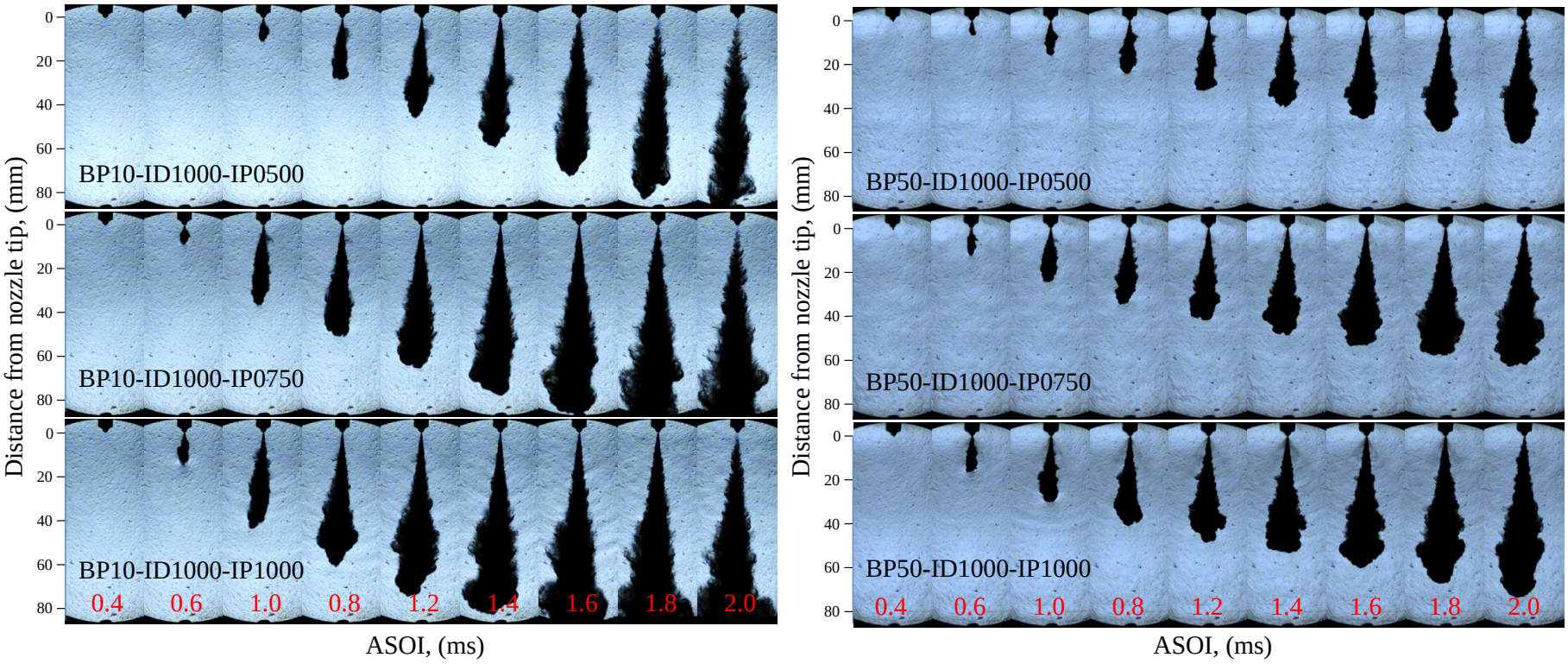

Figure 5-26 Spray developing patterns of GB05 under back pressure (a) 10 bar and (b) 50 bar with injection duration 1,000 μs. injection pressure 500, 750 and 1,000 bar.

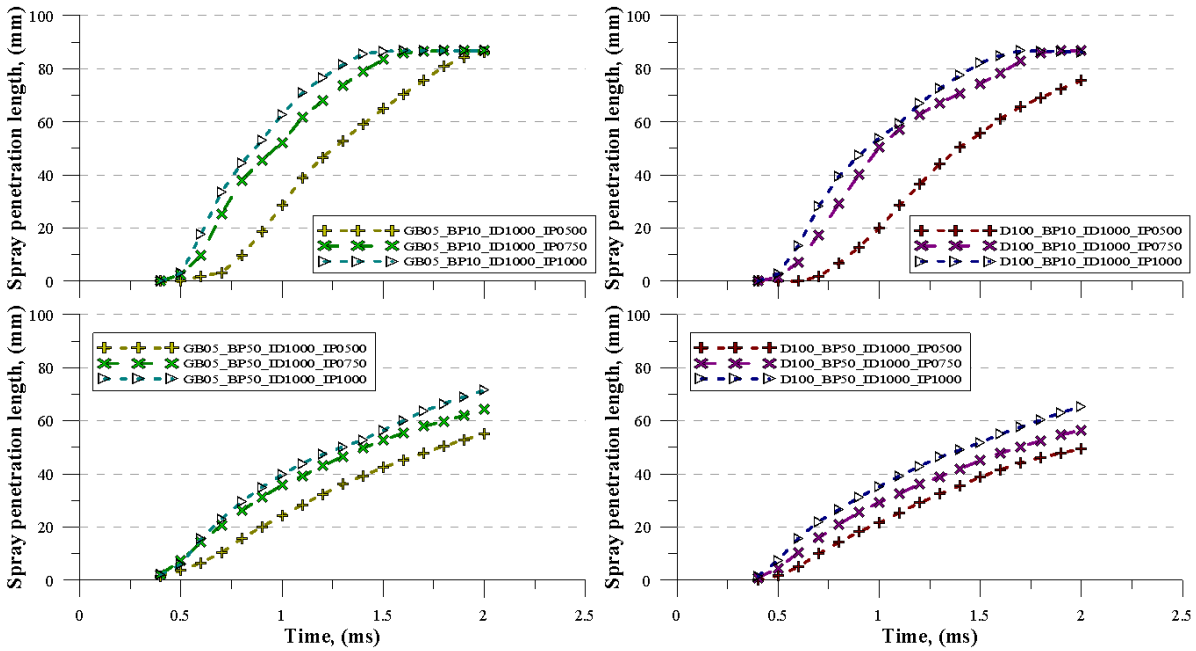

(a) (b)

Figure 5-27 Spray penetrations of (a) GB05 and (b) D100 with injection duration 1,000 μs. at back pressure 10 and 50 bar and injection pressure 500, 750 and 1,000 bar.

The effects of injection pressure and the ambient pressure on the cone angle of GB05 and D100 with injection duration of 1,000 μs are presented in Figure 5-28. Due to the instability of the spray during the beginning of the injection, the cone angle at this period could not be analyzed and compared. For instance, at the beginning of injection, the spray cone angle of D100 around 0.75 ms at back pressure of 10 bar exhibited the slightly narrow cone angle. It might be explained that the fuel spray was affected by the operating transition zone (opening and closing needle) in which the dynamic of the injector needle was heavily influenced by fluid viscosity. Due to the higher viscosity of diesel than those of gasoline, the needle was resisted and opened later. When the needle is lifting, the instability of the spray is formed and results in the difficulty of the analysis. It could be the cause of the spray cone angle increasing or decreasing easily [89].

GB05 showed the same trend as D100 in which the cone angle was decreased when the injection pressure was increased. The cone angle correlates well with the spray penetration length as suggested by the previous study [90] calculated by the following equation.

$$S(t) = K \cdot {\rho_a}^{-1/4} \cdot {M_0}^{1/4} \cdot t^{1/2} \cdot \tan^{-1/2}\left(\frac{\theta}{2}\right) \quad (5.5)$$

Where *K* is a constant depending on the spray internal distribution, ρ_a is gas density, t is time, M_0 is momentum flux and θ is spray angle.

With the narrower cone angle, the spray can travel with the longer distance. On the other hand, the short penetration tip couples with the broaden spray cone angle. This correlation can be clearly proven in the case of the back pressure of 10 bar. Following the large difference of the liquid spray length, the cone angle also showed the large difference between injection pressure of 750 and 500 bar. Note that the large difference is significantly noticed at the early stage of the injection period. This could attribute to the injection rate in which higher injection pressure accelerates the steady state injection rate shape.

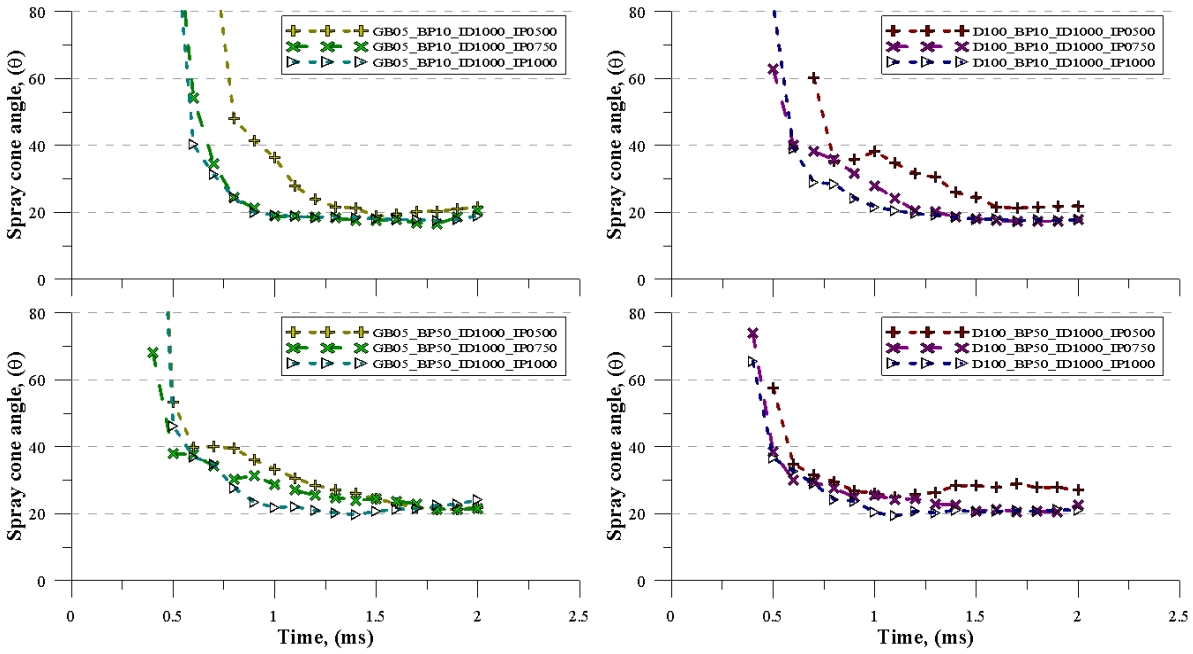

(a) (b)

Figure 5-28 Spray cone angles of (a) GB05 and (b) D100 with injection duration 1,000 µs. at back pressure 10 and 50 bar and injection pressure 500, 750 and 1,000 bar.

When compared to both test fuels, the injection pressure seemed to have more effects on the cone angle of D100. The increased injection pressure resulted in the decreased cone angle. However, for GB05, the cone angle at the injection pressure of 750 and 1,000 bar looked

similar. This is due to the cavitation formation. At low ambient pressure, the cavitation readily happens when the injection pressure is increased in particular for the non-viscous fuel like gasoline [91]. The cavitation leads to enlarging the cone angle [92]. This means that the cone angle, which decreased by the effect of injection pressure, is enlarged by the effect of cavitation phenomena. However, when the ambient pressure increases, the cavitation is hardly induced due to the lower pressure difference. Therefore, the effect of injection pressure on GB05 looked similar to diesel fuel.

As seen in Figure 5-29, the injection and back pressure affected the spray area as the same penetration length. When the injection pressure increased, the spray area increased due to the increased spray length. In addition, the tip of the spray seemed to broaden as in Figure 5-26 because the fuel with the high momentum flux was easily dispersed. The fuel vaporization should easily happen for the spray having the larger area. On the other hand, with the increased ambient pressure, the decreased penetration length was the major cause of the decreased spray area. This means that the evaporation of fuel will be inhibited.

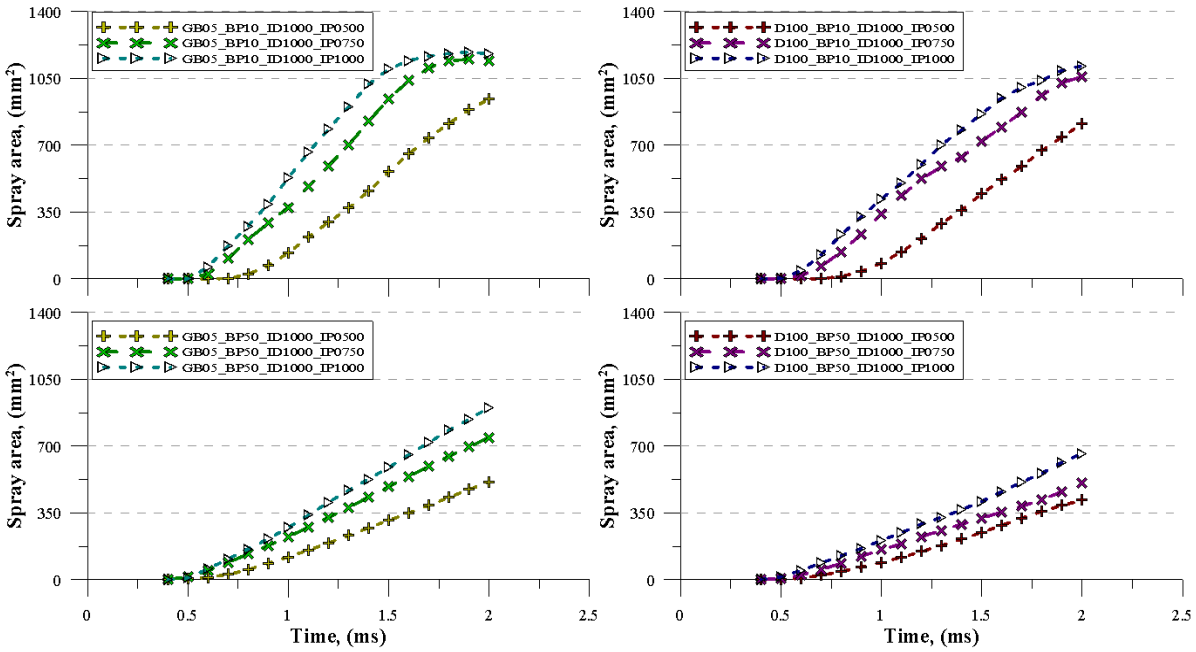

(a) (b)

Figure 5-29 Spray area of (a) GB05 and (b) D100 with injection duration 1,000 μs. at back pressure 10 and 50 bar and injection pressure 500, 750 and 1,000 bar.

Figure 5-30 shows the average speed of spray under back pressure 10 and 50 bar. The average speed of blended fuel trends to increase when injection pressure increases. The spray

injected with injection pressure 1,000 bar under backpressure 10 bar shows the highest average speed due to low ambient density and low momentum flux. On the other hand, the lowest average speed is observed under the back pressure 50 bar and injection pressure 500 bar due to high ambient density and high momentum flux. The average speed rapidly increases in the range of 0.3-1.0 ms of the start of injection (speedy zone) and results in the maximum average speed. After the speedy zone, the average speeds slightly decreases until the end of injection timing. The behavior of average speeds of GB and neat diesel fuel under back pressure 10 and 50 bar are similar.

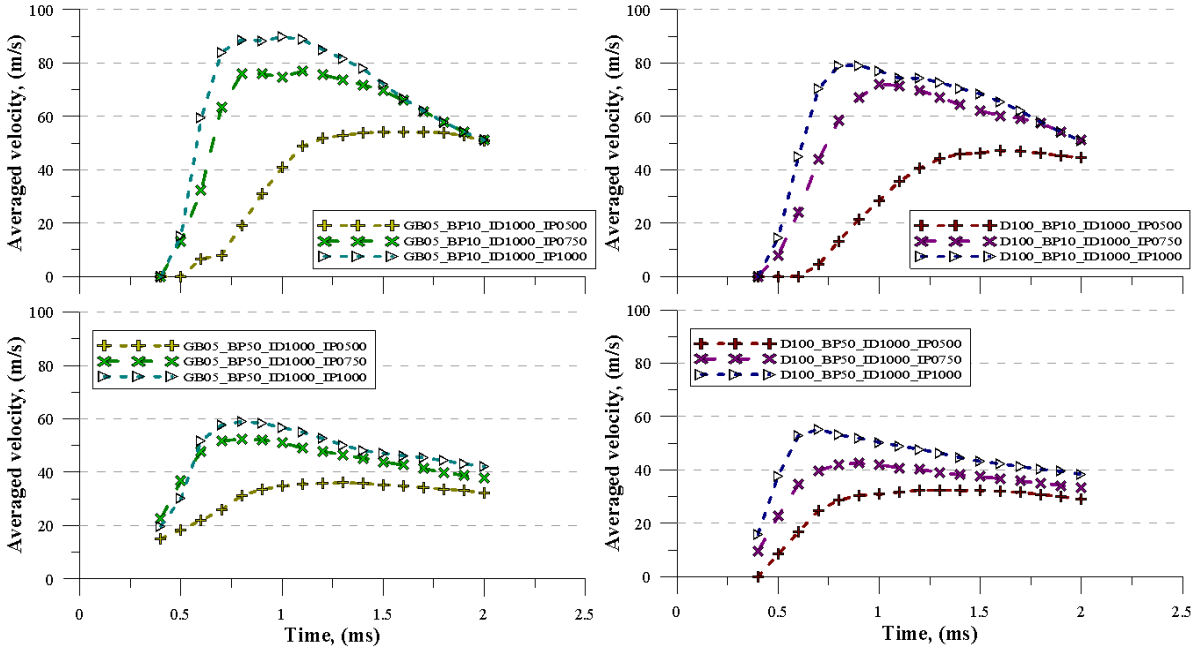

(a) (b)

Figure 5-30 Average velocity of spray penetration of (a) GB05 and (b) D100 with injection duration 1,000 μs. at back pressure 10 and 50 bar and injection pressure 500, 750 and 1,000 bar.

Figure 5-31 shows the instantaneous speed under back pressure 10 and 50 bar. The instantaneous speed of GB05 and neat diesel fuel tends to increase when injection pressure increases. The highest instantaneous speed is observed at the lowest backpressure 10 bar and the injection pressure at 1,000 bar. On the other hand, at the back pressure 50 bar and the lowest injection pressure 500 bar, the free spray has the slowest instantaneous speed. At 0.3 ms of the start of injection, the instantaneous speeds immediately increase and continuously boost the instantaneous speed. It results in the maximum instantaneous speed at 0.7-1.0 ms

with the same speedy zone in the average speed. Then, the instantaneous speed drastically decreases until the end of injection timing. The similarity of instantaneous speeds of GB and neat diesel fuel are found at the same injection pressure and back pressure.

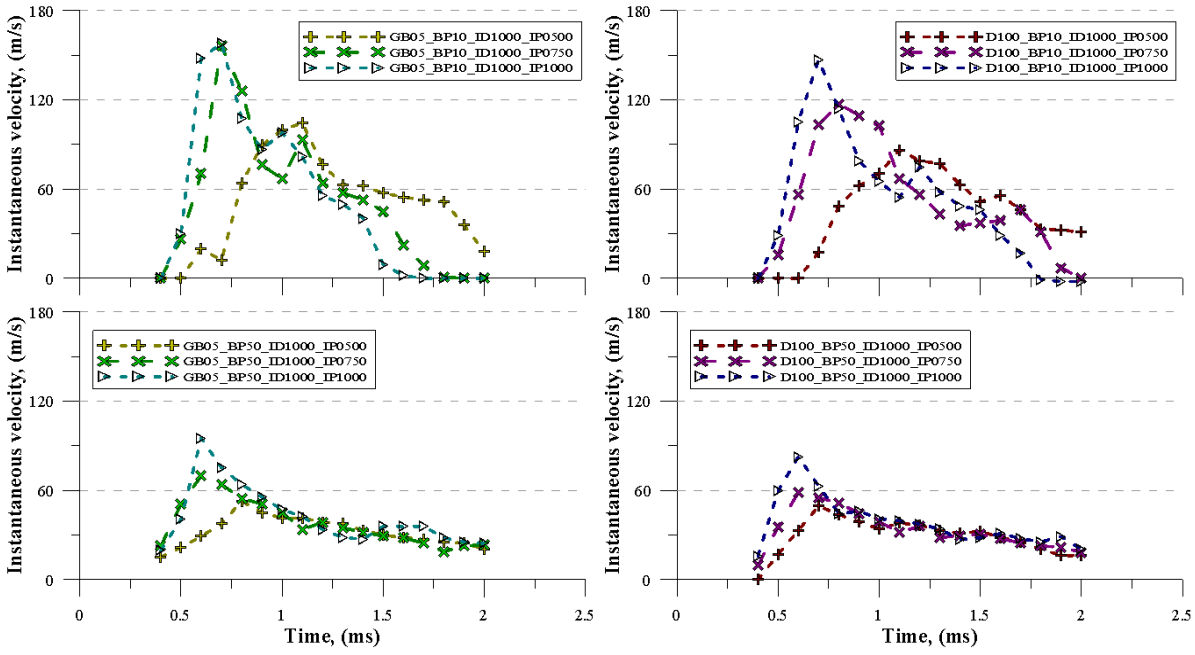

(a) (b)

Figure 5-31 Instantaneous velocity of spray penetration of (a) GB05 and (b) D100 with injection duration 1,000 μs. at back pressure 10 and 50 bar and injection pressure 500, 750 and 1,000 bar.

GB05 spray structure

The PLIF-PIV technique was adopted to investigate the internal spray structure of GB05 fuel. The PLIF-PIV images of GB05, illuminated by the DPSS laser sheet, were recorded by using the high-speed camera. Then, the PLIF-PIV images with the light intensity were converted to the pseudocolor images with 256 levels of colors by using MatLab software to analyze the spray structure. The light intensities of PLIF-PIV images were divided into 256 levels in which 255 is taken to be red and 0 is taken to be black. It means that the pixel having the level color of 256 presents the location of high spray concentration, and no spray droplet is detected at the pixel having the level color of 0. As shown in Figure 5-32, for all test conditions, the dense spray which is the presumable liquid core, which illustrated in the red color, positioned at the center of the spray and slightly right-hand side where the laser source was located and emitted. At the low ambient pressure of 10 bar in Figure 5-32(a), the

liquid jets were observed since the needle started to open. As the needle was continuously lifted, the liquid lengths increased which corresponds to the above results of the spray penetration tip. Finally, the dense spray/liquid core slightly diminished and disappeared when the time passed. At the lower injection pressure of 500 bar, the liquid jet was disappeared sooner than that of the high injection pressure.

Like the low ambient pressure, the liquid jets at the high back pressure of 50 bar in Figure 5-32(b) were detected since the beginning of the spray development process. Then, the liquid length increased with the increased timing. However, unlike the low ambient pressure condition, the liquid jet kept the constant length after the spray reached the quasi-steady state and still remained in the internal spray until the last image captured for all injection pressures. The back pressure significantly affects the spray structure by compressing it in the confined area**.** It is difficult for the fuel to distribute throughout the whole spray and mix with air. As the results, the internal spray structure consists of almost dense spray.

To clearly understand the effects of injection pressure and the back pressure on the internal spray structure, the images taken after the needle fully closed for all test conditions in Figure 5-32 were selected and transformed into 25 contour lines with 256 levels of colors to define the fuel mass concentration boundary as presented in Figure 5-33. The black contour line corresponds to the lowest light intensity, indicating the low spray density area. On the other hand, the red contour line correlates to the highest light intensity, representing the high spray concentration area. The results show that at the ambient pressure of 10 bar, the internal spray structure is approximately asymmetric where the liquid core located at the center. The fuel mass concentration was gradually decreased along the radial direction and downstream of the spray.

At the ambient pressure of 50 bar, the dense spray dominated almost the whole spray area and slightly the right-hand side, in particular at the low injection pressure. More dense spray located near the laser source resulted in the attenuated light at the far area. At the injection pressure of 750 and 1,000 bar, the spray periphery shows a small wavy motion. It might be explained that when the fuel is injected into the surrounding air, some earlier fuel sprays are decelerated, and moved upward as the vortex motion [93]. The fuel droplets in this vortex region formed into the stagnated point. When the later injected part of the fuel reaches this area, it developed the movement to avoid the stagnated point, or it intercepts with the earlier injected part of fuel. Therefore, the later part is bent like the buckling shape.

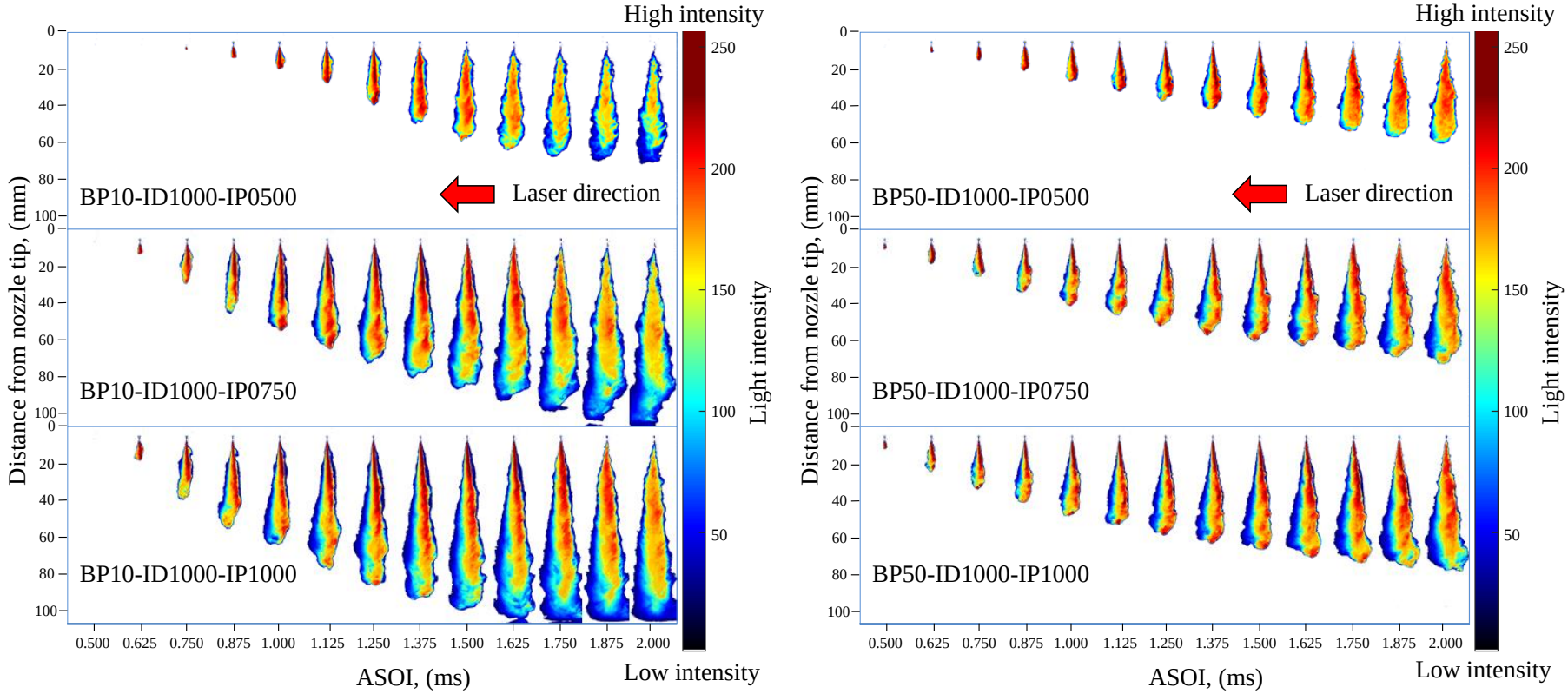

(a) (b)

Figure 5-32 PLIF-PIV image with the pseudocolor of free sprays of GB05 under back pressure (a) 10 bar and (b) 50 bar with injection duration 1,000 μs, and injection pressure 500, 750 and 1,000 bar.

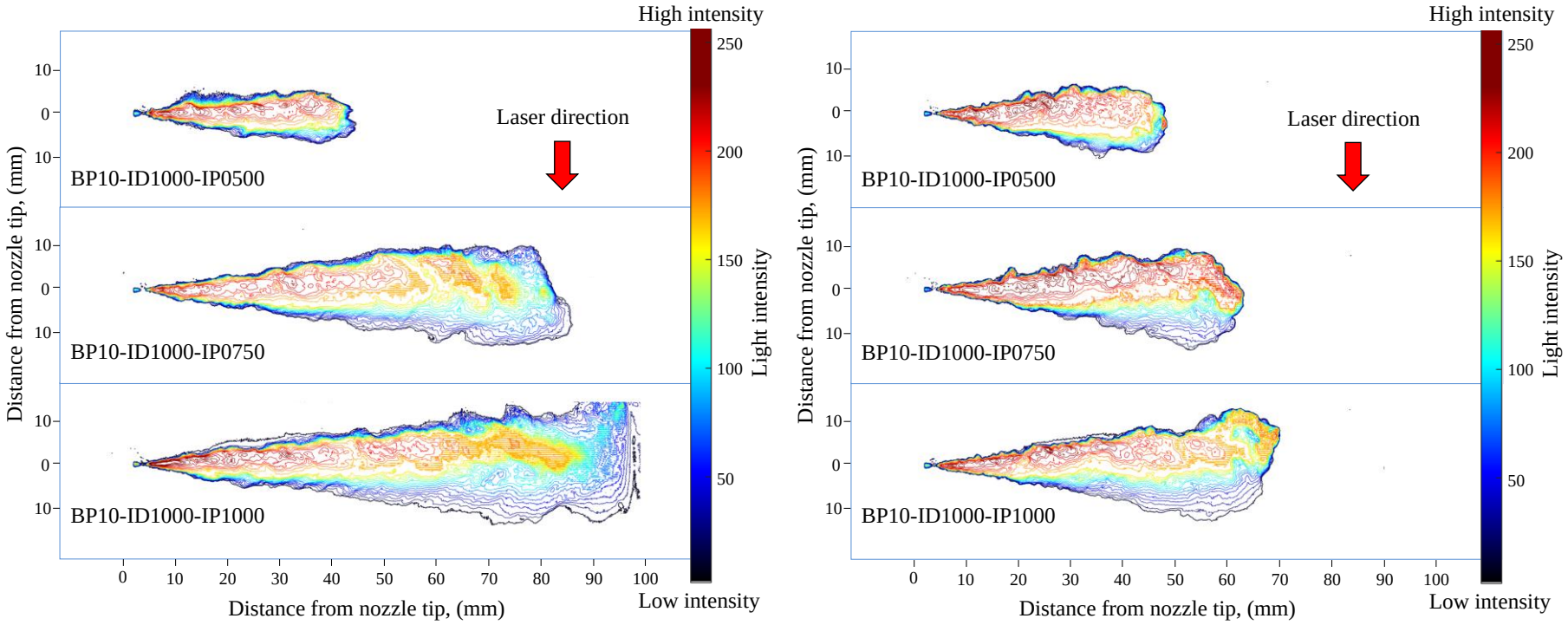

Figure 5-33 The distribution of GB05 spray density under back pressure (a) 10 bar and (b) 50 bar with injection duration 1,000 μs and injection pressure 500, 750 and 1,000 bar.

The flow fields of GB05 spray

Figure 5-34 illustrates the spray internal flow of GB05 which characterized by the vector (velocity) and vorticity distribution at the injection pressure of 500 bar and the back pressure of 10 bar. The whole shape of PLIF-PIV spray image at 2.5 ms ASOI is shown in Figure 5-34 (a) while Figure 5-34 (b) and (c) is the vector and vorticity located in the downstream part of the spray in the range of 35 to 75 mm from the injector tip, which is magnified and analyzed. As shown in Figure 5-34(b) in the red circle, the spray droplets were pushed aside from the streamline and moved upward forming the large scale vortex motion at the side periphery like the diesel spray [94]. These vortex motion areas correspond to the recirculation zone of the surrounding gas flow, hint spray-induced gas flow field [95]. The droplets of the downstream spray at the side periphery which injected earlier lose the momentum and they were forced to the radial direction outward from the core by the successive higher momentum droplets. At the same time, the ambient air resisted the movement of the spray droplet and deviated the spray movement to the upward direction.

The location at which the large scale vortexes happen (in the red circle (b)) is the area of the highest vorticity (c). The rotating movement of the vortex, occurred at the periphery of the spray, induced the surrounding air entrainment thus making fuel-air mixing in this area leaner as shown by the lower light intensity in the red circle (a). In the meanwhile, this vortex resulted in the stagnation of the nearby spray droplets, making the richer mixture formation as seen by the higher light intensity in the PLIF-PIV spray image (a). As the results, the heterogeneous air-fuel mixture distributed throughout the spray area and created the branch-like spray structure as defined by Azetsu et al [96].

Interestingly, the velocity vector at the end of the spray tip region of GB05 encircled by the dash red line in Figure 5-34(b) shows the reverse direction which is backward to the spray injector. This behavior could not be seen clearly in the diesel spray from the past research [94,97]. With the lower surface tension and viscosity of gasoline when compared with those of diesel, the fuel droplets of GB05 are readily broken. In addition, the fuel atomization and break up process are accelerated due to the higher air entrainment according to the low density of gasoline. It is possible that the air could entrain into the spray in this tip region. With the low momentum of the smaller droplets hints low inertia mass, the surrounding gas could against the traveling of the GB05 higher than the diesel spray.

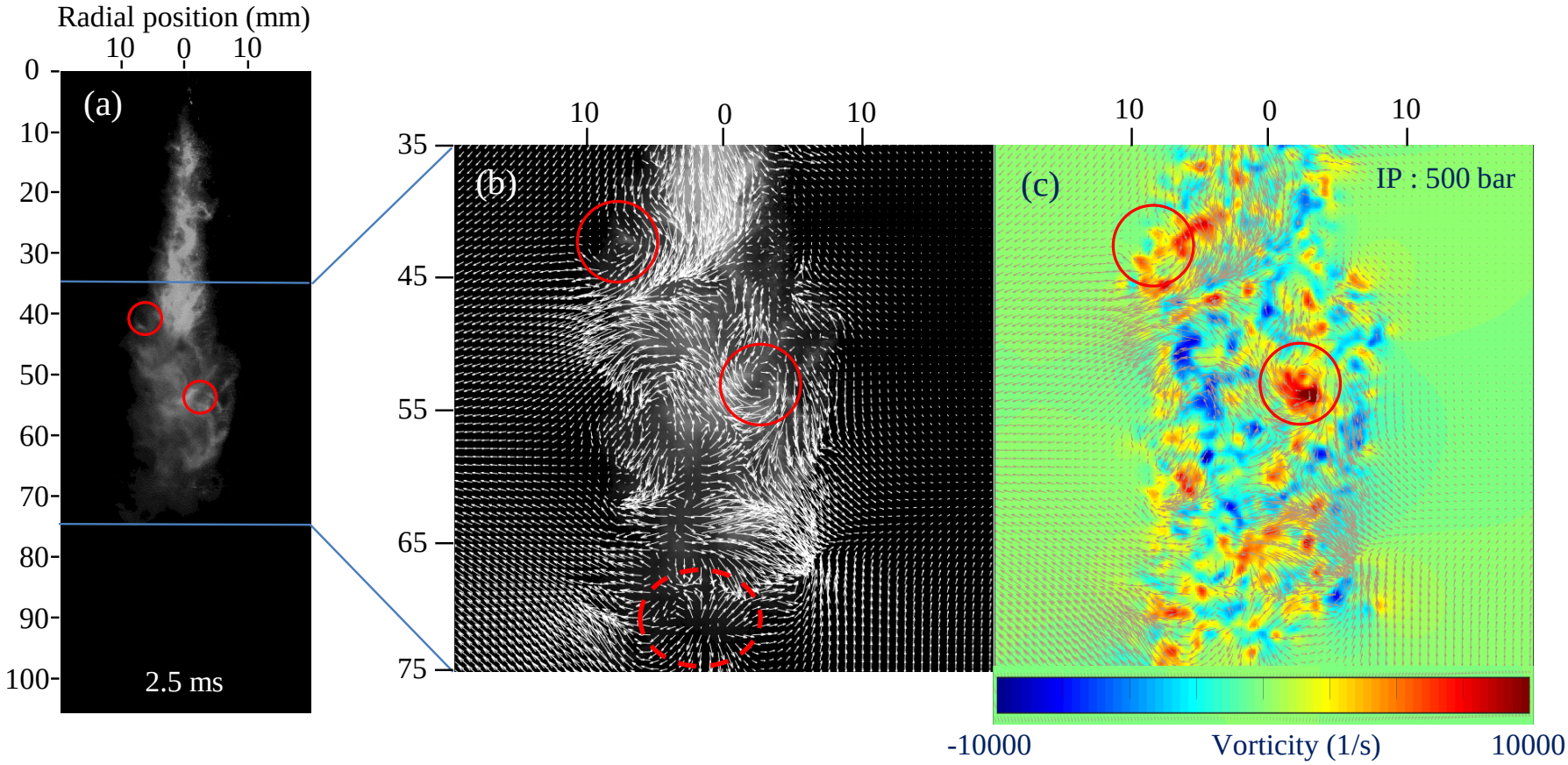

Figure 5-34 The vector and vorticity distribution of GB05 spray under the back pressure of 10 bar with the injection duration 1,000 μs and the injection pressure of 500 bar.

As the results, the GB05 droplets move back straightforward to the opposite direction of the streamline, not along the radial direction as seen in Figure 5-35. Meanwhile, the ambient gas resistance merely diverts the diesel spray from the axial direction as the bifurcate spray at the capturing section of the surrounding gas in the spray tip region [97].

The flow field of GB05 in the DI engine could not be compared with the gasoline spray in the gasoline direct injection (GDI) engine. Due to the different features of the injector and injection pressure, the characteristic of the reverse flow of GB05 could not be found in the gasoline spray in the GDI engine. The counter-rotating vortex motion in the periphery of the spray couples with the straightforward high velocity at the leading edge and the central part of the spray are the key features of gasoline spray injected via GDI system [98].

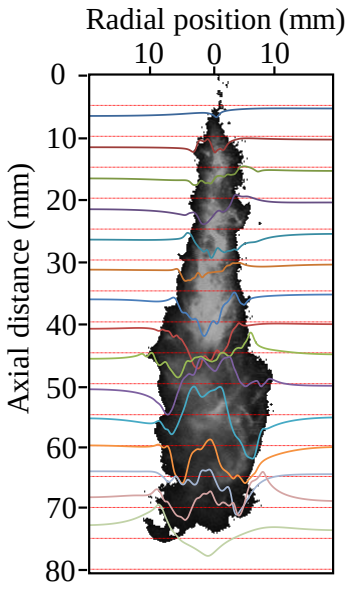

Figure 5-35 The asymmetrical profile of GB05 spray with the spray core at 2.5 ms (back pressure 10 bar and Injection pressure 500 bar).

Presented in Figure 5-35, calculated in the range of 5 to 75 mm with the increment of 5 mm from the injector tip, the axial velocity of GB05 spray showed the asymmetrical profile with the spray core. From 5 mm to 40 mm from the injector tip the axial velocity had only the positive value (the dash red line is the reference; below dash line is the positive value and vice versa). This means that all spray droplets move down to the bottom. Around 45 mm, the axial velocity indicated the negative value at the periphery of the spay with the marginal magnitude while at the 50 and 55 mm the large negative values of axial velocity were seen. The negative velocity relates to the direction of the vector which turns backward to the

injector tip, thus corresponding with the location of the vortex motion. At the end of the spray tip around 70-75 mm, the axial velocity had the negative value around the spray axis which is the same location of the reverse vector shown in Figure 5-34(b).

The effects of injection pressure on the spray flow at the back pressure of 10 and 50 bar are shown in Figure 5-36 and 37, respectively. As can be seen from the time-resolved spatial distribution of the vector and vorticity, the spray at 2.5 ms ASOI showed the higher number of large and small scale vortex than that of 2.0 ms ASOI which showed the higher vortex distribution than that of 1.5 ms. At the earlier injection timing, the surrounding/ambient gas was not perturbed by the injected spray. There are less fuel-air interfaces and interactions.

At the same ambient pressure, when the injection pressure increased, the number and the intensity of the large scale vortex increased. Hint, the higher vorticity occurred. At the higher injection pressure, the spray could travel with the longer penetration tip and the higher speed due to the higher momentum flux. This leads to more drag force to resist the moving spray and turned the axial velocity flow to the radial direction thus forming the vortex and vorticity. In addition, the small scale vortex motion was induced to be created throughout the whole spray. The spray is developed with the high turbulence motion and fluctuation. Consequently, the mixture formation process is enhanced. Compared at each injection pressure in Figure 5-38, when the injection pressure increased, the axial velocity profile calculated at the time of 2.0 ms ASOI presented the first negative value at the distance of the spray shorter than those of the low injection pressure. At injection pressure of 500 bar, the negative velocity was firstly seen at 35 mm from the injector tip while the injection pressure of 750 bar indicated the minus sign of axial velocity at 25 mm. Particularly, the injection pressure of 1000 bar showed the radial flow filed of the spray at 5 mm at which the shortest distance plane from the tip was analyzed. The droplet size of the spray decreases as the injection pressure increases due to the high shear rate. Therefore, the air entrainment could exist earlier in the entrainment section and attempts to push the spray bending to the radial direction thus creating the vortex motion. At the longer distance of the spray, the minus axial velocity distributed along with the radial direction corresponding with the higher number of the vortex created throughout the spray.

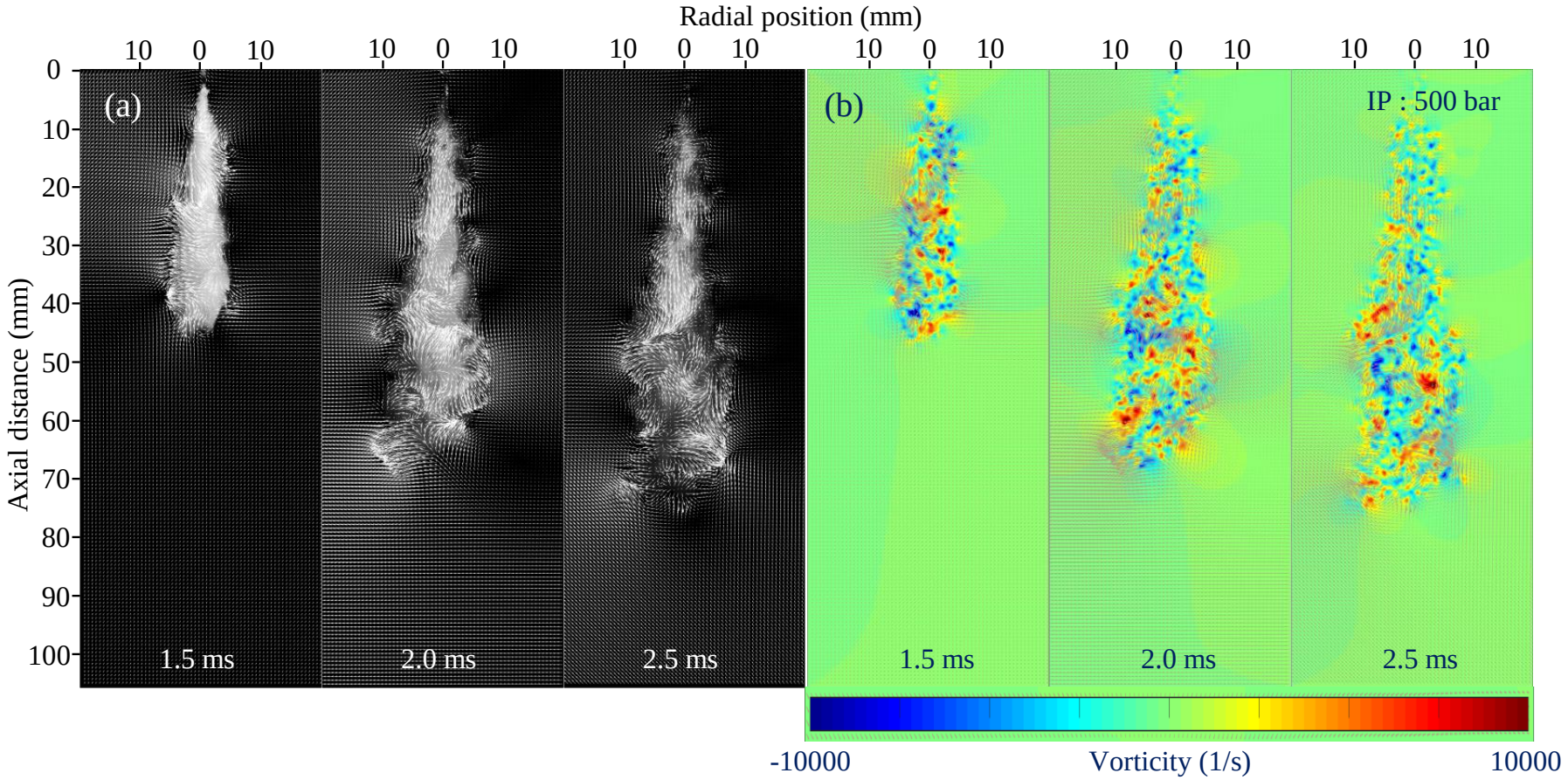

Figure 5-36 The vector (a, c and e) and vorticity distribution (b, d and f) of GB05 spray under the back pressure of 10 bar with the injection duration of 1,000 μs, and the injection pressure of 500, 750 and 1,000 bar.

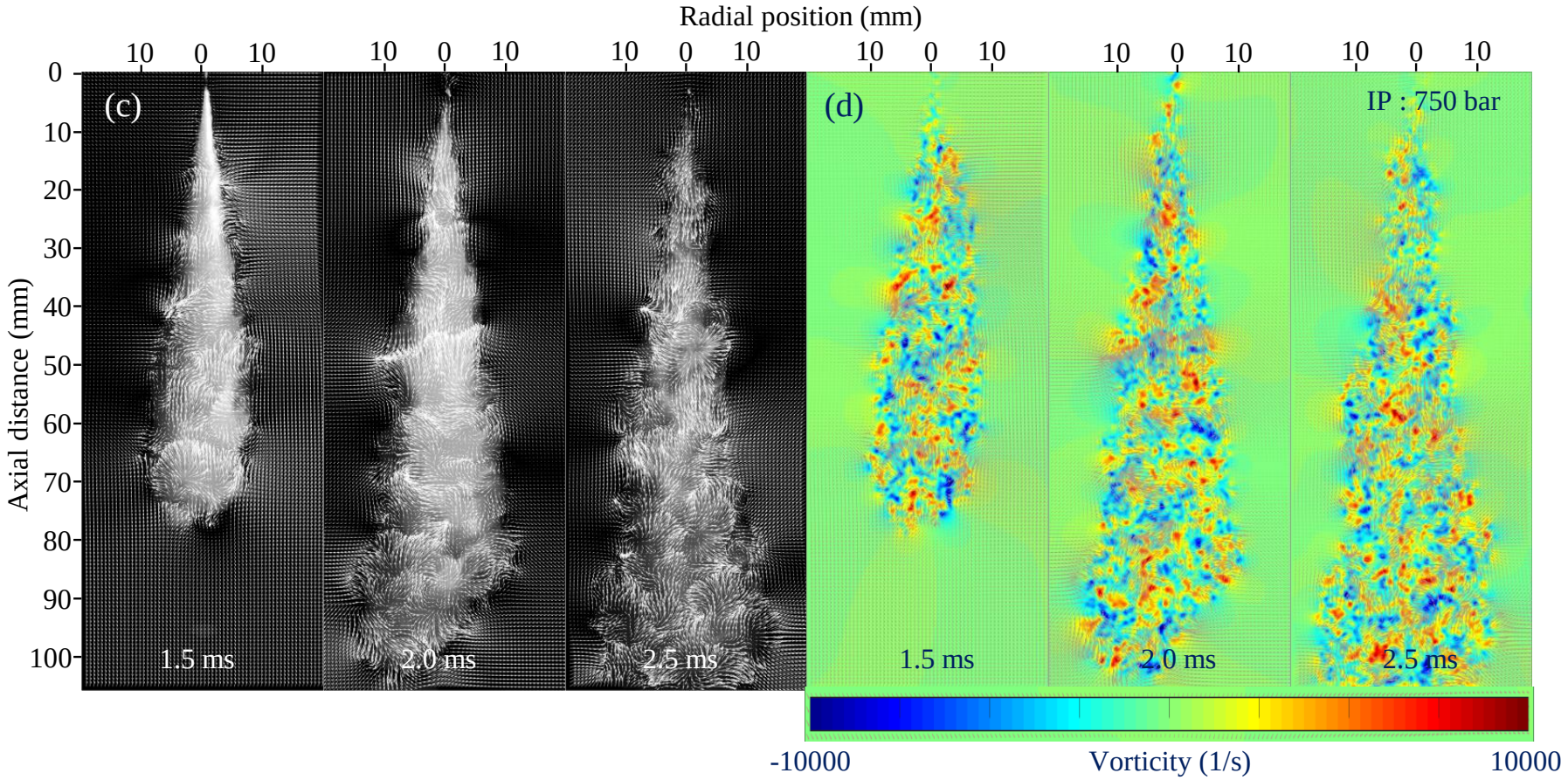

Figure 5-36 The vector (a, c and e) and vorticity distribution (b, d and f) of GB05 spray under the back pressure of 10 bar with the injection duration of 1,000 μs, and the injection pressure of 500, 750 and 1,000 bar. (Cont.)

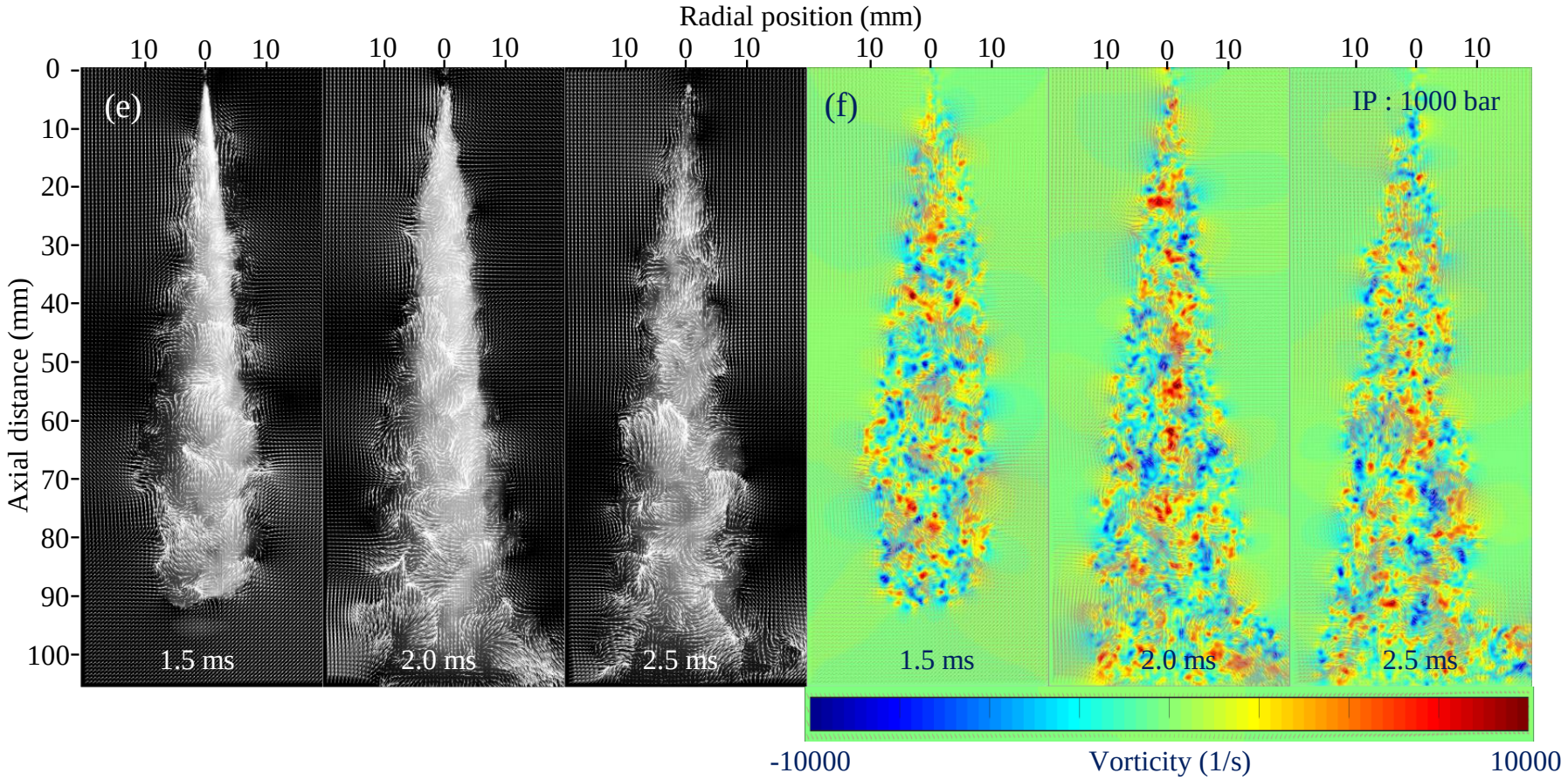

Figure 5-36 The vector (a, c and e) and vorticity distribution (b, d and f) of GB05 spray under the back pressure of 10 bar with the injection duration of 1,000 μs, and the injection pressure of 500, 750 and 1,000 bar. (Cont.)

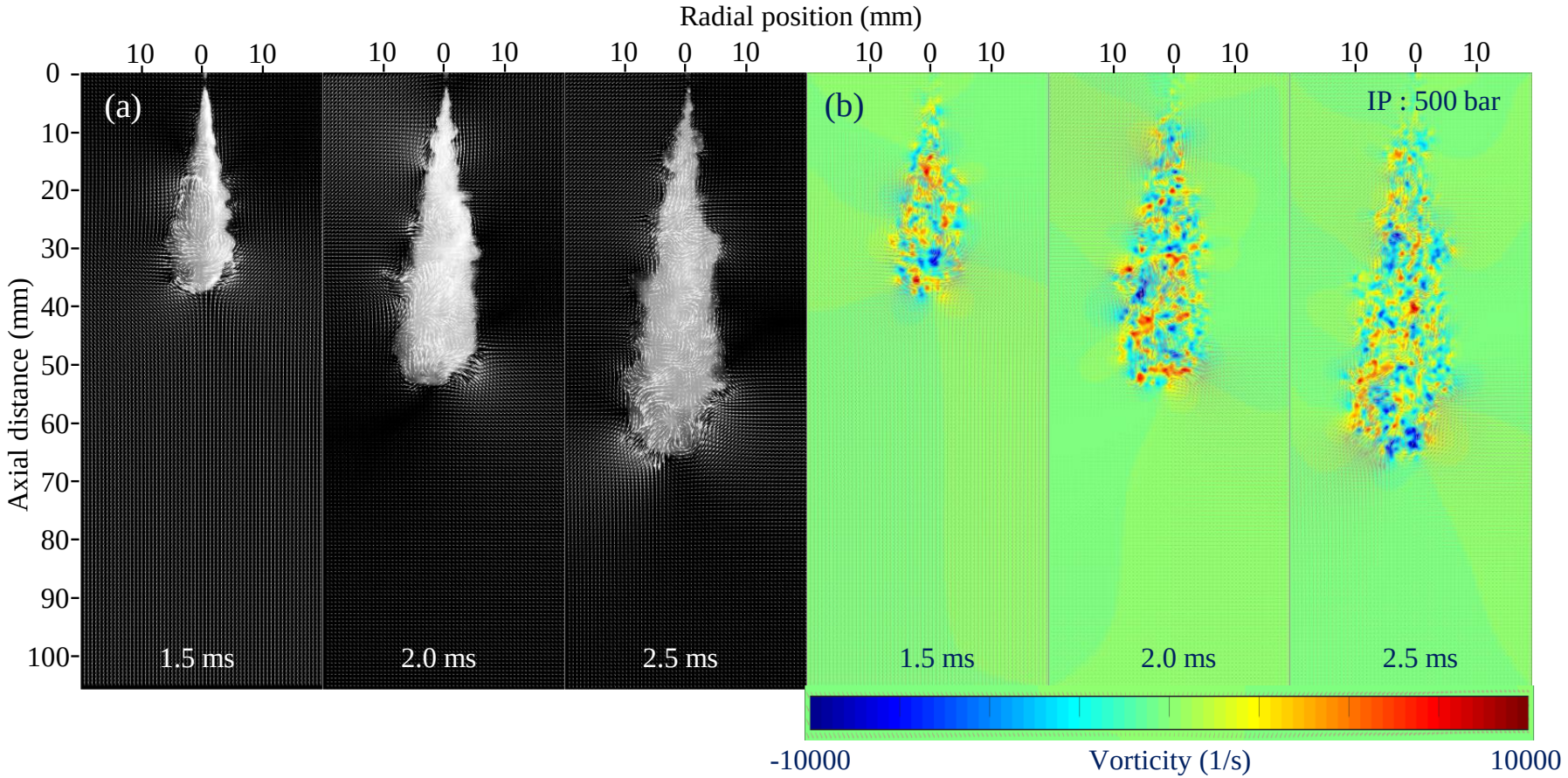

Figure 5-37 The vector (a, c and e) and vorticity distribution (b, d and f) of GB05 spray under the back pressure of 50 bar with the injection duration of 1,000 μs, and the injection pressure of 500, 750 and 1,000 bar.

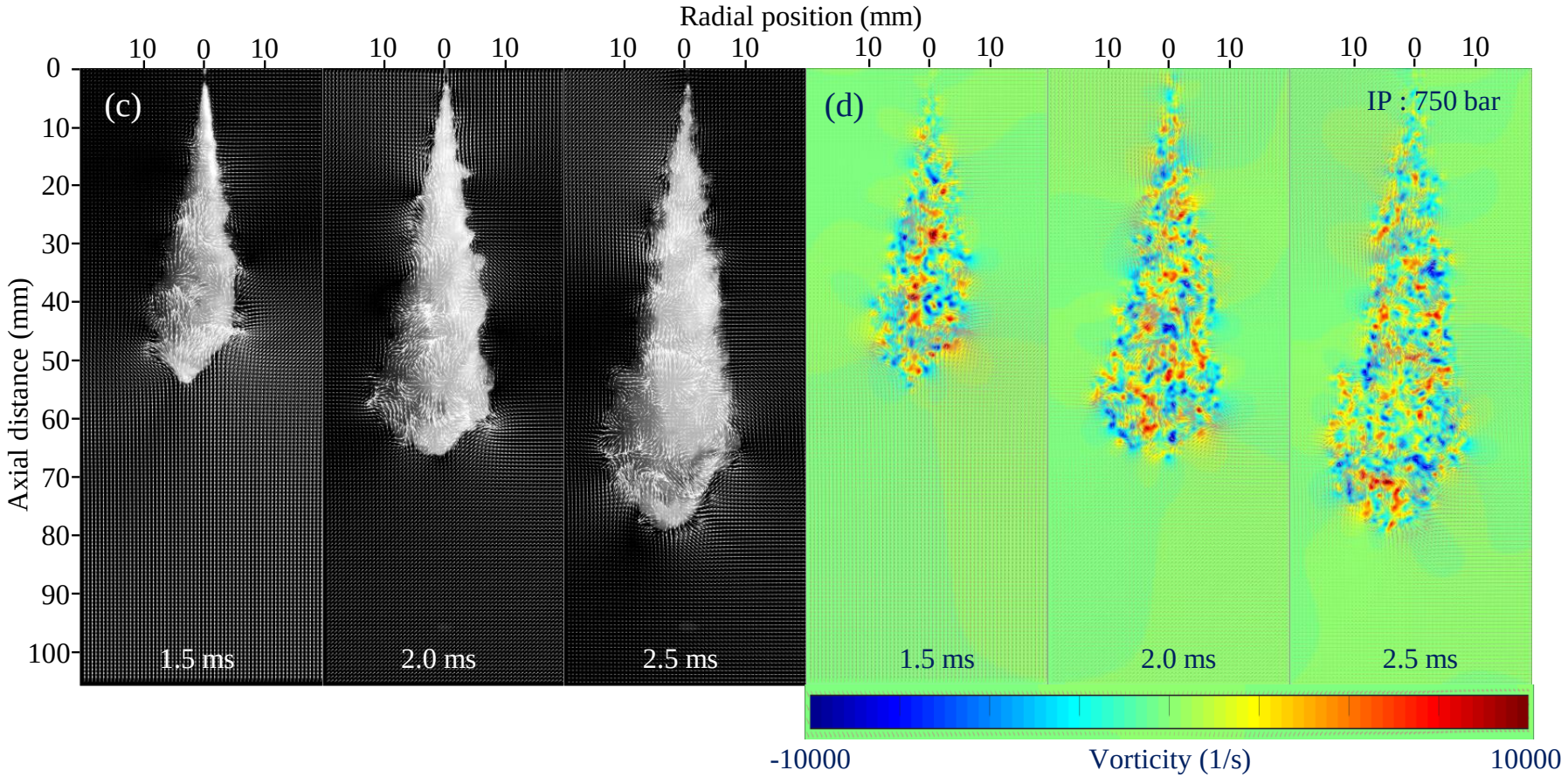

Figure 5-37 The vector (a, c and e) and vorticity distribution (b, d and f) of GB05 spray under the back pressure of 50 bar with the injection duration of 1,000 μs, and the injection pressure of 500, 750 and 1,000 bar. (Cont.)

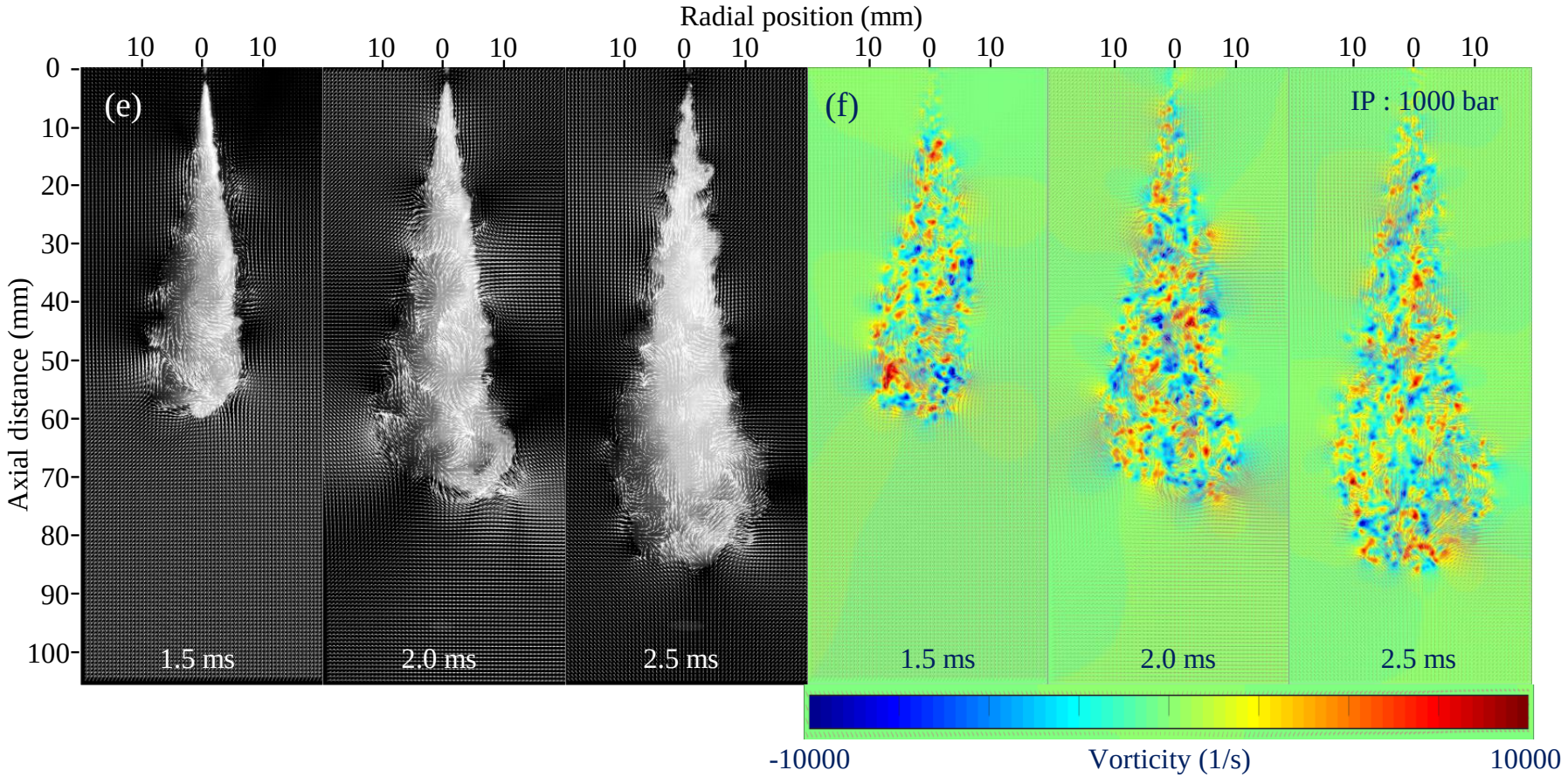

Figure 5-37 The vector (a, c and e) and vorticity distribution (b, d and f) of GB05 spray under the back pressure of 50 bar with the injection duration of 1,000 μs, and the injection pressure of 500, 750 and 1,000 bar. (Cont.)

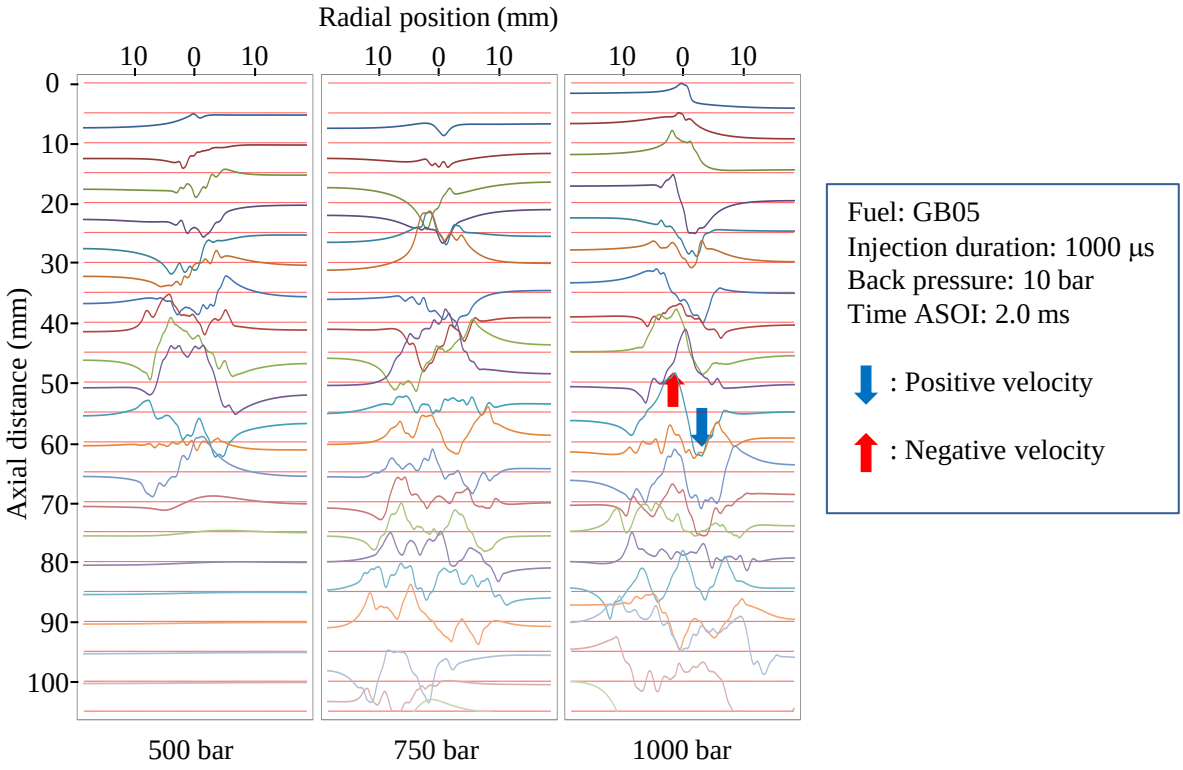

(a)

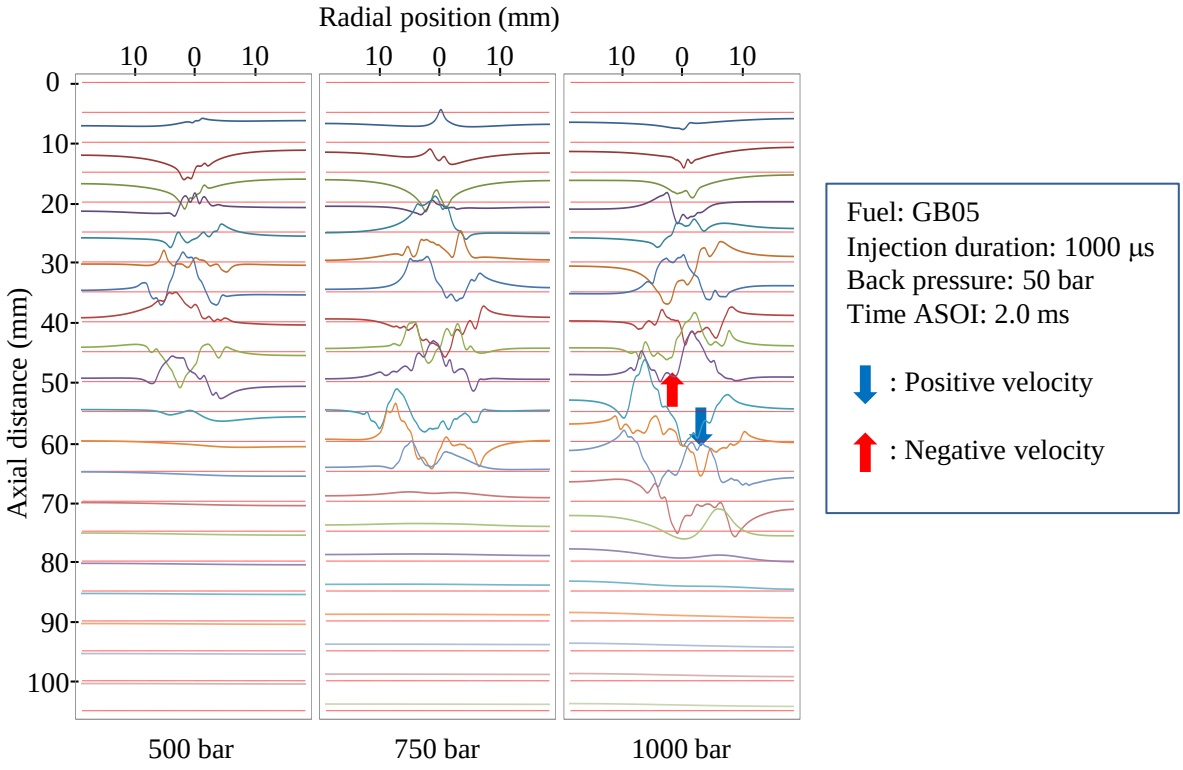

(b)

Figure 5-38 The axial velocity distribution profile of GB05 with different injection pressure at back pressure (a) 10 and (b) 50 bar.

Considering between Figure 5-36 and 37, at the same injection pressure when the back pressure increased, the number and the strength of vortex and vorticity decreased. The spray periphery is relatively smooth and stable. At the higher back pressure, the compact spray was confined by the drag force. The spray could not travel easily. Then the spray distribution was suppressed. This means that the air-fuel mixing process hardly occurred. Compared at the same injection pressure but different back pressure between Figure 5-38(a) and (b), the axial velocity had the less magnitude and distribution along the radial axis as the increased back pressure. In addition, the higher back pressure of 50 bar delayed the first negative axial velocity happen later than that of 10 bar with the injection pressure of 1000 bar. The dense ambient air compresses the spray to travel along the axis. There is less air entrainment to resist the droplet moving with the high momentum. The spray droplets were hardly diverged from the axial direction.

5.2.3.2 Conclusions

Gasoline Spray was investigated by using the Schlieren photography and PLIF-PIV image. The behavior and structure of GB05 and diesel in various injection pressures and back pressures were analyzed. Especially, this paper is the first to clarify the spray flow field of gasoline blended with biodiesel 5%. From this work some important conclusion can be drawn:

- The increased spray length with the increased injection pressure because of the increased momentum flux is not depended directly on the test fuel (fuel properties). Therefore, the effect of injection pressure on the spray penetration length of GB05 and neat diesel fuel are similar. With the higher injection pressure, the spray can travel longer in the chamber.

- Like neat diesel, the spray cone angle of GB05 is enlarged with the increased ambient pressure. However, the magnitude of the increased cone angle of GB05 is smaller than those of neat diesel because cavitation phenomena happen in GB05 flow inhibits the effect of ambient pressure.

- The average speed and the instantaneous speed of GB05 and neat diesel are the similar trends. At SOI 0.3-0.7 ms, the free sprays are immediately increased and continuously boosted the speed. After that, it quite decreases until the end of injection timing.

- The injection pressure and back pressure are the most effects on the spray structure and distribution. At high ambient pressure, the free spray was affected on shape and size. The free sprays clearly contract and the liquid jet still remains after closing needle.

- The spray density of GB05 is continuously distributed along with the free spray at both the low and high-back pressure. Moreover, the wavy motions are found at the medium and high injection pressure. It causes the buckling shape.

- Although the spray flow field of GB05 seems like the diesel spray at the entrainment and recirculation zone, the air entrainment has the effect on the GB05 at the spray tip region but there is no clear evidence of the effect on the diesel from the past research. This may claim that using gasoline injected with common rail injection system could improve better air-fuel mixing process.

- At the high injection pressure and low back pressure, the vortex and vorticity are formed throughout the spray area with the large number and magnitude. This indicates the high turbulence spray structure and heterogeneous fuel-air mixing distribution. In addition, the spray tip penetration of GB05 is lower than that of the diesel spray due to the low viscosity, density and surface tension (from the literature). Therefore, when using gasoline in the high-pressure injection system, the injection pressure can increase with less occurrence of the spray impingement on the piston and the fuel-air mixing process is better than those of using diesel. As the results, the auto-ignition of gasoline should easily occur.

5.3 Combustion and emission characteristics

5.3.1 Combustion characteristics and exhaust emissions of GCI engine fueled with Gasoline-biodiesel blends

The current study investigated the effects of gasoline-biodiesel blends on gasoline compression ignition (GCI) combustion. Biodiesel concentrations blended with gasoline were varied in the range of 0, 10 and 20 %. A single-cylinder engine based on a commercial four-cylinder Hyundai engine was used throughout the experiment. The engine speed and load were set at 2000 rpm and 7 bars of IMEP. The injection timing and duration was altered to keep stoichiometric air-fuel equivalent ratio (λ=1). The combustion characteristics were analyzed by heat release analysis and exhaust emission was measured.

The results showed that gasoline compression ignition combustion can achieve with all blended fuels. Biodiesel content reduced ignition delay and also advanced combustion phasing. NO_X emission decreased with the increased concentration of biodiesel. However, CO emission was not influenced by biodiesel concentration.

5.3.1.1 Results and discussion

Figure 5-39 shows the in-cylinder pressure of each test fuel at every 0.2 degree crank angle. The result found that diesel yielded the highest in-cylinder pressure due to the highest heating value, followed with biodiesel. When compared the amount of biodiesel blended with gasoline, the higher percentage of biodiesel higher in-cylinder pressure was observed. The amount of injected fuels when using high biodiesel concentration in Table5-2 is the cause.

The heat release rate calculated by the first law of thermodynamics is presented. Two stages of combustions including premixed and diffusion combustion were obviously noticed. Neat biodiesel and diesel provided more premixed combustion than that of blends.

In addition, higher biodiesel content in the blends indicated higher premixed combustion mode than those of lower biodiesel concentrations. To keep the constant IMEP of 7 bar and stoichiometric air-fuel equivalent ratio, higher biodiesel content blends and neat diesel required more advance injection timing in Table 5-2 and longer ignition delay which is the cause of higher premixed combustion. Due to the higher latent heat of vaporization of biodiesel and diesel than that of gasoline, longer time was spent to vaporize enough fuel for auto-ignition.

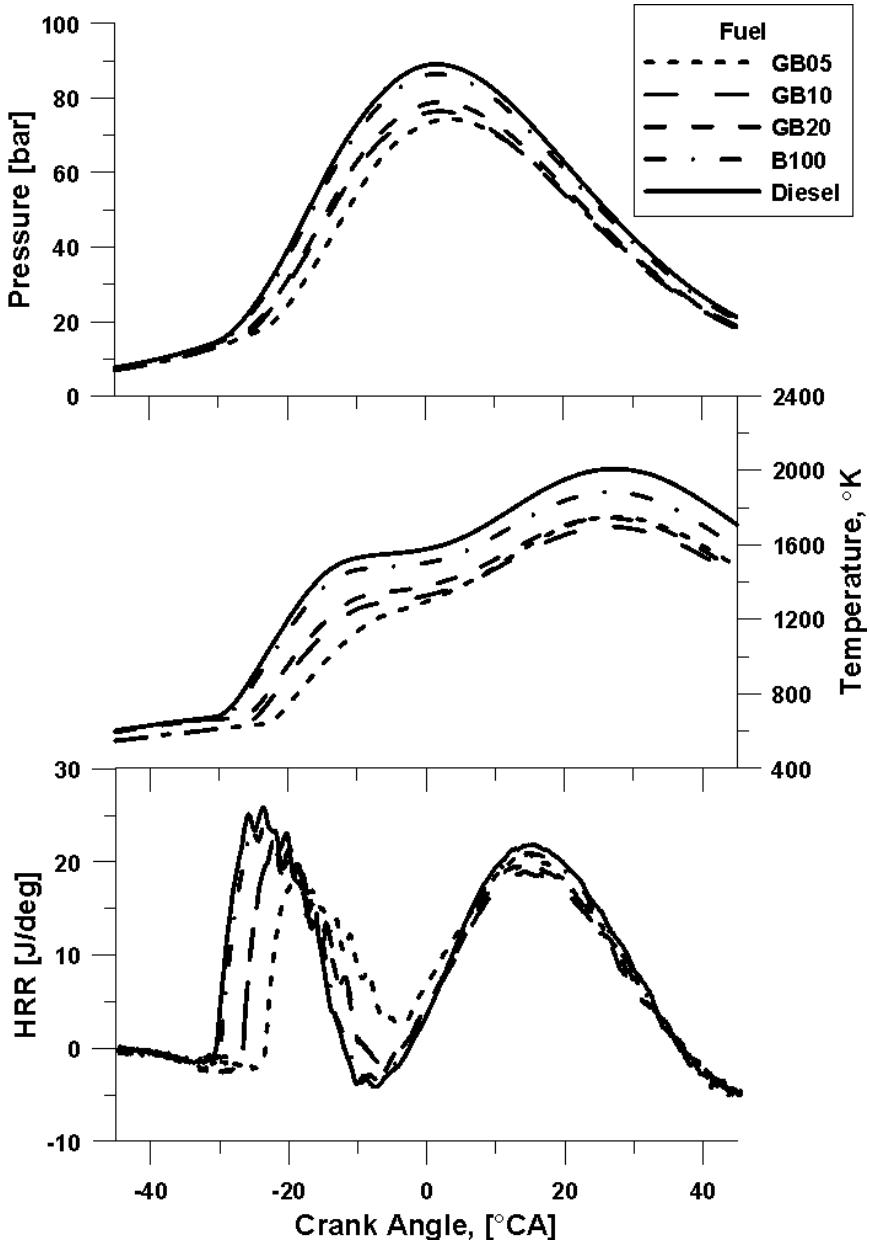

Figure 5-39 In-Cylinder pressures, Combustion temperature and Heat release rate (HRR) of all test fuels.

Table 5-2 Injection strategies for maintaining IMEP 7 bar and $\lambda = 1$.

	GB05	GB10	GB20	Biodisel (B100)	Diesel (D100)
Injection timing (^{o}CA)	25	25	40	44	43
Injection preriod (μSec.)	875	865	930	1020	920

For diffusion combustion, higher biodiesel concentration and neat diesel seemed to provide higher diffusion combustion. To keep the constant IMEP of 7 bar and stoichiometric air-fuel equivalent ratio, longer injection period of injection was needed as in Table 5-2. Hence, higher amounts of biodiesel and diesel were injected into the engine. Therefore, more fuels remained from premixed combustion to combust during the diffusion stage.

The maximum pressure and $(dP/d\theta)_{max}$ significantly increased when the percentage of biodiesel in blends increased in Figure 5-40 and 5-41. In addition, maximum pressure and $(dP/d\theta)_{max}$ of diesel showed higher value than that of biodiesel. Figure 5-42 presents the peak pressure and the crank angle at which it occurs. The higher peak pressures from the combustion of neat diesel and biodiesel were located around TDC whereas the lower peak pressures from blended fuels were located further from TDC. Due to the smaller volume change near the top dead center, the combustion of neat fuels yielded higher peak pressures while the retarded combustion with high dilution of gasoline occurred further after TDC resulting in lower peak pressure.

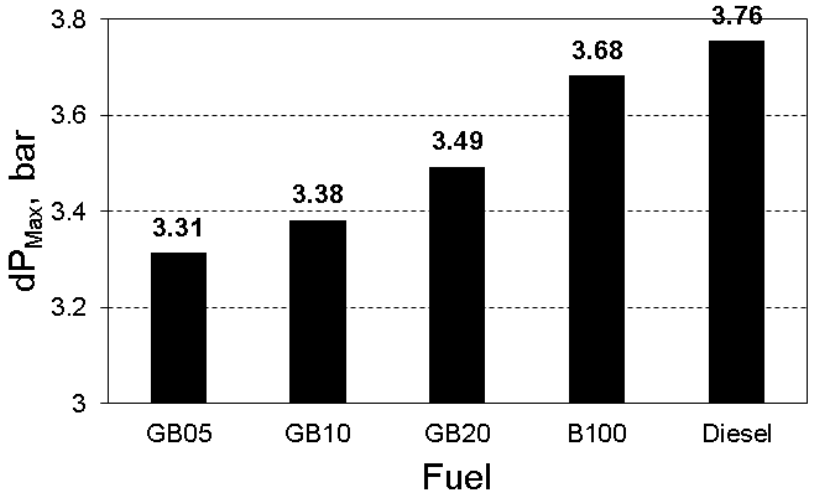

Figure 5-40 Maximum cylinder pressure during combustion.

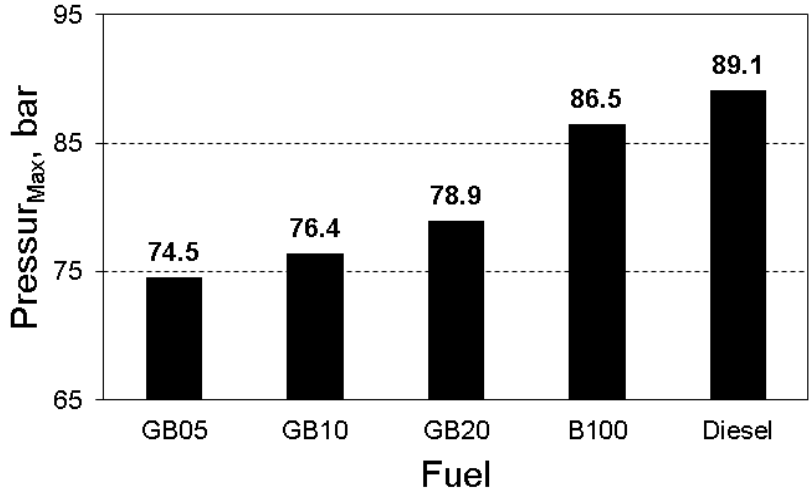

Figure 5-41 Maximum pressure change per degree crank angle.

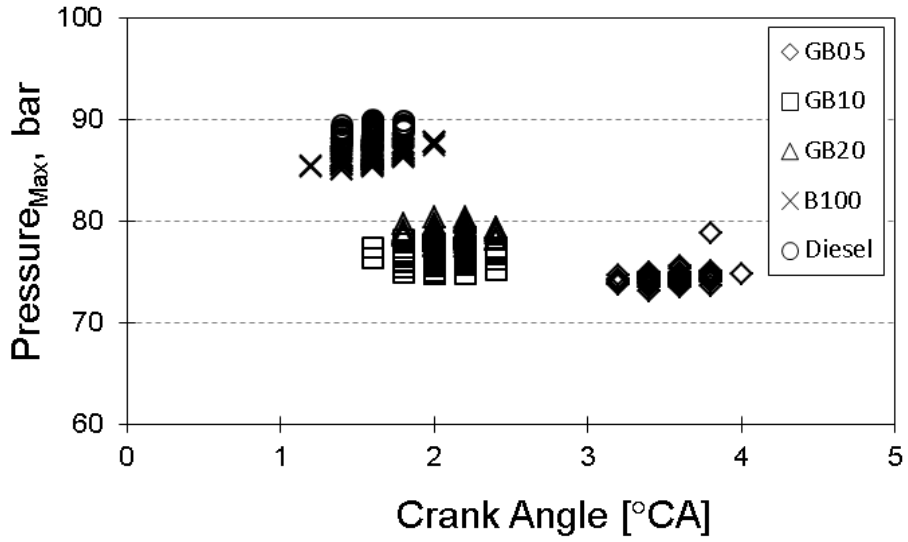

Figure 5-42 Maximum pressure occurred at crank angle.

Figure 5-43 presents a coefficient of variation of maximum pressure (COV of P_{max}). For B05 and B10, biodiesel could not show its effect on COV of P_{max}. However, when blending. 20 % of biodiesel the COV of P_{max} significantly reduced. It is the same trend with COV of indicated mean effective pressure (COV of IMEP) as shown in Figure 5-44. Biodiesel content could reduce the fluctuation of IMEP. Unlike COV of P_{max} , GB05 and GB10 show the noticeable difference of COV of IMEP.

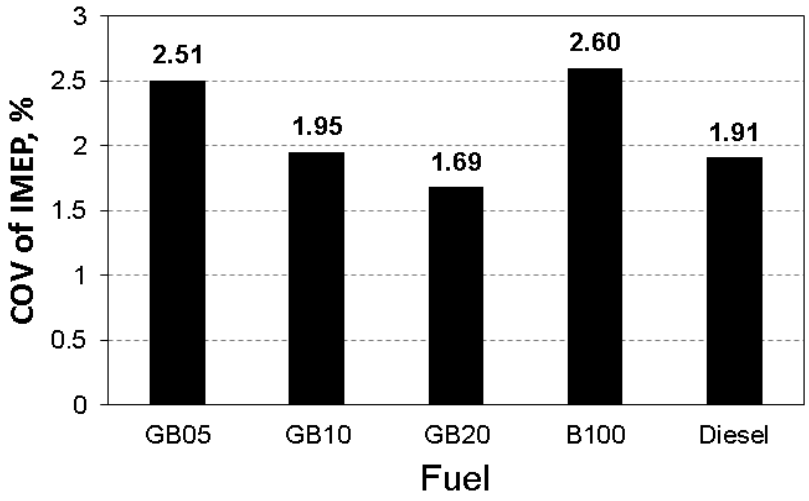

Figure 5-43 COV of Pressure max.

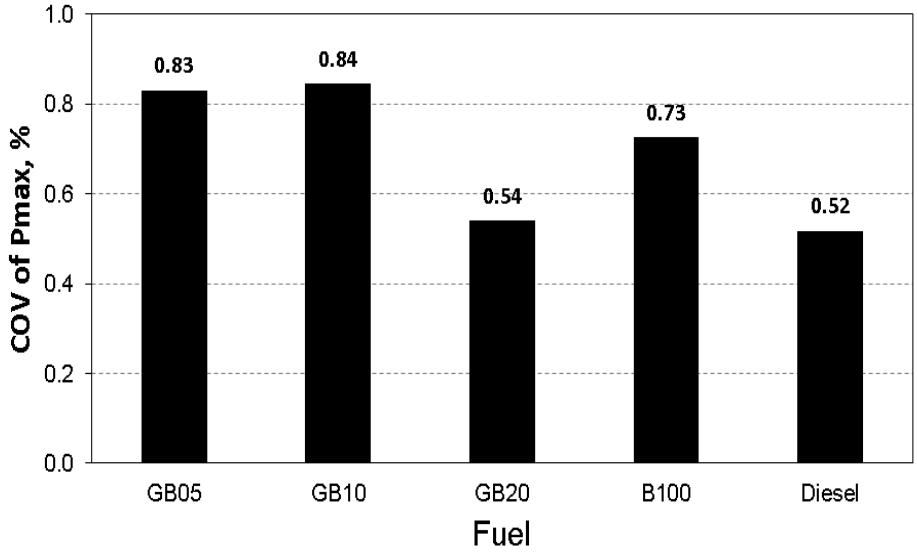

Figure 5-44 COV of IMEP.

Figure 5-45 presents mass fraction burned of each test fuels. The neat diesel, biodiesel and high content of biodiesel in the blends indicated the earlier start of combustion. In addition, the higher mass fraction was burned when compared at the same crank angle. This is due to the advance injection timing in order to keep the constant IMEP and air-fuel ratio as discussed earlier. Defined as the time duration from 10 % to 90 % of mass fraction burned combustion duration in Figure 5-46, the blended fuels in which higher gasoline mixed showed the shortest combustion duration.

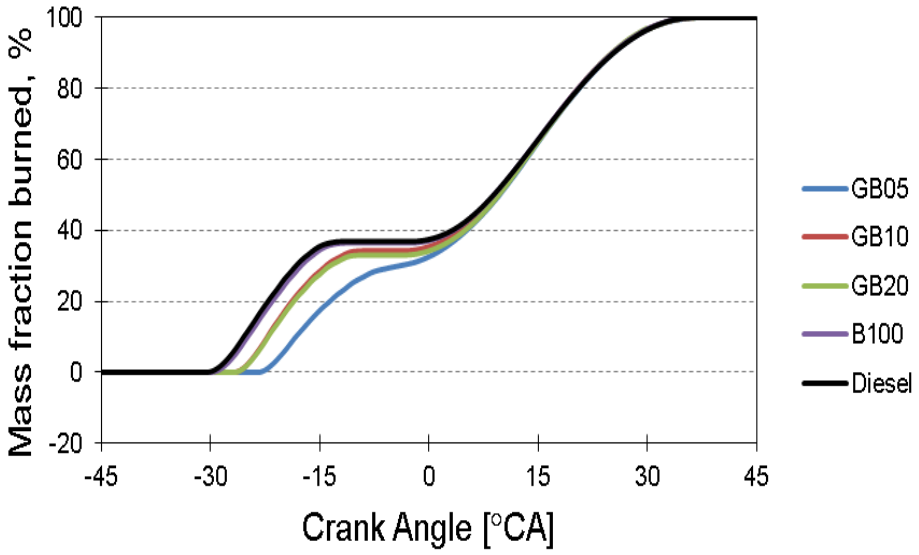

Figure 5-45 Mass fraction burned of all test fuels.

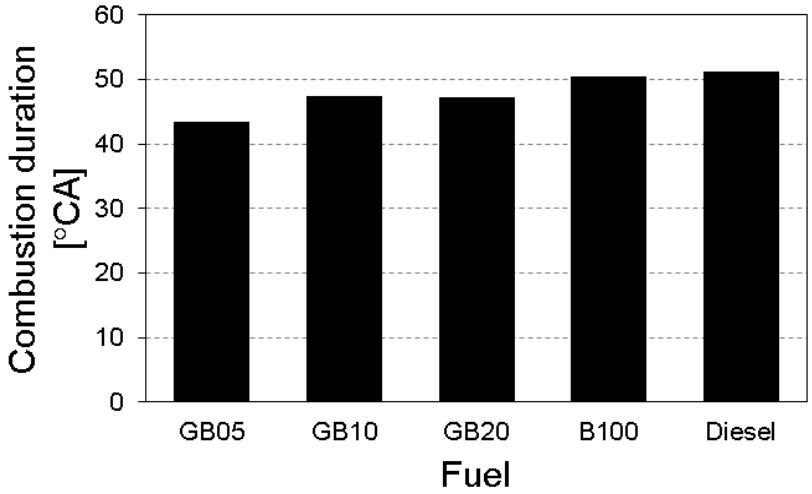

Figure 5-46 Combustion duration of all test fuels.

5.3.1.2 Conclusions

The study on gasoline compressed ignition (GCI) engine was conducted in an experiment using biodiesel addition (5%, 10% and 20%) into gasoline compared to neat gasoline, neat diesel, and neat biodiesel with single injection strategy. The conclusion from this study can be drawn as follows:

- The period of combustion for diesel occurred at 18 to 65 degree bTDC and for GB20at 18 to 75 degree bTDC.

- The highest cylinder pressure for both of diesel and GB20 occurred at 40 degree bTDC.

- The cylinder pressure at 18 degree bTDC for GB20 is higher than diesel fuel.

- Gasoline-biodiesel blends can be used in a compression ignition engine.

- Biodiesel can increase pressure when mixed with gasoline.

- Gasoline-biodiesel blends decreased premixed combustion when compared with diesel and pure biodiesel.

- Gasoline-biodiesel blends showed 5%, 10%, 50% and 90% mass fraction burned later than diesel and pure biodiesel.

5.3.2 Combustion characteristics of gasoline compression ignition engine fueled with gasoline-biodiesel blends at different injection pressure

This study investigates the combustion characteristics of gasoline compression ignition engines fueled with gasoline-biodiesel blends. A single-cylinder diesel engine, modified from a commercial four-cylinder engine, was investigated while working in gasoline compression ignition (GCI) mode throughout the experiment. In addition, the effects of the different gasoline blends on the variation of the fuel flow rate (on a mass basis) were also studied. Gasoline blended with a range of 5-20% biodiesel and pure diesel was injected into the measuring vessel with various injection pressures and durations. A seven-hole Bosch injector and a common-rail system were employed in this experiment. The injection pressures were varied from 200 to 1,350 bar and the injection duration was varied from 800 to 1,050 μs while repeating the injection 1,000 times for each run.

To characterize the combustion, the test engine was mounted with an AC dynamometer and the pressure traces were measured using a piezoelectric pressure transducer. Only pure gasoline mixed with five percent biodiesel as a lubricity enhancer was injected into the cylinder while varying the injection pressure. The injection pressures were set at 600 and 1,000 bar while the injection duration was altered to control the same equivalent ratio (λ=1). Operated in the low-speed condition, the engine speed was fixed at 1,200 rpm. In addition, other engine parameters including engine oil, coolant water, and intake air temperature, were controlled at the same operating condition for each experiment. Moreover, to understand the combustion characteristics such as heat release rate (HRR) and burning duration, the data were analyzed with the one-zone thermodynamic model. The exhaust emissions (CO, NO_X, and THC) were measured using an exhaust gas analyzer for each case, as well. The results showed that fuel properties had an effect on the injection flow rate. Higher viscosity fuel resulted in a lower injection rate. The injection pressure showed the greatest effect on the fuel flow rate. The higher the injection pressure, the higher the injection flow rate. At the same injection pressure and duration, it was revealed that the injection flow rate was reduced with an increase in the amount of biodiesel in the blend. In terms of combustion phenomena, a 5% gasoline-biodiesel blend (GB05) showed the most significant differences in combustion when injected at high versus low injection pressures. At the higher injection pressure, the benefits of using diesel fuel were clear, but GB05 combustion at high pressures resulted in increased concentrations of undesirable emissions. On the other hand, GB05 fuel presented clear

advantages when injected at a lower pressure. Depending on the injection pressure, the merits of gasoline on the exhaust emissions were evaluated, especially with respect to CO, NO_X, and THC emissions reductions.

5.3.2.1 Results and discussion

Effect of biodiesel concentration on the injection flow rate

Gasoline is usually produced from oil refineries. As shown in Table 5-1, the properties of pure gasoline, diesel, and biodiesel are significantly different. The results show that gasoline has a lower density and viscosity than diesel and biodiesel. In particular, the viscosity of gasoline is 3.8 and 5.6 times lower than that of diesel and biodiesel, respectively. When adding biodiesel into gasoline, the densities of the blends are increased. These density-related properties have the greatest effect on the spray mass flow rate and momentum flux [37,99], apart from the effect of nozzle geometry. Moreover, fuel properties also cause changes in engine performance and exhaust emissions.

The injection pressure and duration are also key factors of combustion and emission characteristics. In this section, the effects of varying the injection pressure and duration on the fuel flow rate when using various fuels are investigated and compared. In order to identify the effect of injection pressure, the injection duration was fixed at 800 μs while the injection pressure was set at 800 bar. These conditions are selected to represent typical engine operating conditions.

The fuel flow rates (on a mass basis) when varying the injection pressure from 200-1350 bar with a fixed injection duration of 800 μs are shown in Figure 5-47. Figure 5-47 shows that a higher injection pressure results in a higher the injection flow rate for all test fuels. At every injection pressure, neat diesel (D100) results in a slightly lower injection rate than the blends. This means that relative to the gasoline blends, longer injection duration is required to inject the same amount of fuel when using diesel. Moreover, when the amount of biodiesel blended with gasoline increases, the injection flow rate is reduced (GB05 > GB10 >GB20 >D100). This trend closely corresponds with a previous study [14], in which adding biodiesel in petroleum-based fuel (gasoline) was shown to decrease the fuel injection flow rate. The decreased injection flow rate is related to the increased fuel viscosity. The high viscosity of biodiesel, which results in more friction loss in the orifice, is the cause of slightly decreased injection rates across fuel grades.

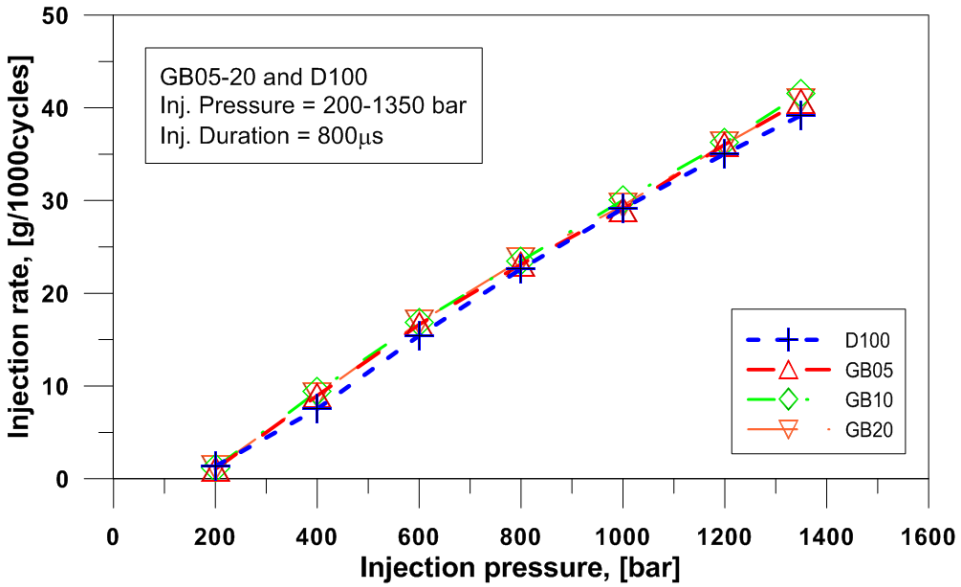

Figure 5-47 Injection rates with different injection pressures at the injection duration of 800 μs when using diesel and gasoline-biodiesel blends.

At the short injection duration around 800-950 μs, due to the lower viscosity, the injection rate of GB05-20 is slightly higher than that of D100. The results have the same trends when varying injection pressure as explained above. However, at the long injection durations between 1,000 and 1,050 μs, there is no significant difference between the injection rate of GB05-20 and D100, as shown in Figure 5-48.

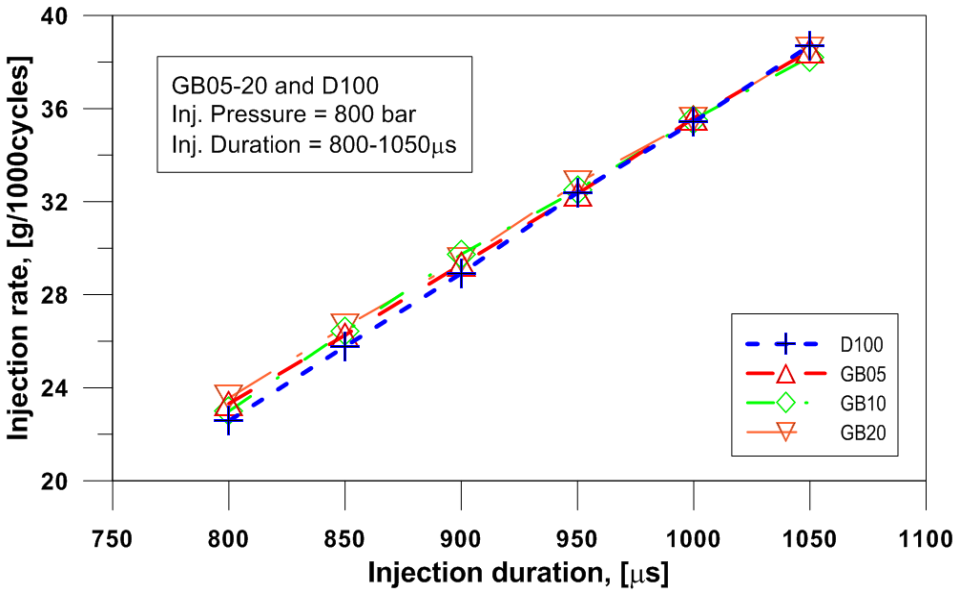

Figure 5-48 The variations of injection flow rates when altering the injection durations between 800 and 1,050 μs with a fixed injection pressure of 800 bar.

Hence, the longer injection duration has no effect on the injection flow rate when using various fuels. This result can be explained because a long injection duration leads to the quasi-steady state flow period in which the different viscosities or densities do not affect the mass flow rate [100]. Therefore, the mass flow rate values for all test fuels are similar.

The combustion characteristics

Figure 5-49 shows the in-cylinder pressure of diesel and GB05 combustion at every 0.2 degree increment of the crank angle. The result shows that diesel yields the highest in-cylinder pressure at injection pressures of 1,000 bar, followed by diesel at a lower injection pressure, while GB05 produces the lowest value at the injection pressure of 600 bar. When the injection pressure of GB05 increases, the in-cylinder pressure decreases and the crank angle at which the maximum pressure occurs moves away from the TDC towards the expansion stroke.

The heat release rate calculated by the first law of thermodynamics and the in-cylinder temperature is also presented in Figure 5-49. Clearly observed, two-stage combustions, including premixed and diffusion combustion, occur for all test conditions. Neat diesel shows a similar shape of heat release rates for both injection pressures while GB05 produces significantly different features of combustion between high and low injection pressure. The ignition delay of diesel combustion is shorter and the rate of heat release during the first-stage combustion and in-cylinder temperature are higher when the injection pressure increases. However, after premixed combustion diminishes, the heat release of second-stage combustion of diesel at a higher injection pressure is slightly lower than it is at a lower injection pressure. When the injection pressure increases, sufficiently rapid fuel-air mixing is easily achieved due to the fast atomization and vaporization of smaller fuel droplets. Therefore, early ignition occurs at higher injection pressures and results in a higher heat release rate. The higher heat release during second-stage combustion at the lower injection pressure results from the increased quantity of remaining fuel following a longer injection duration (1,775 μs compared to 775 μs).

At a low injection pressure of 600 bar, GB05 shows two-stage combustion, in which two peaks of in the heat release rate plot are completely separated. However, two-stage combustion at a high injection pressure results in the continuous occurrence of second stage combustion, just after the premixed combustion. Hence, there is no intermediate decreasing heat release rate of the premixed combustion. With an excessive gasoline injection pressure

of 1,000 bar, it is possible that wall and piston wetting occurs [101]. The liquid fuel forms a film and hardly vaporizes. A longer time is then required for the fuel-air mixing process to form an ignitable mixture and attain auto-ignition, thus lengthening the ignition delay, as clearly shown by the retarded CA5 in Figure 5-50.

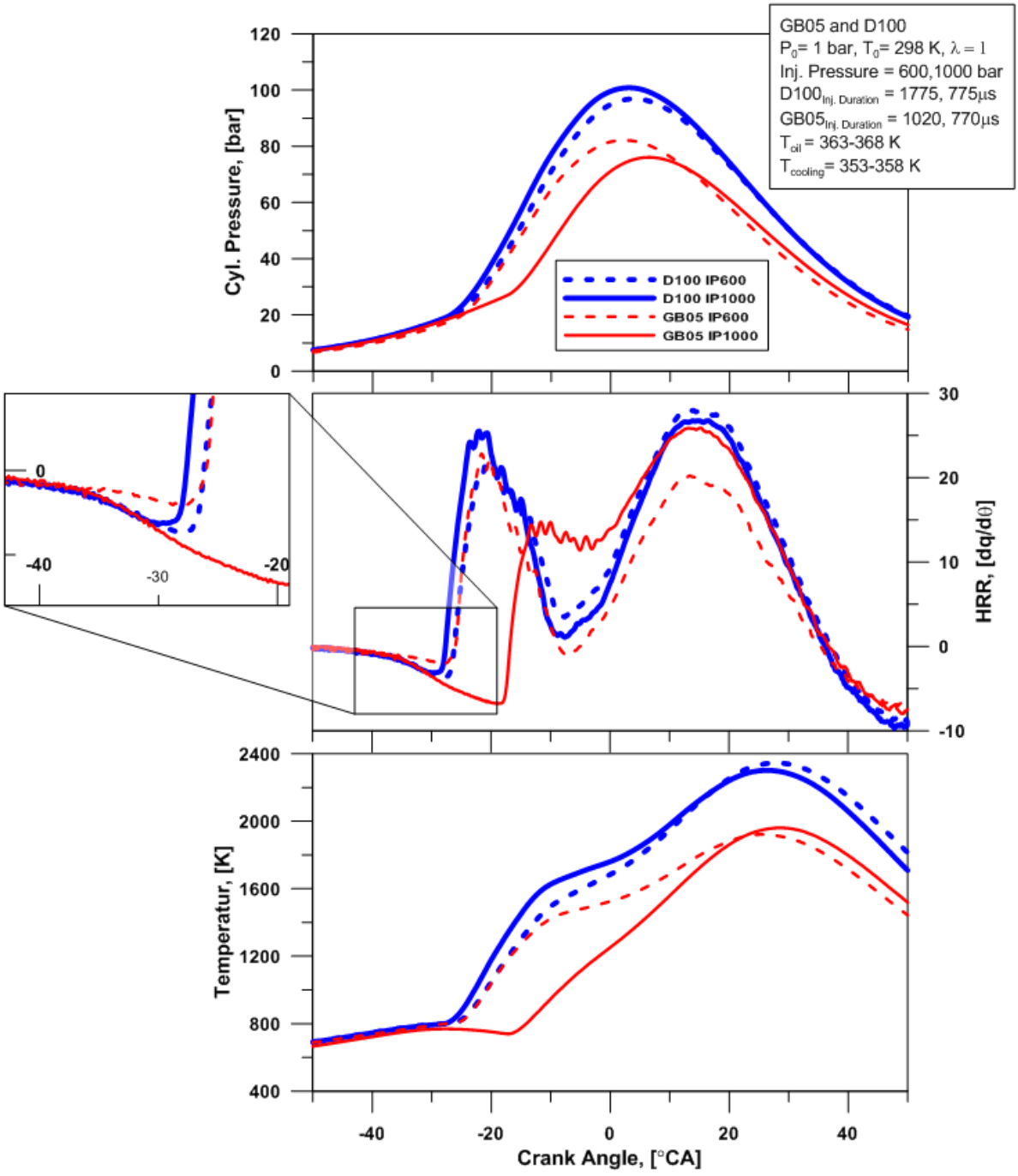

Figure 5-49 Average in-cylinder pressures, heat release rate (HRR), and flame temperature from diesel and GB05 combustion for various injection pressures.

At the injection pressure of 600 bar, diesel and GB05 produce heat release rate curves with a similar shape. Illustrated in Figure 5-50, the crank angle at which 5% of the mass (CA5) is burned occurs early for GB05 combustion. This implies the ignition of GB05 slightly advances that of diesel. Less heat is required for fuel evaporation, indicated by the lower negative heat release rate. The GB05 mixture attains the self-ignition temperature early and multiple spontaneous combustion sites can occur. Therefore, the heat release rate is moderately higher with the shorter duration at the first stage of combustion. Due to the early and rapid heat release, more time is available for heat loss from heat transfer. In addition, less fuel remains for the second stage combustion. As a result, a remarkably lower heat release during diffusion combustion is presented.

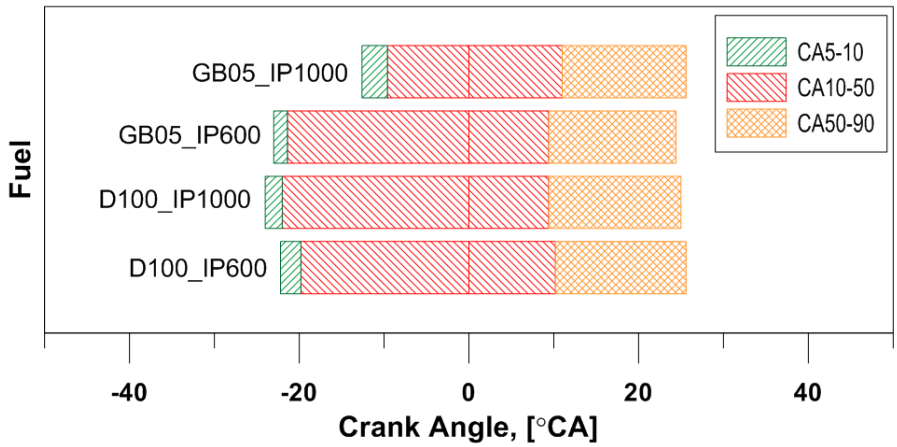

Figure 5-50 Crank angle of the start of combustion (CA5), 50 % mass fraction burned combustion duration (CA50) and combustion duration (CA10 –CA90).

In addition, at high pressures less premixed mixture (12.3% of the total mixture, presented in Figure 5-51) is available during the first-stage combustion. As a result, more fuel is left for the diffusion combustion (mixing-controlled combustion) as shown by the dramatically higher heat release rate relative to the premixed combustion.

As discussed previously, wall and piston wetting occur when injecting GB05 at a high injection pressure. The liquid fuel film requires more heat (contributing to a negative heat release rate) and more time to vaporize. Thus, the ignition delay is significantly lengthened when compared with diesel at the same injection pressure of 1,000 bar, as presented by the CA5 plot of Figure 5-50. In Figure 5-51, only 12.3% of GB05 but 30.6% of the diesel mass burned during the premixed combustion contributes to the heat release rate. As a result, GB05

has an outstandingly lower heat release than that of diesel. On the other hand, more GB05 mixture remains, in conjunction with the fast oxidation (CA10 - CA90) shown in Figure 5-50, leading to a heat release rate comparable to diesel during the second stage combustion.

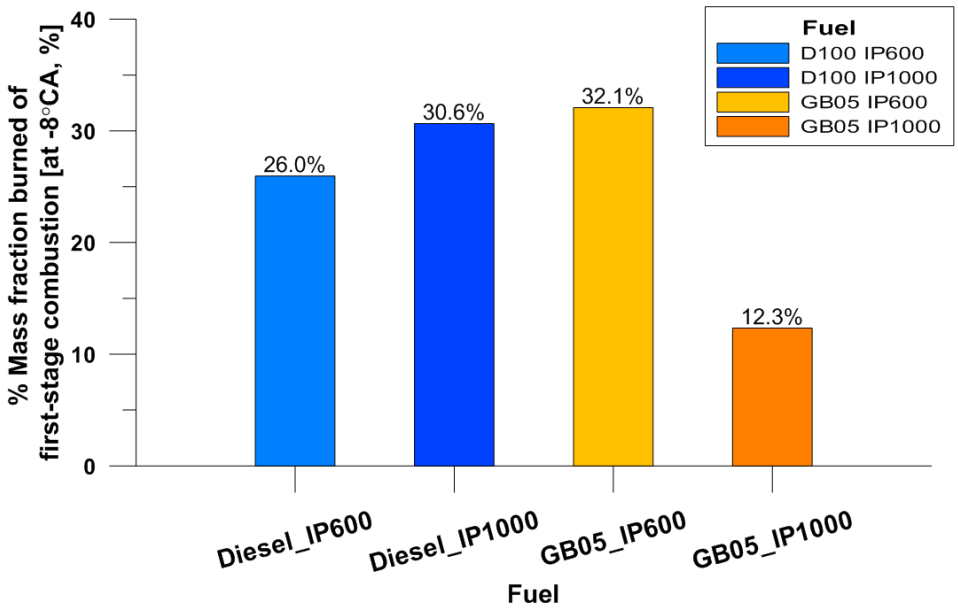

Figure 5-51 Percent of burned mass during the premix combustion (first-stage combustion) from diesel and GB05 fuel for various injection pressures.

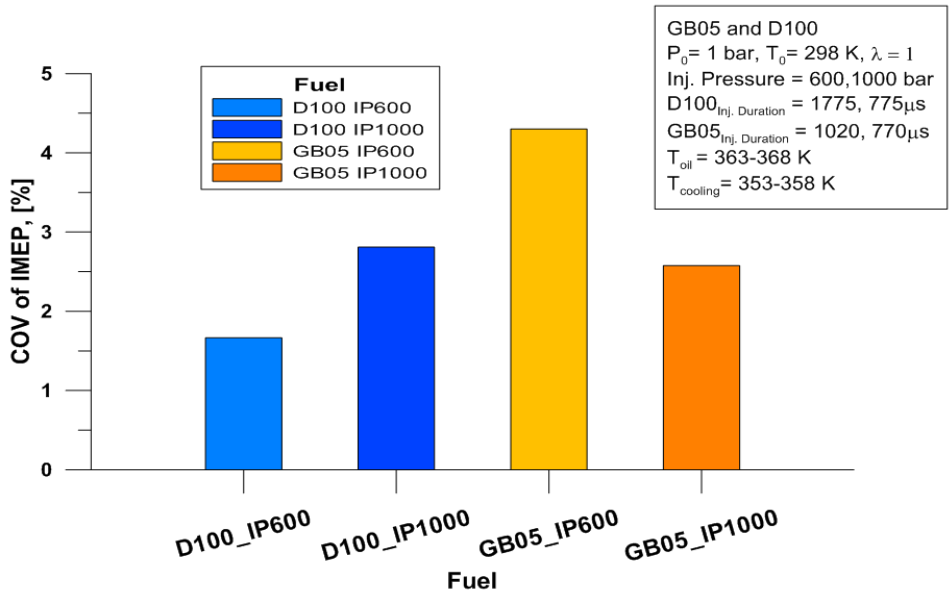

Figure 5-52 COV of IMEP from diesel and GB05 combustions for various injection pressures.

Figure 5-52 presents the coefficient of variation (COV) of the indicated mean effective pressure (IMEP) of each test fuel. The COV of IMEP is concerned with the heat release rate during the first stage of combustion; COV of IMEP increases when the heat release rate increases. Hence, the premixed combustion has a greater effect on engine behavior. Therefore, when the injection pressure increases, the COV of IMEP increases for diesel combustion but decreases for GB05 oxidation.

Gas emissions

Carbon monoxide

As shown in Figure 5-53, diesel and GB05 show different trends of CO emission with varying injection pressure. Compared with the injection pressure of 600 bar, CO emission is suppressed by diesel fuel but significantly increases when combusting GB05 at the higher injection pressure of 1,000 bar. As the results, lower levels of CO were emitted from GB05 than for diesel at a low injection pressure. But GB05 showed a much higher concentration of emitted CO at a high injection pressure. In the case of diesel, the result corresponds well with a previous study in which a higher injection pressure could reduce CO emissions in a PCCI engine [102]. When the injection pressure is increased, the spray velocity is increased and the droplet size is reduced. This leads to fast evaporation of the injected fuel and there is enough available time for the fuel-air mixing process. Thus, the locally rich region, the source of CO emissions, is eliminated.

For GB05 fuel, at the high injection pressure of 1,000 bar, when the injection pressure increased, incomplete combustion occurred due to the wall wetting, as demonstrated by a previous study which used ethanol as a fuel [101]. The previous study showed that when the injection pressure increased, the extent of the wall wetting effect increased and resulted in significant changes in the magnitude and phasing of GCI combustion. The wall wetting issue played an important role in GCI combustion. Therefore, incomplete combustion occurred and led to a higher CO concentration.

At the low injection pressure of 600 bar, GB05 shows the benefit of dramatically lower CO emission than that of diesel fuel. Due to the rapid vaporization process, gasoline can mix with air very quickly. Therefore, a less locally rich mixture results in a lower CO level.

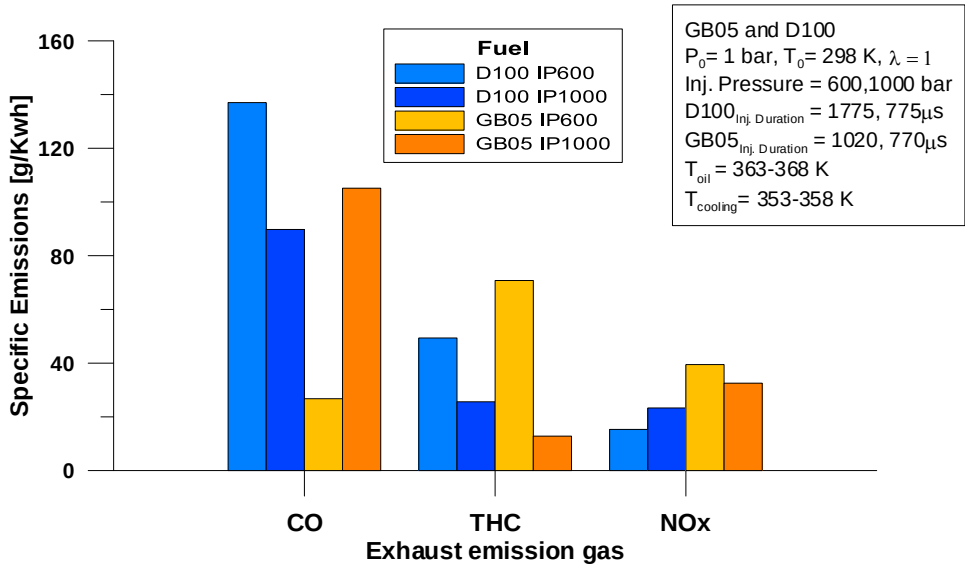

Figure 5-53 Gas emission; CO, THC and NO_X from diesel and GB05 combustions for various injection pressures.

Total hydrocarbons

Unlike CO emissions, total hydrocarbons (THC) decrease for both cases of test fuels when the injection pressure increases, as seen in Figure 5-53. To keep the stoichiometric equivalent ratio, the fuel injections into the cylinder were lengthened when the injection pressure decreased. As a result, there is less available time for the fuel-air mixing process (under mixing). Under these conditions, incomplete combustion may occur. Also, the combustion continued during the expansion stroke. It is possible that flame quenching occurred, causing the higher THC.

At the high injection pressure of 1,000 bar, GB05 yields the lower THC levels than diesel fuel. Heavy components of hydrocarbon (C≥ 6) are the major source of THC for diesel combustion [103]. However, the THC emitted from the GB05 combustion is higher than diesel at the low injection pressure of 600 bar. As shown in Figure 5-49, the lowest heat release rate of GB05 during the mixing-controlled combustion phase leads to a local temperature that is too low to allow complete combustion [104].

Oxides of nitrogen

Presented in Figure 5-53, oxides of nitrogen (NO_X) resulting from diesel combustion increase, but GB05 nitrogen oxides decrease as the injection pressure increases. Figure 5-49

shows a higher combustion temperature during the premixed combustion period, which is the cause of higher NO_X at higher injection pressures for the diesel combustion. Similarly, the higher combustion temperature at lower injection pressures for the GB05 similarly resulted in increased NO_X levels.

When compared to the other test fuels, GB05 results in higher NO_X levels than found in diesel combustions. The burned gas temperature of GB05 combustion during the expansion stroke decreases to a level low enough to prohibit NO reactants. Hence, no decomposition of NO occurs [105].

5.3.2.2 Conclusions

The effects of biodiesel gasoline blends with 5-20% concentrations of biodiesel on the injection fuel flow rate were studied. In addition, a study on a gasoline compression ignition (GCI) engine using 5% biodiesel in gasoline was conducted and compared to neat diesel. To determine the fuel flow rate, the injection pressure and duration were varied. With a single injection, the influence of the injection strategy, in terms of injection pressure on combustion characteristics, and gas emissions were evaluated at 600 and 1,000 bar. In the case of high injection pressure, there are more benefits to using diesel fuel due to its high cetane number and short ignition delay. However, more advanced injection timing and fuel composition studies are needed in order for gasoline-biodiesel blends to approach the performance of diesel. The main conclusions drawn from the study are as follows:

- The injection flow rate is related to the fuel viscosity at every injection pressure with a higher viscosity resulting in a lower injection flow rate. However, the variation of the fuel flow rate can be compensated for with a longer injection duration.
- The combustion characteristics show the benefit of higher injection pressure for diesel combustion, but show drawbacks for GB05 oxidation.
- The premixed combustion phase has the greatest effect on engine behavior (COV of IMEP).
- A lower injection pressure may be suitable for GB05 combustion. Therefore, further research should be performed to optimize the injection pressure for GBO5.
- GB05 can reduce CO but at the expense of increasing NO_X, while THC is depended on the injection pressure.

6. TOTAL CONCLUSIONS

This research has studied the effect of gasoline when using in the compression ignition engine, called Gasoline Compression Ignition (GCI) engines. Due to the advantage of oxygenated fuels and its high lubricity, biodiesel was added in the gasoline. The experiments were divided into three main concepts including physical/chemical fuel properties, fuel spray and combustion characteristics. Firstly, the effect of gasoline and biodiesel concentration in the gasoline-diesel-biodiesel blends on the phase stability was investigated. In addition, the influence of ambient temperature on the phase separation was also experimented to ensure that using the blends in the engine will not have any problem. Then, the selected test fuels without phase separation were measured the physical/chemical fuel properties to clarify the effect of gasoline and biodiesel on the spray and combustion characteristics in the following test.

Secondly, the macroscopic structure of gasoline blended with biodiesel (GB05 -GB20) was deeply clarified and compared with neat gasoline and biodiesel when injected via the high-pressure common rail injection system into the constant volume combustion chamber (CVCC). Injection pressure and ambient pressure were varied to verify the effect of the operating range of the engine on the fuel spray. In addition, the influences of injection strategy including single and multiple injections were conducted with many experiments. The liquid penetration length, the cone angle, spray area and speed were analyzed through the shadowgraph and Schlieren technique images. For better understanding, the effect of using gasoline in the CI engine, the microscopic structure of gasoline blended with 5% biodiesel as the lubricity enhancer was researched by means of the PLIE technique. The flow fields of gasoline spray in terms of velocity and vorticity profile were analyzed to predict the fuel-air mixing process which affects the combustion characteristic.

Finally, combustion characteristics when using gasoline blended with biodiesel varied from 5 to 20 percent were investigated in the single cylinder CI engine. In-cylinder pressure and the subsequent heat release rate were analyzed and compared with pure diesel and biodiesel. Moreover, the effect of injection pressure when using gasoline blended with 5 % biodiesel was identified.

6.1 Overall conclusions

The effect of gasoline and biodiesel on the physical/chemical properties of the blends

The gasoline-diesel-biodiesel blends can keep the phase stability as the homogeneous mixture for all blended ratio at the ambient temperature higher than 5°C. At the ambient temperature ≤ 5°C, the higher biodiesel concentration resulted in the phase separation, appearing as colloids due to the higher cloud point. The strength of colloids relates to biodiesel concertation. However, there is no two/three phase separation occurring for gasoline-diesel-biodiesel blends at all test conditions. Gasoline and diesel are the non-polar substance while one end of biodiesel is polar, and another is non-polar. Therefore, the blend has the high phase stability properties.

Compared among pure gasoline, diesel and biodiesel, the physical/chemical properties of the blends (gasoline and biodiesel) are changed nearly linearly with the amount of biodiesel, except for lubricity. When adding biodiesel 5-20 %, the lubricity was dramatically improved as nearly as diesel fuel. Therefore, gasoline should add biodiesel as the lubricity enhancer when using in the CI engine with the high-pressure common rail injection system to protect the pump and injector failure. The properties of gasoline blended with biodiesel (GBxx) have the significant difference form the diesel, especially viscosity, density and surface tension. These should attribute to the spray behaviors and combustion characteristics when using gasoline instead of diesel in the CI engine.

The effect of biodiesel on the macroscopic spray structure of the gasoline blended fuels

Due to the significant difference of its properties, biodiesel is characterized as the longest liquid spray tip, widest spray cone angle and fastest average speed when compared with neat gasoline and the blends. However, the spray characteristics of the gasoline blended biodiesel are as similar as those of pure gasoline and not depended on the injection strategy. This means that adding biodiesel 5-20 % in gasoline did not alter the spray characteristics both for the single and multiple injections. Biodiesel blended gasoline has the effect on the spray during the internal flow in the injector. When gasoline is injected at the high pressure with the common rail injection system, the cavitation is readily occurred. However, adding biodiesel in gasoline can suppress the occurrence of the cavitation in the nozzle during the

needle lift period. The effect of adding biodiesel in the blends can be significantly observed at the high injection pressure and low back pressure where the cavitation is strongly happened.

The effect of injection pressure on the macroscopic spray structure of the gasoline blended fuels

Generally, the spray penetration length is strongly dominated by the injection pressure. When the injection pressure increases, the spray tip of gasoline blended biodiesel increases like the diesel fuel. With the high viscosity fuel such as biodiesel, the effect of injection pressure on the spray length is noticed from the start of the injection until the fully develop spray length. However, when the cavitation occurs as in the case of gasoline injection, the effect of injection pressure can be observed after the break-up period. Because biodiesel can suppress the cavitation in the blends, the injection pressure affects the spray penetration length of the gasoline blends as same as those of the high viscosity fuel (from the SOI to the fully develop spray). Injection pressure also affects the spray speed and area. When injection pressure increases the speed and area of gasoline blends increases, In contrast to the spray penetration length, the injection pressure shows the marginal effect on the spray cone angle. The cone angle seems to decrease with the increased injection pressure.

The effect of ambient pressure on the macroscopic spray structure of the gasoline blended fuels

Ambient pressure dominates the spray characteristic including the spray penetration length, cone angle and the speed higher than those of injection pressure. This means that the cylinder condition when the fuel is injected has strongly the effect on the spray behavior, hint the air-fuel mixture. When the back pressure increases, the liquid length decreases while the cone angle increases. The ambient pressure has the large effect on the biodiesel fuel and has the less influence on the gasoline spray. The cavitation phenomena in case of gasoline injection which strongly induced at the low backpressure are the cause to conceal the effect of ambient pressure on the variation of the spray length and cone angle. Because biodiesel can suppress the cavitation, the effect of ambient pressure on the GB05 fuel can still be noticed.

The microscopic spray structure of the gasoline blended with 5 % of biodiesel

The spray flow field of GB 05 is created like the branch-like spray structure which similar as the diesel spray and corresponds well with the flow field of the surrounding gas which classified into three regions; the entrainment, recirculation zone and the tip region. The large-scale vortex motion is formed at the side periphery in the recirculation zone where the high vorticity is occurred. Although the spray flow field of GB05 seems like the diesel spray, it seems that the air entrainment has the higher effect on the GB05 at the spray tip region than diesel fuel. In addition, when the injection pressure increases, the air entrainment could exist earlier in the entrainment section and the vortex and vorticity are formed throughout the spray area with the large number and magnitude. This may claim that using gasoline injected with common rail injection system could improve better air-fuel mixing process. As the results, the auto-ignition of gasoline should easily occur.

The effect of biodiesel on the combustion characteristics of the gasoline blended fuels

When injected in the CI engine, gasoline blended biodiesel fuels results in the two-stage combustion including the premixed and diffusion phase like the diesel combustion. However, the in-cylinder pressure of the blends is lower than that of diesel and also the heat release rate. Increasing biodiesel concentration in the gasoline blended fuels can increase the in-cylinder pressure. When the amount of biodiesel increases, much more time is required for fuel evaporation and mix with the air to keep the same engine output. As the results, the ignition delay is lengthening. Consequently, the higher premixed combustion phase of high biodiesel content in the blend is observed. Not only the high premixed combustion phase, but biodiesel content in the blends can also increase the diffusion phase as nearly as the diesel combustion.

Contrary to the diesel, when the injection pressure increases the in-cylinder pressure of gasoline blended with 5% biodiesel decreases. Neat diesel shows a similar shape of heat release rates for high and low injection pressures while GB05 produces significantly different features of combustion. At low injection, pressure gasoline seems to ignite earlier than that of diesel but at the high injection pressure the start of combustion is relatively late and most of the combustion occurs in the expansion stroke. This indicates that a lower injection pressure

may be suitable for GB05 combustion. Therefore, further research should be performed to optimize the injection pressure for GB05.

6.2 Future work

In the future, to understand the air-fuel mixing process at the spray break up region, the liquid core of gasoline-biodiesel sprays should be analyzed by optical techniques and spray droplet size should be investigated by using the PDPA method. In addition, the internal flow test in the injector should be conducted to clarify the cavitation phenomena which are induced by the gasoline fuels. Moreover, gasoline-biodiesel sprays should be investigated at the evaporated condition like the real engine conditions during the compression stroke of the diesel engine. Then, in order to utilize the gasoline-biodiesel spray formations in the future, the numerical spray model of gasoline-biodiesel blended fuel should be developed.

It is also very interesting to investigate the effect of gasoline-biodiesel blends on the combustion flame in combustion chambers by using the optical technique to understand their phenomena and compare with diesel fuel. From this research, the combustion characteristics of GCI engine are influenced by the injection pressure and injection timing. Therefore, the optimization of injection timing and pressure should be experimented to obtain the middle-high engine performance with the low NOx and soot. Also, the multiple injection strategies should be considered to apply to the GCI engine.

7. REFERENCES

[1] EIA. International Energy Outlook 2017 Overview. US Energy Inf Adm 2017;IEO2017:143. doi:www.eia.gov/forecasts/ieo/pdf/0484(2016).pdf.

[2] Noehre C, Andersson M, Johansson B, Hultqvist A. Characterization of Partially Premixed Combustion 2006. doi:10.4271/2006-01-3412.

[3] Hwang J, Qi D, Jung Y, Bae C. Effect of injection parameters on the combustion and emission characteristics in a common-rail direct injection diesel engine fueled with waste cooking oil biodiesel. Renew Energy 2014;63:9–17. doi:10.1016/j.renene.2013.08.051.

[4] Knothe G. The Lubricity of Biodiesel. SAE Tech Pap Ser 2005. doi:10.4271/2005-01-3672.

[5] Wadumesthrige K, Ara M, Salley SO, Ng KYS. Investigation of Lubricity Characteristics of Biodiesel in Petroleum and Synthetic Fuel. Energy & Fuels 2009;23:2229–34. doi:10.1021/ef800887y.

[6] Sasaki S, Ito T, Iguchi S. Smoke-less RichCombustion by Low Temperature Oxidation in Diesel Engines. 9Aachen Colloq Automob Engine Technol 2000:767.

[7] Akihama K, Takatori Y, Inagaki K, Sasaki S, Dean AM. Mechanism of the Smokeless Rich Diesel Combustion by Reducing Temperature. SAE Int 2001. doi:10.4271/2001-01-0655.

[8] Onishi S, Jo SH, Shoda K, Jo P Do, Kato S. Active Thermo-Atmosphere Combustion (ATAC) - A New Combustion Process for Internal Combustion Engines. SAE Int 1979. doi:10.4271/790501.

[9] Noguchi M, Tanaka Y, Tanaka T, Takeuchi Y. A Study on Gasoline Engine Combustion by Observation of Intermediate Reactive Products during Combustion 1979. doi:10.4271/790840.

[10] Tongroon M, Zhao H. Combustion Characteristics of CAI Combustion with Alcohol Fuels. SAE Int 2010. doi:10.4271/2010-01-0843.

[11] Kimura S, Aoki O, Ogawa H, Muranaka S, Enomoto Y. New Combustion Concept for Ultra-Clean and High-Efficiency Small DI Diesel Engines 1999. doi:10.4271/1999-01-3681.

[12] Tong L, Wang H, Zheng Z, Reitz R, Yao M. Experimental study of RCCI combustion and load extension in a compression ignition engine fueled with gasoline and PODE.

Fuel 2016;181:878–86. doi:10.1016/j.fuel.2016.05.037.

[13] Kokjohn SL, Hanson RM, Splitter DA, Reitz RD. Fuel reactivity controlled compression ignition (RCCI): a pathway to controlled high-efficiency clean combustion. Int J Engine Res n.d.;12:209–26.

[14] Putrasari Y, Lim O. A study on combustion and emission of GCI engines fueled with gasoline-biodiesel blends. Fuel 2017;189:141–54. doi:10.1016/j.fuel.2016.10.076.

[15] Putrasari Y, LIM O. A study of a GCI engine fueled with gasoline-biodiesel blends under pilot and main injection strategies. Fuel 2018;221:269–82. doi:10.1016/j.fuel.2018.01.063.

[16] Thongchai S, Lim O. Investigation of the combustion characteristics of gasoline compression ignition engine fueled with gasoline-biodiesel blends. J Mech Sci Technol 2018;32:959–67. doi:10.1007/s12206-018-0146-9.

[17] Adams CA, Loeper P, Krieger R, Andrie MJ, Foster DE. Effects of biodiesel-gasoline blends on gasoline direct-injection compression ignition (GCI) combustion. Fuel 2013;111:784–90. doi:10.1016/j.fuel.2013.04.074.

[18] Cracknell R, Ariztegui Cortijo J, Dubois T, Engelen B, Manuelli P, Pellegrini L, et al. Exploring a gasoline compression ignition (GCI) engine concept. SAE Int 2014. doi:10.4271/2013-01-0911.

[19] Najt PM, Foster DE. Compression-Ignited Homogeneous Charge Combustion 1983. doi:10.4271/830264.

[20] Christensen M, Hultqvist A, Johansson B. Demonstrating the Multi Fuel Capability of a Homogeneous Charge Compression Ignition Engine with Variable Compression Ratio. SAE Tech Pap 1999:1999-01–3679. doi:10.4271/1999-01-3679.

[21] Willand J, Nieberding R-G, Vent G, Enderle C. The Knocking Syndrome - Its Cure and Its Potential 1998. doi:10.4271/982483.

[22] Lavy J, Dabadie J-C, Angelberger C, Duret P, Willand J, Juretzka A, et al. Innovative Ultra-low NOx Controlled Auto-Ignition Combustion Process for Gasoline Engines: the 4-SPACE Project 2000. doi:10.4271/2000-01-1837.

[23] Splitter D, Wissink M, DelVescovo D, Reitz RD. Improving the Understanding of Intake and Charge Effects for Increasing RCCI Engine Efficiency. SAE Int J Engines 2014;7:913–27. doi:10.4271/2014-01-1325.

[24] Kalghatgi GT. Auto-Ignition Quality of Practical Fuels and Implications for Fuel Requirements of Future SI and HCCI Engines 2005. doi:10.4271/2005-01-0239.

[25] Kalghatgi GT, Risberg P, Ångström H-E. Advantages of Fuels with High Resistance to Auto-ignition in Late-injection, Low-temperature, Compression Ignition Combustion 2006. doi:10.4271/2006-01-3385.

[26] Hanson R, Splitter D, Reitz RD. Operating a Heavy-Duty Direct-Injection Compression-Ignition Engine with Gasoline for Low Emissions 2009. doi:10.4271/2009-01-1442.

[27] Kokjohn SL, Hanson RM, Splitter DA, Reitz RD. Experiments and Modeling of Dual-Fuel HCCI and PCCI Combustion Using In-Cylinder Fuel Blending. SAE Int J Engines 2009;2:24–39. doi:10.4271/2009-01-2647.

[28] Manente V, Johansson B, Tunestal P. Partially Premixed Combustion at High Load using Gasoline and Ethanol, a Comparison with Diesel. SAE Int 2009. doi:10.4271/2009-01-0944.

[29] Manente V, Tunestal P, Johansson B, Cannella WJ. Effects of Ethanol and Different Type of Gasoline Fuels on Partially Premixed Combustion from Low to High Load 2010. doi:10.4271/2010-01-0871.

[30] Woo C, Goyal H, Kook S, Hawkes ER, Chan QN. Double Injection Strategies for Ethanol-Fuelled Gasoline Compression Ignition (GCI) Combustion in a Single-Cylinder Light-Duty Diesel Engine. SAE Int 2016. doi:10.4271/2016-01-2303.

[31] Kolodziej CP, Sellnau M, Cho K, Cleary D. Operation of a Gasoline Direct Injection Compression Ignition Engine on Naphtha and E10 Gasoline Fuels. SAE Int J Engines 2016;9:2016-01–0759. doi:10.4271/2016-01-0759.

[32] Sellnau M, Sinnamon J, Hoyer K, Husted H. Gasoline Direct Injection Compression Ignition (GDCI) - Diesel-like Efficiency with Low CO2 Emissions. SAE Int J Engines 2011;4:2010–22. doi:10.4271/2011-01-1386.

[33] Sellnau M, Foster M, Hoyer K, Moore W, Sinnamon J, Husted H. Development of a Gasoline Direct Injection Compression Ignition (GDCI) Engine. SAE Int J Engines 2014;7:835–51. doi:10.4271/2014-01-1300.

[34] Cracknell, R., Rickeard, D., Ariztegui, J., Rose K et al. Advanced Combustion for Low Emissions and High Efficiency Part 2: Impact of Fuel Properties on HCCI Combustion. SAE Tech Pap 2008-01-2404 2008:776–90.

[35] Sellnau MC, Sinnamon J, Hoyer K, Kim J, Cavotta M, Husted H. Part-Load Operation of Gasoline Direct-Injection Compression Ignition (GDCI) Engine. SAE Int 2013. doi:10.4271/2013-01-0272.

[36] Kim K, Bae C, Johansson B. Spray and Combustion Visualization of Gasoline and Diesel under Different Ambient Conditions in a Constant Volume Chamber. SAE Int 2013. doi:10.4271/2013-01-2547.

[37] Payri R, Garcia A, Domenech V, Durrett R, Plazas Torres A. Hydraulic Behavior and Spray Characteristics of a Common Rail Diesel Injection System Using Gasoline Fuel. SAE Int 2012. doi:10.4271/2012-01-0458.

[38] Szybist JP, Boehman AL. Behavior of a Diesel Injection System with Biodiesel Fuel. SAE Pap 2003:1–11. doi:10.4271/2003-01-1039.

[39] Desantes JM, Payri R, Salvador FJ, Manin J. Influence on Diesel Injection Characteristics and Behavior Using Biodiesel Fuels. SAE Int 2009. doi:10.4271/2009-01-0851.

[40] Allocca L, Mancaruso E, Montanaro A, Vaglieco BM, Vassallo A. Renewable Biodiesel/Reference Diesel Fuel Mixtures Distribution in Non-Evaporating and Evaporating Conditions for Diesel Engines. SAE Int 2009. doi:10.4271/2009-24-0054.

[41] Postrioti L, Grimaldi CN, Ceccobello M, Gioia R Di. Diesel Common Rail Injection System Behavior with Different Fuels. SAE Tech Pap Ser 2004. doi:10.4271/2004-01-0029.

[42] Kamimoto T, Kando H, Kobayashi H. An experimental study on the applicability of the light extinction method to a high density particle cloud. vol. 53. 1987. doi:10.1299/kikaib.53.1468.

[43] Manaka Y, Ohta T, Saito M, Furuhata T, ARAI M. Effect of High Ambient Pressure on Behavior and Structure of Diesel Spray. ICLASS 2009, 11th Trienn. Int. Conf. Liq. At. Spray Syst., Vail, Colorado, USA: 2009, p. 1–6.

[44] Zama Y, Ochiai W, Furuhata T, Arai M. Experimental study on spray angle and velocity distribution of diesel spray under high ambient pressure conditions. vol. 21. 2011. doi:10.1615/AtomizSpr.2012004722.

[45] Arai M. Diesel Spray Behaviour and Air Entrainment 2018;2.

[46] Macian V, Payri R, Margot X, Salvador FJ. A CFD analysis of the influence of diesel nozzle geometry on the inception of cavitation. vol. 13. 2003. doi:10.1615/AtomizSpr.v13.i56.80.

[47] Goney KH, Corradini ML. SAE TECHNICAL Isolated Effects of Ambient Pressure , Nozzle Cavitation and Hole Inlet Geometry on Diesel Injection Spray Characteristics 2015.

[48] Nurick WH. Orifice Cavitation and Its Effect on Spray Mixing. J Fluids Eng 1976;98:681–7.

[49] Arai M. Physics behind Diesel Sprays. Iclass 2012:1–18.

[50] Adrian R. Particle-Imaging Techniques For Experimental Fluid-Mechanics. vol. 23. 1991. doi:10.1146/annurev.fluid.23.1.261.

[51] Lee J, NISHIDA K, YAMAKAWA M. An Analysis of Ambient Air Entrainment into Split Injection D.I. Gasoline Spray by LIF-PIV Technique 2002. doi:10.4271/2002-01-2662 .

[52] Driscoll KD, Sick V, Gray C. Simultaneous air / fuel-phase PIV measurements in a dense fuel spray 2003;35:112–5. doi:10.1007/s00348-003-0647-4.

[53] Yeom J. Diagnosis of the behavior characteristics of the evaporative diesel spray by using images analysis 2008;22. doi:10.1007/s12206-008-0602-7.

[54] Sepret V, Bazile R, Marchal M, Couteau G. Effect of ambient density and orifice diameter on gas entrainment by a single-hole diesel spray. vol. 49. 2010. doi:10.1007/s00348-010-0869-1.

[55] Rhim D-R, Farrell P V. Effect of Gas Density and the Number of Injector Holes on the Air Flow Surrounding Non-Evaporating Transient Diesel Sprays 2001. doi:10.4271/2001-01-0532 .

[56] G.S.Settles. Schlieren and shadowgraph Techniques. 1st editio. Springer Science & Business Media; 2001.

[57] Settles GS, Hargather MJ. A review of recent developments in schlieren and shadowgraph techniques 2017. doi:10.1088/1361-6501/aa5748.

[58] Manaka Y, Ohta T, Saito M, Furuhata T. Effect of High Ambient Pressure on Behavior and Structure of Diesel Spray. Engineering 2009:2009–2009.

[59] Gonzalez RC, Woods RE, Eddins SL. Digital Image Processing Using MATAB. Second edi. Gatesmark Publishing; 2009.

[60] Mathworks. Image Processing Toolbox ™ User's Guide R2014b. The MathWorks, Inc.; 2014.

[61] Thielicke W, Stamhuis EJ. PIVlab – Towards User-friendly, Affordable and Accurate Digital Particle Image Velocimetry in MATLAB. J Open Res Softw 2014;2. doi:10.5334/jors.bl.

[62] Du C, Andersson M, Andersson S. The Influence of Ethanol Blending in Diesel fuel on the Spray and Spray Combustion Characteristics. SAE Int 2014. doi:10.4271/2014-

01-2755.

[63] Huang H, Dabiri D, Gharib M. On errors of digital particle image velocimetry. Meas Sci Technol 1997;8:1472–1440.

[64] Lee KH, Lee CH, Lee CS. An experimental study on the spray behavior and fuel distribution of GDI injectors using the entropy analysis and PIV method. Fuel 2004;83:971–80. doi:10.1016/j.fuel.2003.10.021.

[65] Heywood JB. Internal Combustion Engine Fundementals. vol. 21. 1988. doi:10987654.

[66] Shahir SA, Masjuki HH, Kalam MA, Imran A, Fattah IMR, Sanjid A. Feasibility of diesel-biodiesel-ethanol/bioethanol blend as existing CI engine fuel: An assessment of properties, material compatibility, safety and combustion. Renew Sustain Energy Rev 2014;32:379–95. doi:10.1016/j.rser.2014.01.029.

[67] Hu J, Du Z, Li C, Min E. Study on the lubrication properties of biodiesel as fuel lubricity enhancers. Fuel 2005;84:1601–6. doi:10.1016/j.fuel.2005.02.009.

[68] Muñoz M, Moreno F, Monné C, Morea J, Terradillos J. Biodiesel improves lubricity of new low sulphur diesel fuels. Renew Energy 2011;36:2918–24. doi:10.1016/j.renene.2011.04.007.

[69] Atadashi IM, Aroua MK, Aziz AA. High quality biodiesel and its diesel engine application: A review. Renew Sustain Energy Rev 2010;14:1999–2008. doi:10.1016/j.rser.2010.03.020.

[70] Bao Y, Chan QN, Kook S, Hawkes E. Spray Penetrations of Ethanol Gasoline and Iso-Octane in an Optically Accessible Spark-Ignition Direct-Injection Engine. SAE Int 2014. doi:10.4271/2014-01-9079.

[71] K-Petro. Quality Standard Chart according to laws, 2018, https://www.kpetro.or.kr/%0Aeng/lay1/S210T239C379/contents.do 2018.

[72] Ejim CE, Fleck BA, Amirfazli A. Analytical study for atomization of biodiesels and their blends in a typical injector: Surface tension and viscosity effects. Fuel 2007;86:1534–44. doi:10.1016/j.fuel.2006.11.006.

[73] Naber JD, Siebers DL. Effects of Gas Density and Vaporization on Penetration and Dispersion of Diesel Sprays 1996.

[74] Fansler TD, Parrish SE. Spray measurement technology: A review. Meas Sci Technol 2015;26. doi:10.1088/0957-0233/26/1/012002.

[75] Zigan L, Shi J, Automotive D, Schmitz I, Wensing M. Fuel property and fuel

temperature effects on internal nozzle flow , atomization and cyclic spray fluctuations of a direct injection spark ignition – injector 2014. doi:10.1177/1468087413482320.

[76] H. Nurick W. Orifice Cavitation and Its Effect on Spray Mixing. vol. 98. 1976. doi:10.1115/1.3448452.

[77] Hayashi T, Suzuki M, Ikemoto M. Visualization of Internal Flow and Spray Formation with Real Size Diesel Nozzle. 12th Int Conf Liq At Spray Syst (ICLASS 2012) 2012:1–7.

[78] Desantes JM, Payri R, Salvador FJ, Manin J, Valencia UP De. Influence on Diesel Injection Characteristics and Behavior Using Biodiesel Fuels. SAE Int 2009.

[79] Kook S, Pickett LM. Liquid length and vapor penetration of conventional, Fischer-Tropsch, coal-derived, and surrogate fuel sprays at high-temperature and high-pressure ambient conditions. Fuel 2012;93:539–48. doi:10.1016/j.fuel.2011.10.004.

[80] Siebers DL. Liquid-Phase Fuel Penetration in Diesel Sprays. SAE Trans 1998;107:1205–27.

[81] Canaan RE, Dec JE, Green RM, Daly DT. The Influence of Fuel Volatility on the Liquid-Phase Fuel Penetration in a Heavy-Duty D.I. Diesel Engine. SAE Trans 1998;107:583–602.

[82] Higgins BS, Mueller CJ, Siebers DL. Measurements of Fuel Effects on Liquid-Phase Penetration in DI Sprays. SAE Trans 1999;108:630–643. doi:10.4271/1999-01-0519.

[83] Wakuri Y, Fujii M, Amitani T, Tsuneva R. Studies on the Penetration of Fuel Spray in a Diesel Engine. JSME 1960;3(9):123–30.

[84] Payri R, Salvador FJ, Gimeno J, García A. Flow regime effects on non-cavitating injection nozzles over spray behavior. Proc Inst Mech Eng Part D J Automob Eng 2012;226:133–44. doi:10.1177/0954407011413056.

[85] Agarwal AK, Chaudhury VH. Spray characteristics of biodiesel/blends in a high pressure constant volume spray chamber. Exp Therm Fluid Sci 2012;42:212–8. doi:10.1016/j.expthermflusci.2012.05.006.

[86] Battistoni M, Grimaldi CN. Numerical analysis of injector flow and spray characteristics from diesel injectors using fossil and biodiesel fuels. Appl Energy 2012;97:656–66. doi:10.1016/j.apenergy.2011.11.080.

[87] Kim K, Kim D, Jung Y, Bae C. Spray and combustion characteristics of gasoline and diesel in a direct injection compression ignition engine. Fuel 2013;109:616–26. doi:10.1016/j.fuel.2013.02.060.

[88] Kim J-K, Jeon C-H, Yim E-S, Chung C-S. Lubricity Characterization of Hydrogenated Biodiesel as an Alternative Diesel Fuel. J KSTLE 2012;28:321–7. doi:http://dx.doi.org/10.9725/kstle-2012.28.6.321.

[89] Payri R, Gimeno J, Viera JP, Plazas AH. Schlieren visualization of transient vapor penetration and spreading angle of a prototype diesel direct-acting piezoelectric injector. Iclass 2012 2012:1–8.

[90] Desantes JM, Payri R, Salvador FJ, Manin J. Influence on Diesel Injection Characteristics and Behavior Using Biodiesel Fuels. SAE Int 2009. doi:10.4271/2009-01-0851.

[91] Yao Z, Wang G. No Title. J Chem Pharm Res 2013;5(11):649–54.

[92] Payri F, Bermúdez V, Payri R, Salvador FJ. The influence of cavitation on the internal flow and the spray characteristics in diesel injection nozzles. Fuel 2004;83:419–31. doi:10.1016/j.fuel.2003.09.010.

[93] Jeon J, Moon S. Ambient density effects on initial flow breakup and droplet size distribution of hollow-cone sprays from outwardly-opening GDI injector. Fuel 2018;211:572–81. doi:10.1016/j.fuel.2017.09.016.

[94] Yokogawa K, Kobashi Y, Kato S. Analysis of Turbulence in Diesel Spray Using Time-Resolved PIV. ICLASS 2015, 13th Int. Conf. Liq. At. Spray Syst., Tainan, Taiwan: 2015, p. 1–7.

[95] Jingyu Zhu, Kut OA, Nishida K. An Investigation of the Effects of Fuel Injection Pressure, Ambient Gas Density and Nozzle Hole Diameter on Surrounding Gas Flow of a Single Diesel Spray by laer-induced fluorescence-particle image velocimetry Technique. Int J Engine Res 2013. doi:10.1177/1468087412458778.

[96] Azetsu A, Dodo S, Someya T, Oikawa C. A Study on the Structure of Diesel Spray (2-D Visualization of the Non-Evaporating Spray). Int. Symp. COMODIA 90, Kyoto, Japan: 1990, p. 199–204.

[97] Zhu JY, Nishida K, Kuti O a. PIV Study on Flow Fields of Spray and Surrounding Gas under Non-Evaporating and Evaporating Conditions 2012:1–8.

[98] Lee J, Yamakawa M, Isshiki S, Nishida K. An Analysis of Droplets and Ambient Air Interaction in a D.I. Gasoline Spray Using LIF-PIV Technique Reprinted From: SI Combustion and Flow Diagnostics. SAE Tech Pap Ser 2016. doi:10.4271/2002-01-0743.

[99] Payri R, García A, Domenech V, Durrett R, Plazas AH. An experimental study of

gasoline effects on injection rate, momentum flux and spray characteristics using a common rail diesel injection system. Fuel 2012;97:390–9. doi:10.1016/j.fuel.2011.11.065.

[100] Tinprabath P, Hespel C, Chanchaona S, Foucher F. Influence of biodiesel and diesel fuel blends on the injection rate under cold conditions. Fuel 2015;144:80–9. doi:10.1016/j.fuel.2014.12.010.

[101] Woo C, Kook S, Hawkes ER. Effect of intake air temperature and common-rail pressure on ethanol combustion in a single-cylinder light-duty diesel engine. Fuel 2016;180:9–19. doi:10.1016/j.fuel.2016.04.005.

[102] Opat R, Ra Y, Gonzalez D. MA, Krieger R, Reitz RD, Foster DE, et al. Investigation of Mixing and Temperature Effects on HC/CO Emissions for Highly Dilute Low Temperature Combustion in a Light Duty Diesel Engine 2007. doi:10.4271/2007-01-0193.

[103] Koci CP, Ra Y, Krieger R, Andrie M, Foster DE, Siewert RM, et al. Detailed Unburned Hydrocarbon Investigations in a Highly-Dilute Diesel Low Temperature Combustion Regime. SAE Int J Engines 2009;2:858–79. doi:10.4271/2009-01-0928.

[104] Mendez S, Kashdan JT, Bruneaux G, Thirouard B, Vangraefschepe F. Formation of Unburned Hydrocarbons in Low Temperature Diesel Combustion. SAE Int J Engines 2009;2:205–25. doi:10.4271/2009-01-2729.

[105] Heywood JB. Internal Combustion Engine Fundamentals. McGRAW HILL; 1988.

APPENDICES - A: Publications

Journal

1. **Title:** A Study of Macroscopic Gasoline Spray Added Biodiesel 5% on a Single-hole Common rail Diesel Injector by Varying Injection Pressure
   Author: Sakda Thongchai, Kyeonghun Jwa, and Ocktaeck Lim
   Journal: Applied Energy (Under review)
2. **Title:** A Study of High-Pressure Gasoline Spray Added Biodiesel 5% in a Constant Volume Combustion Chamber
   Author: Sakda Thongchai, Kyeonghun Jwa, and Ocktaeck Lim
   Journal: Energy Procedia, 158 (2019) 607–611
3. **Title:** The Influence of Biodiesel Blended in Gasoline-Based Fuels on Macroscopic Spray Structure from a Diesel Injector
   Author: Sakda Thongchai and Ocktaeck Lim
   Journal: International Journal of Automotive Technology, Vol. 20(4) (2019) 701-711.
4. **Title:** An Investigation on the Spray Characteristics of a Compressed Natural Gas Injector
   Author: Sakda Thongchai, Yujin Kang, Ocktaeck Lim
   Journal: Trans. of Korean Hydrogen and New Energy Society, Vol. 29, No. 2, 2018, pp. 219~225, DOI: https://doi.org/10.7316/KHNES.2018.29.2.219
5. **Title:** Investigation of the combustion characteristics of gasoline compression ignition engine fueled with gasoline-biodiesel blends
   Author: Sakda Thongchai and Ocktaeck Lim
   Journal: Journal of Mechanical Science and Technology, 30 (10) (2016) 4773~4779, DOI 10.1007/s12206-016-0949-0
6. **Title:** Influence of Injection Strategy on a Compression Ignition Engine Fueled with Gasoline
   Author: Sakda Thongchai and Ocktaeck Lim
   Journal: Energy Procedia, 105 (2017) 1757 – 1763
7. **Title:** A Study on the Particle Size and Velocity Profile on a Gasoline Port Injector Using a Phase Doppler Particle Analyzers (PDPA)
   Author: Hyojin Kim, Hyun Jo, **Sakda Tongchai**, Ocktacke Lim

Journal: Trans. of the Korean Hydrogen and New Energy Society (2015. 6), Vol. 26, No. 3, pp. 287~293

8. **Title:** The effects of gasoline-biodiesel blended fuels on spray characteristics
   Author: Sakda Thongchai, and Ocktaeck Lim
   Journal: Trans. of the Korean Hydrogen and New Energy Society (2015.6), Vol.26, No.3, ppp.287−293, DOI: http://dx.doi.org/10.7316/KHNES.2015.26.3.287
9. **Title:** A Comprehensive Study on Fuel Injector Test Bench for Heavy Duty Engine
   Author: Shubhra Kanti Das, **Sakda Thongchai**, Ocktaeck Lim
   Journal: Journal of ILASS-Korea, http://dx.doi.org/10.15435/JILASSKR.2015.20.3.195
10. **Title:** Ignition Delay Prediction of Gasoline-diesel blended fuel at Diesel Engine Condition Using Constant Volume Combustion Chamber
    Author: Shubhra Kanti Das **Sakda Thongchai**, Ocktaeck Lim(임옥택)
    Journal: (한국자동차공학회 부문종합 학술대회, Vol.2016 No.5, [2016])
11. **Title:** A Study on Fuel Injector Test bench for Heavy Duty Engine
    Author: Shubhra Kanti Das, **Sakda Thongchai**(삭다), Ocktaeck Lim(임옥택), Sangjin Yoon)
    Journal: (한국자동차공학회 학술대회 및 전시회, Vol.2015 No.11, [2015]

Proceeding

1. **Title:** Compatibility of Motorcycle and Agricultural Engines in Ethanol Blended Fuels
   Author: Sakda Thongchai, Ocktaeck Lim, Mongkon Kananont, Amornpoth Suebwong, Nuwong Chollacoop, Peerawat Saisirirat, and Manida Tongroon
   Paper: KSAE 부문 종합학술대회, 2014.5, 332-332 (1 page)
2. **Title:** A Study on the Autoignition Characteristics of the Pre-mixture of DME/LPG in a HCCI Engine
   Author: Thongchai Sakda, Jamsran Naranhuu, Park Kyuyeol, Lee Youngjae, and Lim Ocktaeck
   Paper: Thai Society of Mechanical Engineers, 10.14455/TSME.res.2014.286
3. **Title:** Spray Characteristics of Gasoline-Biodiesel blends on a Common Rail System
   Author: S. Thongchai, T. Ahmed, S. K. Das, O. Lim
   Paper: 13th International Conference on Liquid Atomization and Spray Systems, Tainan, Taiwan, 2015, August 23-27, B1-3-214, p. 63

4. **Title:** The Effects of Gasoline-Biodiesel Blends on Fuel Properties, Phase Separation and Spray Characteristics of Diesel Engines
   Author: Sakda Thongchai, Tushar Ahmed, Shubhra Kanti Das and Ocktaeck Lim
   Paper: The 6th TSME International Conference on Mechanical Engineering, 6-18 December 2015, Thailand
5. **Title 1:** The Spray Characteristics of Ethanol-Biodiesel-Diesel Blended Fuel (B10E10)
   Author: Manida Tongroon, **Sakda Thongchai**, Nuwong Chollacoop and Ocktaeck Lim
   Title 2: Investigation of Gasoline Spray Added Biodiesel 5% on the Common Rail Diesel System
   Author: Sakda Thongchai and Ocktaeck Lim
   Paper: Journal of ILASS-America, The 14th International Conference on Liquid Atomization and Spray Systems, 2018, 146 and 255

APPENDICE - B: Conferences

1. **Name of conference:** KSAE Annual Conference and Exhibition, Busan Exhibition & Convention Center (BEXCO), Busan, Korea, May 29-31, 2014
   Title: Compatibility of Motorcycle and Agricultural Engines in Ethanol Blended Fuels
   Author: Sakda Thongchai*, Ocktaeck Lim, Mongkon Kananont, Amornpoth Suebwong, Nuwong Chollacoop, Peerawat Saisirirat, and Manida Tongroon
2. **Name of conference:** KSAE Annual Conference and Exhibition, KINTEX (Korea International Exhibition Center), Gyeonngido, Korea, Nov 19-22, 2014
   Title: An Investigation on the Spray Characteristics of Gasoline-Biodiesel Blends
3. **Name of conference:** The 5th TSME International Conference on Mechanical Engineering, 17-19th December 2014, The Empress, Chiang Mai
   Title: A Study on the Autoignition Characteristics of the Pre-mixture of DME/LPG in a HCCI Engine
4. **Name of conference:** The 21st International Symposium on Alcohol Fuels, ISAF2015 , March 10-14, 2015, KDJ convention center in Gwangju Republic of Korea
   Title: Fuel and Spray Characteristics of Gasoline-Biodiesel Blends
5. **Name of conference:** KSAE Spring Conference, Gwangju, Korea (28-30 May 2015)
   Title: The effects of Gasoline-Biodiesel Blended Fuels on Spray Characteristics
6. **Name of conference:** KSME, 대한기계학회 울산지회 2015 년도 춘계학술대회, 2015 년 5 월 13 일(수요일) 14:00~18:00
   Title: The investigation of Gasoline-Biodiesel Blended Fuels on Multi-injection Spray Characteristics
7. **Name of conference:** ICLASS, 13th Triennial International Conference on Liquid Atomization and Spray Systems, Tainan, Taiwan, August 23~27, 2015
   Title: Spray Characteristics of Gasoline-Biodiesel blends on a Common Rail System
8. **Name of conference:** KSAE Annual Conference and Exhibition, Hwabaek International Convention Center, Gyeongju, Korea, November 17-21, 2015
   Title: Combustion Characteristics and Emissions of Gasoline-biodiesel blends in Gasoline Compression Ignition (GCI) engine
9. **Name of conference:** TSME, The 6th TSME International Conference on Mechanical Engineering, 16-18 December 2015

Title: The Effects of Gasoline-Biodiesel Blends on Fuel Properties, Phase Separation and Spray Characteristics of Diesel Engines

10. **Name of conference:** ISAF2016, The 22st International Symposium on Alcohol Fuels, 9, 10 e 11 de Maech 2016, Hotel Las Americas, Cartagena - Colômbia,
    Title: A Study on Combustion and Emission characteristics of GCI Engine Fueled by Gasoline-biodiesel Blends
    Author: Sakda Thongchai and Ocktaeck Lim
11. **Name of conference:** KSAE Annual Spring Conference, Ramada Plaza, JEJU, Korea, 19 ~ 21 May 2016
    Title: Effects of injection pressure on combustion characteristics of gasoline fuel in Gasoline Compression Ignition (GCI) Engine
12. **Name of conference**: The 8th International Conference on Applied Energy, October 8-11, 2016, Beijing, Chaina.
    Title: Influence of Injection Pressure on a Compression Ignition Engine Fueled with Gasoline
    Author: Sakda Thongchai, and Ocktaeck Lim
13. **Name of conference**: The 7th TSME International Conference on Mechanical Engineering, 13-16 December 2016, Chiang Mai, Thailand
    Title: The Effects of Injection Strategy on a Gasoline Compression Ignition (GCI) Engine
    Author: Sakda Thongchai, and Ocktaeck Lim
14. **Name of conference:** The 19th Annual Conference of ILASS–Asia 2017, Oct. 18-21, 2017, Jeju, Korea
    Title: An Investigation on the Spray Characteristics of an 800kPa CNG Port Injector
    Author: Sakda Thongchai and Ocktaeck Lim
15. **Name of conference:** The 1st Faculty of Industrial Technology International Conference October 9-11, 2017, Itenas Bandung, West Java – INDONESIA
    Title: A Study on the Spray Characteristics of an 800kPa CNG Port Injector
    Author: Sakda Thongchai and Ocktaeck Lim
16. **Name of conference:** TSME, the 8th International Conference on Mechanical Engineering, 12-15 December 2017, Bangkok, Thailand
    Title: An Investigation on the Spray Characteristics of an 800kPa CNG Port Injector
    Author: Sakda Thongchai and Ocktaeck Lim

17. **Name of conference:** KSAE Annual Fall Conference, Ramada Plaza, High One Resort, Gangwon-Do, Korea, 14 ~ 17 November 2018
    Title: Investigation of Gasoline Spray Added Biodiesel 5% on the Common Rail Diesel System
    Author: Sakda Thongchai and Ocktaeck Lim
18. **Name of conference:** International Conference on Advanced Automotive Technology (ICAT), July 5-7, 2018, Gwangju, Korea
    Title: A Study of High-Pressure Gasoline Spray Added Biodiesel 5% in a Constant Volume Combustion Chamber (Poster)
    Author: Sakda Thongchai and Ocktaeck Lim
19. **Name of conference:** ILASS-America, The 14th International Conference on Liquid Atomization and Spray Systems, University of Illinois, Chicago(IL), USA, 2018, 146
    Title 1: The Spray Characteristics of Ethanol-Biodiesel-Diesel Blended Fuel (B10E10)
    Author: Manida Tongroon, **Sakda Thongchai**, Nuwong Chollacoop and Ocktaeck Lim
    Title 2: Investigation of Gasoline Spray Added Biodiesel 5% on the Common Rail Diesel System
    Author: Sakda Thongchai and Ocktaeck Lim
20. **Name of conference:** The 10th International Conference on Applied Energy, August 22-25, 2018, Hong Kong, China.
    Title: A Study of High-Pressure Gasoline Spray Added Biodiesel 5% in a Constant Volume Combustion Chamber
    Author: Sakda Thongchai and Ocktaeck Lim
21. **Name of conference:** TSME, the 9th International Conference on Mechanical Engineering, 11-14 December 2018, Thavorn Palm Beach Resort, Phuket, Thailand.
    Title: The investigation of macroscopic features of a gasoline spray in a non-evaporative condition
    Author: Sakda Thongchai and Ocktaeck Lim
22. **Name of conference:** KSAE Annual Spring Conference, Ramada Plaza, JEJU, Korea, 9 ~ 11 May 2019
    Title: An investigation of gasoline spray characteristics in a constant volume combustion chamber (Poster)
    Author: Sakda Thongchai and Ocktaeck Lim

APPENDICE - C: Certificate of fuel property test

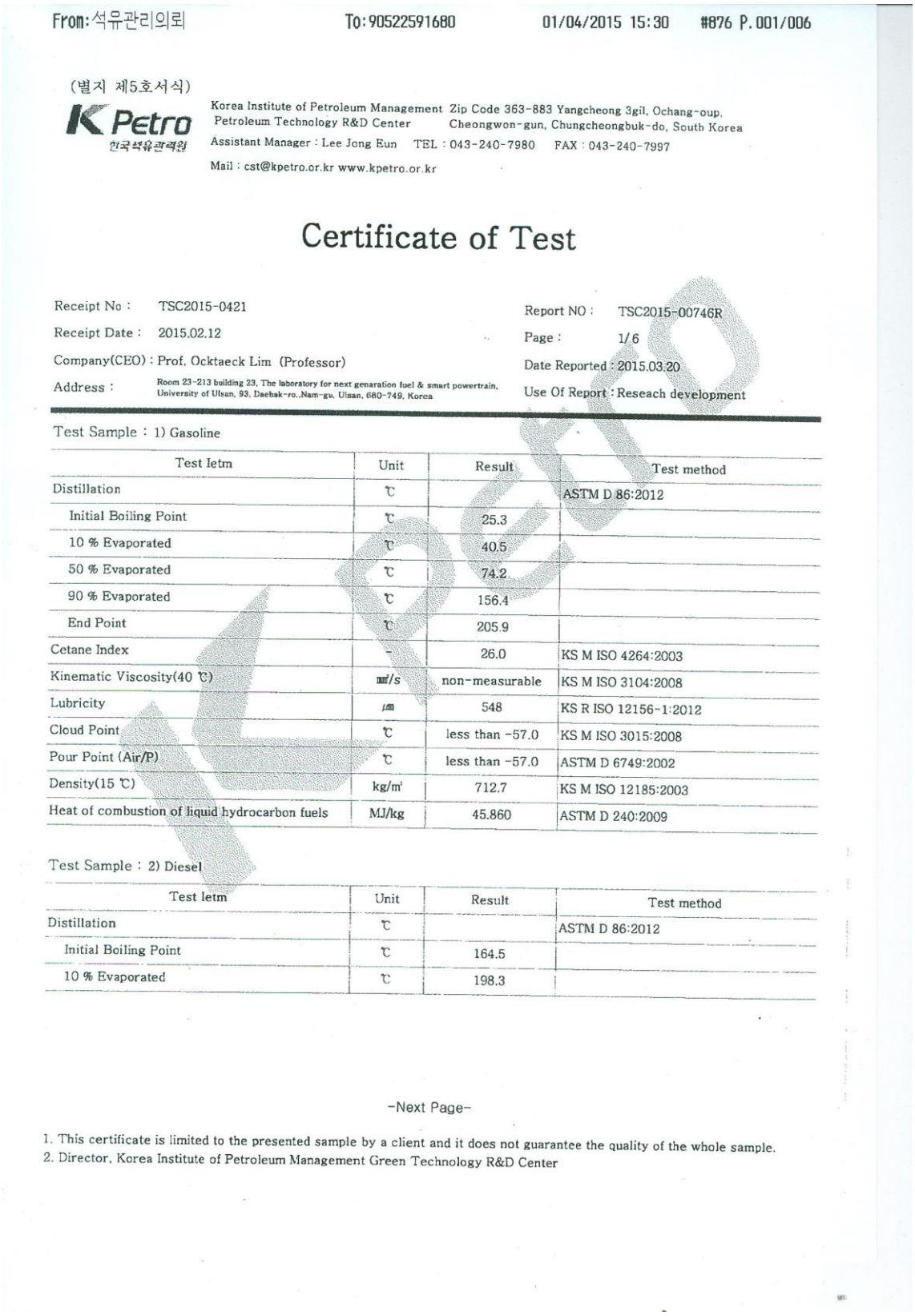

From:석유관리의뢰 To:90522591680 01/04/2015 15:30 #876 P.001/006

(별지 제5호서식)

KPetro 한국석유관리원

Korea Institute of Petroleum Management Zip Code 363-883 Yangcheong 3gil, Ochang-oup,
Petroleum Technology R&D Center Cheongwon-gun, Chungcheongbuk-do, South Korea
Assistant Manager : Lee Jong Eun TEL : 043-240-7980 FAX : 043-240-7997
Mail : cst@kpetro.or.kr www.kpetro.or.kr

Certificate of Test

Receipt No : TSC2015-0421
Receipt Date : 2015.02.12
Company(CEO) : Prof. Ocktaeck Lim (Professor)
Address : Room 23-213 building 23, The laboratory for next genaration fuel & smart powertrain, University of Ulsan, 93, Daehak-ro, Nam-gu, Ulsan, 680-749, Korea

Report NO : TSC2015-00746R
Page : 1/6
Date Reported : 2015.03.20
Use Of Report : Reseach development

Test Sample : 1) Gasoline

Test Ietm	Unit	Result	Test method
Distillation	℃		ASTM D 86:2012
Initial Boiling Point	℃	25.3	
10 % Evaporated	℃	40.5	
50 % Evaporated	℃	74.2	
90 % Evaporated	℃	156.4	
End Point	℃	205.9	
Cetane Index	-	26.0	KS M ISO 4264:2003
Kinematic Viscosity(40 ℃)	㎟/s	non-measurable	KS M ISO 3104:2008
Lubricity	㎛	548	KS R ISO 12156-1:2012
Cloud Point	℃	less than -57.0	KS M ISO 3015:2008
Pour Point (Air/P)	℃	less than -57.0	ASTM D 6749:2002
Density(15 ℃)	kg/㎥	712.7	KS M ISO 12185:2003
Heat of combustion of liquid hydrocarbon fuels	MJ/kg	45.860	ASTM D 240:2009

Test Sample : 2) Diesel

Test Ietm	Unit	Result	Test method
Distillation	℃		ASTM D 86:2012
Initial Boiling Point	℃	164.5	
10 % Evaporated	℃	198.3	

-Next Page-

1. This certificate is limited to the presented sample by a client and it does not guarantee the quality of the whole sample.
2. Director, Korea Institute of Petroleum Management Green Technology R&D Center

Figure C1 The properties of test fuels

(별지 제5호서식)

K Petro 한국석유관리원
Korea Institute of Petroleum Management Petroleum Technology R&D Center
Zip Code 363-883 Yangcheong 3gil, Ochang-oup, Cheongwon-gun, Chungcheongbuk-do, South Korea
Assistant Manager : Lee Jong Eun TEL : 043-240-7980 FAX : 043-240-7997
Mail : cst@kpetro.or.kr www.kpetro.or.kr

Certificate of Test

Receipt No : TSC2015-0421
Receipt Date : 2015.02.12
Company(CEO) : Prof. Ocktaeck Lim (Professor)
Address : Room 23-213 building 23, The laboratory for next genaration fuel & smart powertrain, University of Ulsan, 93, Daehak-ro.,Nam-gu, Ulsan, 680-749, Korea

Report NO : TSC2015-00746R
Page : 2/6
Date Reported : 2015.03.20
Use Of Report : Reseach development

50 % Evaporated	℃	280.6	
90 % Evaporated	℃	335.3	
End Point	℃	361.1	
Cetane Index	-	57.9	KS M ISO 4264:2003
Kinematic Viscosity(40 ℃)	㎟/s	2.798	KS M ISO 3104:2008
Lubricity	㎛	238	KS R ISO 12156-1:2012
Cloud Point	℃	-5.0	KS M ISO 3015:2008
Pour Point (Air/P)	℃	-9.0	ASTM D 6749:2002
Density(15 ℃)	kg/㎥	826.3	KS M ISO 12185:2003
Heat of combustion of liquid hydrocarbon fuels	MJ/kg	45.933	ASTM D 240:2009

Test Sample : 3) Biodiesel

Test Ietm	Unit	Result	Test method
Distillation	℃		ASTM D 86:2012
Initial Boiling Point	℃	non-measurable	
10 % Evaporated	℃	non-measurable	
50 % Evaporated	℃	non-measurable	
90 % Evaporated	℃	non-measurable	
End Point	℃	non-measurable	
Cetane Index	-	non-measurable	KS M ISO 4264:2003
Kinematic Viscosity(40 ℃)	㎟/s	4.229	KS M ISO 3104:2008

-Next Page-

1. This certificate is limited to the presented sample by a client and it does not guarantee the quality of the whole sample.
2. Director, Korea Institute of Petroleum Management Green Technology R&D Center

Figure C1 The properties of test fuels (Cont.)

(별지 제5호서식)

KPetro 한국석유관리원
Korea Institute of Petroleum Management Petroleum Technology R&D Center
Zip Code 363-883 Yangcheong 3gil, Ochang-oup, Cheongwon-gun, Chungcheongbuk-do, South Korea
Assistant Manager : Lee Jong Eun TEL : 043-240-7980 FAX : 043-240-7997
Mail : cst@kpetro.or.kr www.kpetro.or.kr

Certificate of Test

Receipt No : TSC2015-0421
Receipt Date : 2015.02.12
Company(CEO) : Prof. Ocktaeck Lim (Professor)
Address : Room 23-213 building 23, The laboratory for next genaration fuel & smart powertrain, University of Ulsan, 93, Daehak-ro, Nam-gu, Ulsan, 680-749, Korea

Report NO : TSC2015-00746R
Page : 3/6
Date Reported : 2015.03.20
Use Of Report : Reseach development

Lubricity	㎛	189	KS R ISO 12156-1:2012
Cloud Point	℃	3.0	KS M ISO 3015:2008
Pour Point (Air/P)	℃	1.0	ASTM D 6749:2002
Density(15 ℃)	kg/㎥	882.3	KS M ISO 12185:2003
Heat of combustion of liquid hydrocarbon fuels	MJ/kg	39.794	ASTM D 240:2009

Test Sample : 4) GB05

Test Ietm	Unit	Result	Test method
Distillation	℃		ASTM D 86:2012
Initial Boiling Point	℃	28.5	
10 % Evaporated	℃	43.3	
50 % Evaporated	℃	79.9	
90 % Evaporated	℃	174.6	
End Point	℃	328.9	
Cetane Index	-	24.6	KS M ISO 4264:2003
Kinematic Viscosity(40 ℃)	㎟/s	non-measurable	KS M ISO 3104:2008
Lubricity	㎛	290	KS R ISO 12156-1:2012
Cloud Point	℃	-37.0	KS M ISO 3015:2008
Pour Point (Air/P)	℃	less than -57.0	ASTM D 6749:2002
Density(15 ℃)	kg/㎥	722.3	KS M ISO 12185:2003
Heat of combustion of liquid hydrocarbon fuels	MJ/kg	45.323	ASTM D 240:2009

-Next Page-

1. This certificate is limited to the presented sample by a client and it does not guarantee the quality of the whole sample.
2. Director, Korea Institute of Petroleum Management Green Technology R&D Center

Figure C1 The properties of test fuels (Cont.)

(별지 제5호서식)

Korea Institute of Petroleum Management Petroleum Technology R&D Center
Zip Code 363-883 Yangcheong 3gil, Ochang-eup, Cheongwon-gun, Chungcheongbuk-do, South Korea
Assistant Manager : Lee Jong Eun TEL : 043-240-7980 FAX : 043-240-7997
Mail : cst@kpetro.or.kr www.kpetro.or.kr

Certificate of Test

Receipt No : TSC2015-0421
Receipt Date : 2015.02.12
Company(CEO) : Prof. Ocktaeck Lim (Professor)
Address : Room 23-213 building 23, The laboratory for next genaration fuel & smart powertrain, University of Ulsan, 93, Daehak-ro, Nam-gu, Ulsan, 680-749, Korea

Report NO : TSC2015-00746R
Page : 4/6
Date Reported : 2015.03.20
Use Of Report : Reseach development

Test Sample : 5) GB10

Test Ietm	Unit	Result	Test method
Distillation	℃		ASTM D 86:2012
Initial Boiling Point	℃	26.9	
10 % Evaporated	℃	45.1	
50 % Evaporated	℃	86.4	
90 % Evaporated	℃	316.2	
End Point	℃	334.9	
Cetane Index	-	10.6	KS M ISO 4264:2003
Kinematic Viscosity(40 ℃)	㎟/s	non-measurable	KS M ISO 3104:2008
Lubricity	㎛	282	KS R ISO 12156-1:2012
Cloud Point	℃	-32.0	KS M ISO 3015:2008
Pour Point (Air/P)	℃	less than -57.0	ASTM D 6749:2002
Density(15 ℃)	kg/㎥	732.2	KS M ISO 12185:2003
Heat of combustion of liquid hydrocarbon fuels	MJ/kg	44.924	ASTM D 240:2009

Test Sample : 6) GB15

Test Ietm	Unit	Result	Test method
Distillation	℃		ASTM D 86:2012
Initial Boiling Point	℃	non-measurable	
10 % Evaporated	℃	non-measurable	

-Next Page-

1. This certificate is limited to the presented sample by a client and it does not guarantee the quality of the whole sample.
2. Director, Korea Institute of Petroleum Management Green Technology R&D Center

Figure C1 The properties of test fuels (Cont.)

(별지 제5호서식)

K Petro 한국석유관리원
Korea Institute of Petroleum Management Petroleum Technology R&D Center
Zip Code 363-883 Yangcheong 3gil, Ochang-oup, Cheongwon-gun, Chungcheongbuk-do, South Korea
Assistant Manager : Lee Jong Eun TEL : 043-240-7980 FAX : 043-240-7997
Mail : cst@kpetro.or.kr www.kpetro.or.kr

Certificate of Test

Receipt No : TSC2015-0421
Receipt Date : 2015.02.12
Company(CEO) : Prof. Ocktaeck Lim (Professor)
Address : Room 23-213 building 23, The laboratory for next genaration fuel & smart powertrain, University of Ulsan, 93, Daehak-ro, Nam-gu, Ulsan, 680-749, Korea

Report NO : TSC2015-00746R
Page : 5/6
Date Reported : 2015.03.20
Use Of Report : Reseach development

50 % Evaporated	℃	non-measurable	
90 % Evaporated	℃	non-measurable	
End Point	℃	non-measurable	
Cetane Index	-	non-measurable	KS M ISO 4264:2003
Kinematic Viscosity(40 ℃)	㎟/s	non-measurable	KS M ISO 3104:2008
Lubricity	㎛	252	KS R ISO 12156-1:2012
Cloud Point	℃	-20.0	KS M ISO 3015:2008
Pour Point (Air/P)	℃	less than -57.0	ASTM D 6749:2002
Density(15 ℃)	kg/㎥	742.6	KS M ISO 12185:2003
Heat of combustion of liquid hydrocarbon fuels	MJ/kg	44.569	ASTM D 240:2009

Test Sample : 7) GB20

Test letm	Unit	Result	Test method
Distillation	℃		ASTM D 86:2012
Initial Boiling Point	℃	non-measurable	
10 % Evaporated	℃	non-measurable	
50 % Evaporated	℃	non-measurable	
90 % Evaporated	℃	non-measurable	
End Point	℃	non-measurable	
Cetane Index	-	non-measurable	KS M ISO 4264:2003
Kinematic Viscosity(40 ℃)	㎟/s	non-measurable	KS M ISO 3104:2008

-Next Page-

1. This certificate is limited to the presented sample by a client and it does not guarantee the quality of the whole sample.
2. Director, Korea Institute of Petroleum Management Green Technology R&D Center

Figure C1 The properties of test fuels (Cont.)

(별지 제5호서식)

Korea Institute of Petroleum Management Petroleum Technology R&D Center
Zip Code 363-883 Yangcheong 3gil, Ochang-oup, Cheongwon-gun, Chungcheongbuk-do, South Korea
Assistant Manager : Lee Jong Eun TEL : 043-240-7980 FAX : 043-240-7997
Mail : cst@kpetro.or.kr www.kpetro.or.kr

Certificate of Test

Receipt No : TSC2015-0421
Report NO : TSC2015-00746R
Receipt Date : 2015.02.12
Page : 6/6
Company(CEO) : Prof. Ocktaeck Lim (Professor)
Date Reported : 2015.03.20
Address : Room 23-213 building 23, The laboratory for next genaration fuel & smart powertrain, University of Ulsan, 93, Daehak-ro, Nam-gu, Ulsan, 680-749, Korea
Use Of Report : Reseach development

Lubricity	㎛	236	KS R ISO 12156-1:2012
Cloud Point	℃	-16.0	KS M ISO 3015:2008
Pour Point (Air/P)	℃	less than -57.0	ASTM D 6749:2002
Density(15 ℃)	kg/m³	757.1	KS M ISO 12185:2003
Heat of combustion of liquid hydrocarbon fuels	MJ/kg	43.580	ASTM D 240:2009

END.

2015. 03. 20.

Director, Korea Institute of Petroleum Management Petroleum Technology R&D Center

1. This certificate is limited to the presented sample by a client and it does not guarantee the quality of the whole sample.
2. Director, Korea Institute of Petroleum Management Green Technology R&D Center

Figure C1 The properties of test fuels (Cont.)